SEMI-ACTIVE VIBRATION CONTROL OF WIND TURBINE BLADES USING A TIME-FREQUENCY APPROACH

by

John Arrigan

Thesis submitted to the University of Dublin, Trinity College, for the Degree of Doctor of Philosophy

October 2010

DECLARATION

The author hereby declares that, except where reference has been given, this thesis is entirely the author's own work, and has not been not been submitted, in whole or part, to any other University as an exercise for a degree.

The author confirms that the library may, for academic purposes, lend or copy this thesis upon request.

SUMMARY

This thesis proposes the use of structural control devices to mitigate the response of wind turbines, particularly the blades. Theoretical and experimental investigations have been carried out to ascertain the effectiveness of passive and semi-active dampers in controlling the response of wind turbines.

A structural dynamic model was formulated using Lagrange's Equations taking account of the coupling between the blades and tower, and the centrifugal stiffening which occurs due to blade rotation. A model for both flapwise and edgewise vibrations was developed. Dampers were added to the turbine model in the form of Tuned Mass Dampers (TMDs), or equivalent Tuned Liquid Dampers (TLDs), represented by mass-spring-dashpot systems. The effectiveness of these passive devices in controlling the dynamic response of the turbine was studied in detail.

A semi-active algorithm was proposed based on a time-frequency approach using a Short Time Fourier Transform (STFT) technique to allow real-time tuning of the dampers to the dominant frequencies in the system. This adaptive control system allowed the time varying frequency content of the turbine model to be determined. The algorithm updated every second allowing real-time tracking of the dominant frequencies in the turbine model. The dampers were then tuned in real-time to these dominant peaks. The effectiveness of the proposed control algorithm was investigated for variations in the three main dynamic parameters of the turbine. Variations in rotational speed, Ω, and a loss in stiffness of both the blades and nacelle, were considered.

Finally, experimental development of a semi-active TLD was investigated for its use as a smart control device in a wind turbine. A passive TLD was first designed and experimentally characterised to verify the relationship between the natural frequency of the TLD and the still water depth. The TLD was tested on a simple Single Degree of Freedom (SDOF) structure with a natural frequency similar to that of a modern wind turbine blade. The passive TLD was

extended to a semi-active device by means of an STFT control algorithm, similar in nature to that used in the numerical investigations earlier in the thesis. Real-time tuning of the TLD was achieved by controlling the depth of water in the container using an automated computer controlled valve. The adaptive control system was then tested on the SDOF structure which experienced a loss in stiffness during excitation. This enabled assessment of the ability of the semi-active TLD to identify and tune to the new dominant frequency in the primary structure. Loading representative of a turbulent wind load was applied to the test structure to determine the effectiveness of the control system in mitigating vibrations due to a real life wind load experienced by a wind turbine.

ACKNOWLEDGEMENTS

This research was carried out in the Department of Civil, Structural and Environmental Engineering, Trinity College Dublin. The work was funded by the Irish Research Council for Science, Engineering and Technology.

I would like to thank my supervisor, Professor Biswajit Basu, for all his guidance and support over the last three and a half years. His enthusiasm for my work never failed and without his expertise this thesis would not have been completed.

I would also like to express my sincere thanks to all the staff in the Vibrations Laboratory of Trinity College Dublin; Chief Technician Chris O'Donovan, and in particular Dr. Kevin Ryan for all his patience and help over the experimental phases of this thesis.

This PhD is dedicated to my family; my parents, Martin and Catherine, and my brothers, Martin, Thomas and Mal.

TABLE OF CONTENTS

LIST OF FIGURES

LIST OF TABLES

CHAPTER 1 – Introduction

1.1 Brief History of Wind Energy

Wind energy has its origins around the 10th century when the Persians were one of the first to build windmills used for mechanical purposes. The technology spread to Europe during the Middle Ages where windmills were used for tasks such as grinding grain and water pumping. By the early 19th century wind energy had grown considerably, with about 20,000 modern windmills in operation in France alone (Ackermann and Söder, 2000). These windmills generally consisted of 4 or more blades, unlike today's modern wind turbines which mostly have 3 blades. An example of a traditional windmill is illustrated in figure 1.1.

Figure 1.1: Early windmill used for grinding grain

However, with the occurrence of the Industrial Revolution wind energy began to decline in popularity. The emergence of fossil fuels such as coal, and further down the line oil, carried with them significant advantages over wind energy. They could be transported easily and used to output energy whenever required, unlike the energy that came from the wind. Some developments still took place in wind energy technology in countries such as Denmark and

Germany, and it was a Dane, Poul LaCour, who built the first electricity generating wind turbine in 1891.

Work into developing larger wind turbines continued into the 20th century but interest in large scale wind power generation largely died out after World War II. The re-emergence of wind energy came about due to two reasons: global warming and the 1970s oil crisis. With the increasing awareness of climate damage from fossil fuels and the realization that oil is a finite source of energy, investment into alternative, renewable and environmentally friendly energy sources began. This resulted in a 'wind rush' in both Europe and the United States. Denmark continued to lead the field in Europe due to the successes seen in the early part of the century, while California saw large installations of wind turbines due to the financial incentives available for companies who invested. This saw the emergence of the first modern wind farms with several wind turbines connected together in a grid (Manwell et al., 2002). However, these early modern turbines turned out to be quite unreliable and as the oil crisis eased the next several decades saw fossil fuels continuing to dominate energy production.

As the end of the 20th century beckoned, concerns relating to climate change started to gather momentum and the use of fossil fuels again became a major issue, with environmental groups around the world campaigning against them. In 1992 the United Nations drafted the first major environmental treaty; The Kyoto Protocol, which was adopted in 1997 in Kyoto, Japan. The goal of this agreement was:

> "stabilization of greenhouse gas concentrations in the atmosphere at a level that would prevent dangerous anthropogenic interference with the climate system" (UNFCCC, 1992).

With subsequent world summits now frequently debating the issues of climate change, development has continued into renewable energy resources. Over the last 15-20 years, huge leaps forward have been made in wind energy technology, addressing issues such as cost and reliability. Furthermore with the move towards offshore wind energy gathering momentum the potential for wind energy is almost limitless. This has resulted in wind energy leading the way forward as an affordable, reliable and environmentally friendly alternative to traditional fossil fuels.

1.2 Wind Turbine Basics

A wind turbine is a machine that converts kinetic energy in the wind into electricity. The most common type of wind turbine is a Horizontal Axis Wind turbine (HAWT). This is a turbine whose blades rotate in a vertical plane, i.e. about a horizontal axis. The blade cross-section is essentially an aerofoil that tapers towards the blade tip. The lift force that is produced when wind flows over their surface generates the rotor torque which is converted into electricity.

Modern wind turbines are generally classified according to several properties: the orientation of the rotor (upwind or downwind), the rotor control system (pitch or stall), the hub design (rigid or teetering), the alignment with the wind (free yaw or active yaw) and the number of blades (two or three). Figure 1.2 below shows a photo of a modern wind turbine. It has an upwind rotor and contains three blades which is the most popular configuration. The main components are labelled in the figure.

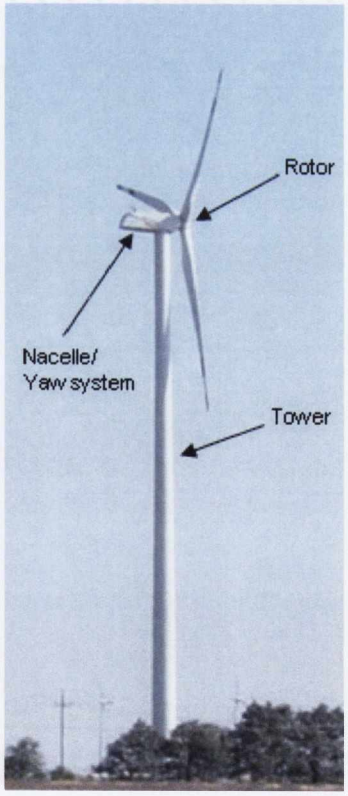

Figure 1.2: Modern three bladed HAWT

1.2.1 Rotor

The rotor of the turbine consists of the blades and supporting hub. These are the most important components of the turbine from a cost and efficiency viewpoint. As in figure 1.2 above, most modern turbines consist of a rotor with three blades in an upwind position. Downwind rotors have the added requirement of taking account of an effect known as tower shadow. This is a wake that forms downwind of the turbine tower which periodically affects the airflow around the blades as they pass by the tower. An upwind rotor configuration avoids this effect. The power output by a wind turbine is controlled by two main methods; stall controlled or pitch controlled blades. Stall controlled blades have a fixed angle of attack. As the wind speed increases above a certain value stall occurs controlling the power generated by the turbine. Pitch control involves changing the pitch angle of the blades in real time. This also serves to control the torque generated. Variable pitch provides more control than a stall mechanism and is therefore more popular, especially in the larger multi-megawatt turbines. However, it does create the requirement for a more expensive hub because of the need for pitch bearings. Some modern wind turbines have partial pitch control systems which allow just the pitch angle of the outer part of the blade to be changed. Yaw control is a third and less popular method for controlling the output of a turbine. This simply involves turning the rotor away from the wind when a reduction in power output is required. This also results in the need for the hub to be designed to take account of gyroscopic loads which occur due to the yawing motion.

As mentioned previously there are two main types of hubs; rigid and teetering. Rigid hubs prevent movement of the blades both in and out of the plane of rotation, known as the edgewise and flapwise directions. A teetering hub is one mounted on bearings which allows the hub to teeter back and forth in both the edgewise and flapwise directions.

1.2.2 Nacelle/Yaw System

The nacelle is the box-like structure at the top of the turbine tower that houses the mechanical and electrical components such as the gearbox and generator. The majority of wind turbines

use induction generators due to their durability, cost effectiveness and the ease at which they can be connected to the electrical grid.

The purpose of a yaw system is to keep the rotor aligned correctly with the wind. Upwind turbines generally have an active yaw drive which uses a wind sensor mounted on the nacelle to ascertain the wind direction. One or more yaw motors are then used to accurately orientate the rotor. Self-aligning or free yaw systems are usually used on downwind turbines.

1.2.3 Tower

The supporting tower of the turbine simply raises the rotor into the air. Wind speeds generally increase with elevation above the ground and are less turbulent in nature; therefore the higher the tower, the better. A trade-off between increased cost versus increased energy capture is generally made, with most tower heights between 1 to 1.5 times the diameter of the rotor. Different types of tower exist with the most popular being tubular steel towers as seen in figure 1.2. Lattice and pre-cast towers are also used, while for small turbines guyed towers are sometimes constructed. The stiffness of the turbine tower is very important due to the coupled vibrations that can occur between the blades and tower. This shall be discussed in more detail later in this thesis.

1.3 Wind Energy Resource

Wind is the flow of air that occurs as a result of pressure differences across the surface of the earth. These pressure differences are caused by uneven heating of the earth by the sun's radiation.

1.3.1 Power in the Wind

Air flows from areas of high pressure to low pressure with the power in the wind expressed as

$$P = \frac{1}{2}\rho A U^3 \tag{1.1}$$

where ρ = air density, A = area considered and U = wind speed. From this equation it can be seen that the power generated by a wind turbine is proportional to the area swept by the rotor and the cube of the wind speed. Thus, if the wind speed doubles the power increases by a factor of eight. This highlights the importance of wind farm location as even a small increase in wind speed can significantly affect power production. Random wind speed fluctuations known as turbulence also occur. Turbulent flows cause rapidly varying aerodynamics loads, particularly on the turbine blades which can reduce the overall efficiency of the turbine. Higher wind speed and a less turbulent flow are two of the main reasons for the current drive towards offshore wind energy. The actual power produced by a wind turbine is also dependent on the fluid mechanics of the flow and the aerodynamics and efficiency of the rotor/generator. In practice, the best modern wind turbines extract a maximum of 45% of the wind energy available (Manwell et al., 2002).

1.3.2 Logarithmic Law

As mentioned previously, wind speed tends to increase with elevation. The variation of wind speed with height, known as the wind profile, can be described by a logarithmic law, details of which can be found in wind engineering textbooks such as Simiu and Scanlon (1996, p-39). This states

$$U(z) = \frac{1}{k} u^* \ln\left(\frac{z}{z_0}\right) \tag{1.2}$$

where z is the height above the surface, z_0 is the roughness length (dependent on terrain type), k is Von-Karman's constant (≈ 0.4), u^* is the friction velocity and $U(z)$ is the mean wind speed at height z. The logarithmic law can be used to estimate wind speed from a reference height, z_r, to another height using the following relationship

$$\frac{U(z)}{U(z_r)} = \frac{\ln\left(\frac{z}{z_0}\right)}{\ln\left(\frac{z_r}{z_0}\right)} \tag{1.3}$$

The instantaneous wind speed, u, is expressed as

$$u = U(z) + \tilde{u} \tag{1.4}$$

where $\tilde{u}$ is the fluctuating or turbulent component of the wind flow. Turbulence in the wind can be simulated by use of spectra such as that developed by Kaimal et al. (1972). More details of this will be given later in this thesis.

1.3.3 Global Availability

The global wind resource has been recently quantified in a study by Archer and Jacobson (2005). Their study used five years of wind data (1998-2002) from the US National Climatic Data Centre and the Forecast Systems Laboratory. They collected measurements from 7,500 surface and 500 balloon-launch monitoring stations to determine global wind speeds at 80 metres above ground level. After finding about 13% of these sites had an average wind speed sufficient for economical wind power generation (above 6.9 m/s) they assumed only 20% of this resource to be harvested. However, the power available still amounted to seven times the world's electricity demand in the year 2000. Their study also excluded the potential of offshore wind resources.

1.3.4 Europe and Ireland's Role

With wind energy technology now at the stage where it can efficiently exploit this huge energy resource from an economic point of view, rapid growth has been seen in the wind energy sector across different regions of the globe. In 2008 alone, an increase of 28.8% was seen in installed global wind energy (GWEC, 2008).

Here in Europe, investment into wind energy is increasing year on year. Europe is indeed leading the way forward with 60% of the world's wind energy capacity installed here at the end of 2007 (EWEA, 2009a). Ireland itself is heavily involved in the push towards wind energy due to the enormous and relatively untapped resources available in this country, particularly on our Atlantic coastline. Several wind farms have been constructed over the last

number of years with many more under construction. At the end of 2008, Ireland had a total of 1,002 Megawatts (MW) of installed wind energy, a growth of over 25% on the previous year. Furthermore, 2008 was the first year in Europe that Wind Energy lead the way ahead of any other energy resource in terms of new annual installed capacity (EWEA, 2009b). As the technology continues to expand more and more research is being carried out into all areas of wind energy technology, from the aerodynamics of the blades to the design of the gearbox and generator used to output the electricity to the grid. This thesis considers the structural dynamic behaviour of wind turbines and the motivation for this work is outlined in the next section.

1.4 Motivation/Aim of this Thesis

With the huge growth in the wind energy sector, particularly over the last decade, single turbines with outputs as large as 5MW are now being constructed. These structures consist of tower heights of up to 80m with rotor diameters of 120m. With this increased size comes increased flexibility leading to potential structural vibration problems, particularly in the turbine blades. This can lead to a reduction in the lifespan of the blades and hence economic viability of the turbine. The aim of this thesis is to investigate the structural dynamic behaviour of wind turbines. A theoretical model has been developed to capture the dynamic behaviour of the blades when excited by wind loading and their interaction with the supporting tower. Dampers modelled as mass-spring-dashpot systems representative of a Tuned Mass Damper (TMD) or equivalent Tuned Liquid Damper (TLD) have been attached to the blades and nacelle, and their vibration mitigation effects studied. A semi-active algorithm has been proposed which enables the dampers to tune in real-time to the dominant frequencies in the system thus achieving a more effective reduction in response. Numerical simulations have been carried out to assess the effectiveness of the control algorithm developed. The intelligent nature of the algorithm allows the control system to cater for any changes in the parameters of the turbine such as the rotational speed.

Experimental investigation into TLDs has also been carried out with the development of a semi-active TLD by real-time adjustment of the volume and hence height of the liquid in the damper. A similar semi-active algorithm to the one developed in the numerical studies was

applied to the TLD to allow real-time identification of the resonant frequencies of the structure being damped. An automated valve then allowed the level of liquid to be adjusted to cater for any loss in stiffness that might occur over the lifetime of the blades or structure being damped.

1.5 Layout of the Thesis

This thesis has been split up into seven chapters outlined below:

Chapter 2 provides a detailed review of literature relevant to the topics dealt with throughout the thesis. It highlights current state of the art research into the area of wind turbine dynamics and gives a comprehensive summary of vibration control techniques.

Chapter 3 introduces the dynamic model and outlines its formulation. Numerical simulations are performed on the model for two different load cases. The first considers a uniform wind load which varies with height, while the second contains an added turbulent component to the steady wind flow.

Chapter 4 details the addition of TMDs to the dynamic model developed in chapter 3. The coupling between the blades and tower is studied to highlight the transfer of vibrations between the two components. Passive tuning of the TMDs is carried out for a steady wind load to determine their effectiveness in reducing vibrations in both the tower and blades of the turbine.

Chapter 5 describes the development of the semi-active algorithm used to tune the dampers in real-time to the frequencies present in the dynamic model of the turbine. The performance of the control system is studied for variations in the dynamic parameters of the system such as the operational speed of the turbine, and the stiffness of the tower and blades.

Chapter 6 focuses on the experimental development and validation of the semi-active damper proposed for use in mitigating vibrations in wind turbines. A semi-active TLD is developed using an algorithm similar to that used for the numerical studies on the turbine model in

chapter 5. This TLD is tested on a simple single degree of freedom structure with a fundamental frequency comparable to that of a large wind turbine blade. Modelling of a TLD as an equivalent TMD is also discussed.

Chapter 7 summarises the work carried out in this thesis and looks at the conclusions that can be drawn from this study. Recommendations are also made for areas requiring further research.

CHAPTER 2 - Literature Review

2.1 Introduction

This chapter aims to give an overview of current published literature and basic theory relevant to the topics dealt with in this thesis. A brief summary of general research into wind turbine design is first presented to provide an insight into the background to the area. The focus then shifts towards the area most relevant to this work, namely wind turbine blade dynamics including coupling with the tower. Vibration control techniques are then outlined to give the reader a detailed understanding of the different control methods available for mitigating vibrations in flexible structures.

2.2 Wind Turbines

As mentioned in the previous chapter, the emergence of wind energy has resulted in a huge volume of research being carried out into all aspects of wind engineering. With their increased size and flexibility, research has recently focussed on understanding the dynamic behaviour of these structures. A paper written by Quarton (1998) provides an overview of the evolution of wind turbine design and analysis giving a detailed account of the many issues faced when designing modern wind turbines.

2.2.1 Turbine Tower

With turbine towers now reaching heights of up to 80m more consideration has to be given to their design and dynamic behaviour. Bazeos et al. (2002) studied the dynamic behaviour of a steel wind turbine tower including soil-structure interaction. The tower was modelled using a Multi-Degree of Freedom (MDOF) oscillator with 18 concentrated masses located at characteristic elevations. They calculated the first three resonant frequencies for both a fixed-base analysis and an elastic subgrade analysis. They found that for each of the first three eigenvalues, the eigenfrequencies for the elastic subgrade analysis were significantly less then for the fixed base, highlighting the importance of knowing the soil-structure interaction

conditions for an accurate assessment of the tower's natural frequencies. Lavassas et al. (2003) also studied the dynamic behaviour of a wind turbine tower employing a detailed finite element analysis. They too considered two separate models to determine the effect of soil-structure interaction on the static and dynamic behaviour of the tower. Work has also been carried out into the optimisation of wind turbine towers (Uys et al., 2007), while Sutherland (2000) investigated the fatigue properties of the different materials used in wind turbine construction, from the steel used in the turbine tower to the composites used in blade design. Martinez et al. (2009) developed a Life-Cycle Assessment (LCA) model of a 2MW wind turbine to determine the environmental effects caused by its manufacture, operation and decommission. They considered not only the tower but all main components of the turbine, such as the foundations and rotor system.

2.2.2 Wind Turbine Blades

With the increased size of modern turbines, the blades in particular are becoming more flexible and their dynamic behaviour is an important design consideration. Ahlstrom (2005) carried out a study investigating the effect of increased flexibility in wind turbine blades and found that it could lead to a significant fall in power output. In general wind turbine blades have two main modes of vibration; flapwise and edgewise. Flapwise vibrations occur out of the plane of blade rotation, while edgewise vibrations (also known as lead-lag) are those occurring in the plane of rotation.

2.2.2.1 Rotating Beams

Research into the dynamics of rotating beams has long been of interest due to applications in helicopter theory, turbo machinery etc. Naguleswaran (1994) used the Frobenius method to determine the natural frequency of a rotating Euler-Bernoulli beam under different boundary conditions, while more recently Oxdemier and Kaya (2006) applied the Differential Transform Method (DTM) to perform a similar study. Yoo and Shin (1998) also investigated the dynamic behaviour of rotating cantilever beams considering stretching and bending motions.

Work in this area now has particular applicability in wind turbine dynamics as turbine blades can be easily modelled by rotating cantilevers. Several studies using rotating beams to model wind turbine blades have recently been carried out. Murtagh et al. (2004a) presented a time domain analytical approach for evaluating the displacement response in the flapwise direction of rotating wind turbine blades. As expected the effect of centrifugal stiffening led to a so-called stiffening of the blades as the rotational speed increased. Kallesoe (2007) performed an in-depth study into the dynamics of a rotating turbine blade considering gravity forces, pitch changes and rotor speed variations.

2.2.2.2 Blade Design and Analysis

Structural and aerodynamic design/analysis of wind turbine blades has been well reported in the literature. Bechly and Clausen (1997) looked at optimising the structural design of a wind turbine blade. They carried out a non-linear analysis of an aerodynamically loaded rotating blade using a finite element model. Their analysis showed that while operating at its design rotational speed the natural frequencies of vibration of the blades were higher than for the stationary/non-rotating case. This was a result of centrifugal stiffening of the blades complementing the results presented above by Murtagh et al. (2004a). Snel (2003) provided a detailed overview of current state of the art knowledge in wind turbine blade aerodynamics and discussed the use of Computational Fluid Dynamics (CFD) as a way to model the aerodynamic behaviour of the blades.

Sicot et al. (2008), Schreck and Robinson (2005) and Larsen et al. (2007) all studied the behaviour of wind turbine airfoils under stall. Baumgart (2002), developed a mathematical model for an elastic wind turbine blade and compared the model with experimental results. Good agreement was seen between the two. Research performed by Ronold et al. (1999) derived a probabilistic model for analysis of the safety of a wind turbine blade against fatigue failure in the flapwise bending direction, while Shokrieh and Rafiee (2006) presented a technique to predict the fatigue lifespan of a composite blade. Marin et al. (2009) adopted a more practical approach, physically examining the fatigue damage in wind turbine blades to try to identify the reasons for the onset of the cracks which occurred during the design life.

Full-scale experimental tests have also been carried out. Kong et al. (2005) designed and tested a full scale blade. They also presented a technique to estimate the fatigue lifespan of wind turbine blades. Another study by Jensen et al. (2006) loaded a 34m composite blade to failure under flapwise bending and compared the results to a finite element model. Good agreement was seen between the experimental and numerical results but for high loads some discrepancies occurred. They stated this to be most likely a result of material non-linearity in the blade which was not accounted for in the finite element model.

2.2.2.3 Flapwise and Edgewise Vibrations

As mentioned previously, there are two main modes of vibration in wind turbine blades; flapwise and edgewise. Most work such as that performed by Ronold and Larsen (2000) has focussed on flapwise vibration as in extreme cases this has led to catastrophic failures through the rotating blades striking the turbine tower. However, the issue of edgewise vibrations is now becoming more problematic in large multi-megawatt turbines and hence more prominent in literature. One such study by Thomsen et al. (2000) states the problem of edgewise vibrations to be a result of the total damping in the blades in the edgewise direction becoming negative. Chaviaropoutos (2001) also noted the occurrence of violent edgewise vibrations presenting a numerical model to investigate the aeroelastic stability of a wind turbine blade.

This thesis considers both flapwise and edgewise vibrations of wind turbine blades. The differences between the two and the significance of their coupling with the turbine tower will be discussed in the subsequent chapters.

2.2.3 Blade-Tower Interaction

To accurately capture the full dynamic behaviour of a wind turbine, one of the most important dynamic effects to consider is the coupling that occurs between the tower and rotating blades. Vibrations are transferred through shear forces in the roots of the blades onto the low speed drive shaft and through the nacelle to the tower. A simplified method for analysing the dynamic behaviour of the whole turbine involves lumping the blades and nacelle together as a single mass at the top of the tower. Murtagh et al. (2004b) derived a closed form expression to

get the natural frequencies for such a system. However, this omits rotation of the blades and associated effects such as centrifugal stiffening which can have a considerable effect on the dynamics of the entire structure.

In a subsequent study, Murtagh et al. (2005) developed a model of a three-bladed wind turbine including blade rotation and blade-tower interaction and compared it to their previous model (Murtagh et al., 2004b). They found that inclusion of the dynamic interaction from the rotating blades could lead to significant increases in blade tip displacements and could therefore not be ignored. Stol et al. (2002) also looked at the interaction between the blades and tower but for a two-bladed turbine. Another study by Lee et al. (2002) represented a two-blade HAWT as a multi-flexible body system with both rigid and flexible subsystems. The equations of motion were first derived for the individual subsystems and then combined to get the complete system equations. Due to its periodic nature, Floquet theory was used to get the characteristic components of the system. A comprehensive study carried out by Hansen (2003) considered both flapwise and edgewise vibration in a 3 bladed wind turbine and the resulting interaction with the tower and other components. He first formulated expressions for the kinetic and potential energy in the system and used Lagrange's method to derive the equations of motion. The periodic terms which subsequently arose in the equations of motion were then eliminated by use of a multi-blade co-ordinate transformation. He found the different blade modes to be highly dependent on the dynamic behaviour of the shaft, nacelle and tower.

2.2.4 Offshore Wind Turbines

While this thesis will not deal directly with offshore wind turbines, it is worth highlighting the shift that is occurring towards locating wind turbines at sea. This is due to the higher and more uniform wind speeds that occur offshore which have the potential to provide a greater and more consistent supply of energy. Construction of a wind farm offshore has many additional challenges to an onshore environment, the most critical being the foundations. Expertise from the offshore platform industry is being transferred to the wind energy industry to find practical and economical ways of supporting offshore turbines. These foundations vary from fixed based platforms in shallow water to Tension Leg Platforms (TLPs) and spars that

are used in deeper offshore environments. In an effort to harness the power available offshore larger turbines are being constructed with energy ratings of 10MW and above. These turbines have even larger more flexible blades making their dynamic behaviour an increasingly important consideration.

Efforts to model the dynamic behaviour of offshore turbines with different foundation types has been performed by Zaaijer (2006). Other work by Henderson et al. (2003) investigated the effect of wave loading on an offshore wind turbine. They stated the importance of considering the wave frequency as small waves with a natural frequency close to that of the turbine can have a more severe effect on the response than a large wave that is far away from the natural frequency. Veldkamp and van der Tempel (2005) stated that linear wave water theory may not be sufficient in modelling the hydrodynamic loads experienced by an offshore turbine as non-linearities in waves can have a significant effect. The possibility of a floating wind turbine has also been investigated. Henderson and Patel (2003) developed analytical tools for evaluating such a structure. They proposed a method for analysing the effect of base motion on the performance of the turbine and also considered the effect it would have on the fatigue loads experienced by the structure. Tavner et al. (2006) looked at the reliability of large wind turbines when installed offshore.

2.3 Vibration Control

The control of vibrations has long been an area of interest across many engineering disciplines. Mitigation of oscillations in vehicles while travelling over an uneven road surface has been thoroughly investigated by mechanical engineers. Meanwhile, in civil engineering where structures have been over-designed for decades, modern design codes now allow for a more daring approach resulting in taller buildings, more slender bridges etc. Skyscrapers over five hundred metres in height and suspension bridges with main spans over a kilometre long are now relatively common around the world. Understanding the structural dynamics of these systems is therefore of critical importance for their design and construction to ensure their structural integrity remains intact throughout their design life. Figure 2.1 below shows the Burj-Dubai skyscraper in the United Arab Emirates; currently the world's tallest building at 818m.

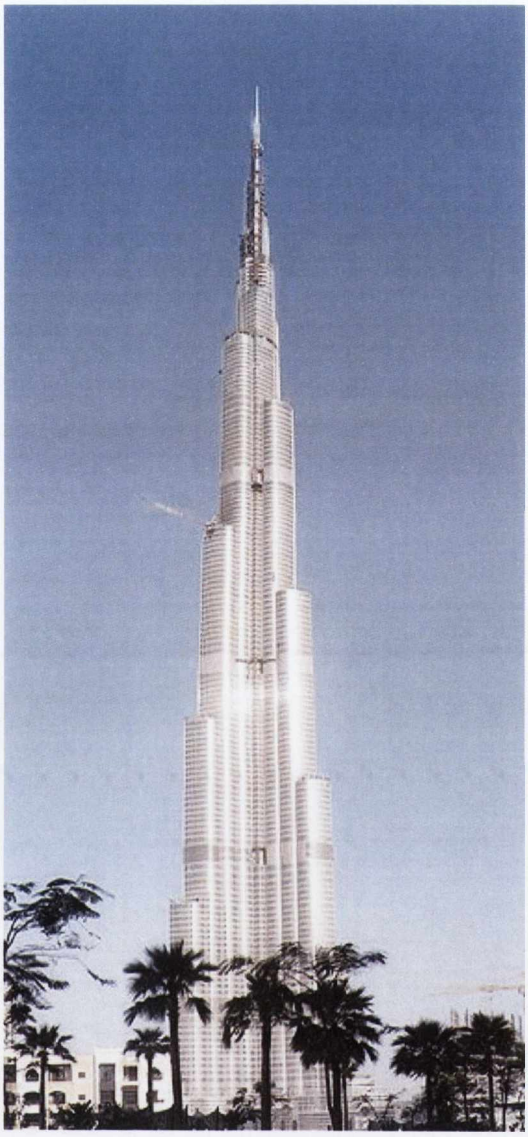

Figure 2.1: Burj-Dubai skyscraper

2.3.1 Tuned Mass Damper

The simplest vibration control device is the Tuned Mass Damper (TMD). This is essentially a small mass connected to the primary structure by springs and dashpots. Figure 2.2 below shows a single degree of freedom (SDOF) structure with a TMD attached.

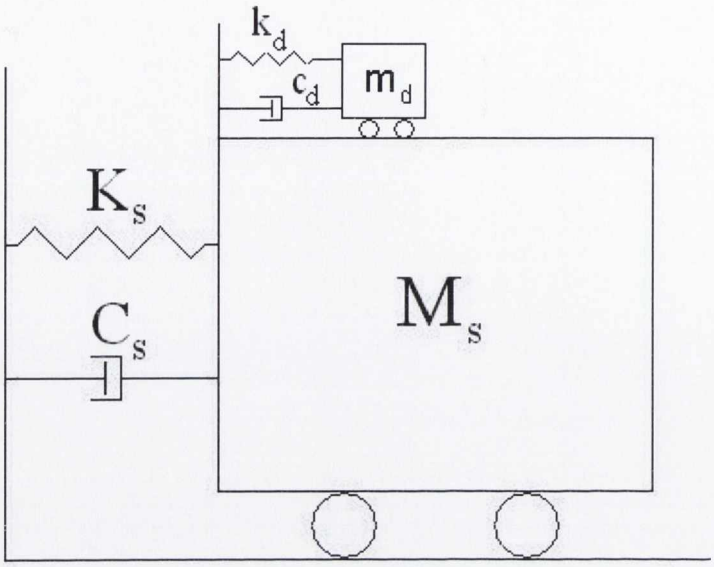

Figure 2.2: Simple structure TMD system

The primary structure is represented by the large mass, M_s, with K_s and C_s represented its stiffness and structural damping respectively. Similarly, the TMD is modelled by its own mass-spring-dashpot system with m_d, k_d and c_d denoting the mass, stiffness and damping values. By tuning the natural frequency of the TMD to the fundamental frequency of the primary system, vibrations in the structure can be considerably reduced through the out of phase motion of the TMD to that of the structure. The natural frequency of the structure, ω_s is found from equation 2.1 below

$$\omega_s = \sqrt{\frac{K_s}{M_s}} \tag{2.1}$$

Similarly, the natural frequency of the TMD can be found as the square root of its stiffness divided by its mass. Tuning the TMD to the natural frequency of the primary structure can therefore be achieved by choosing an appropriate damper mass and stiffness. Kareem (1983) showed that an equivalent SDOF system such as that shown in figure 2.2 can be effectively used to represent a MDOF system in designing a TMD for tall buildings, provided the natural

frequencies are well separated. Designing a simple TMD for successful vibration control requires knowledge of their basic properties as outlined below.

The two most important parameters of a TMD system are the mass ratio and tuning ratio. The mass ratio is simply the ratio of the mass of the TMD to that of the primary system. For figure 2.2 above the mass ratio, μ, is given by

$$\mu = \frac{m_d}{m_s} \tag{2.2}$$

Mass ratios between 1-4% are generally used as high mass ratios can result in an increase in the response of the structure when excited off resonance as the TMD contributes adversely to the overall inertial force. Similarly, the tuning ratio is the ratio of the natural frequency of the TMD to that of the structure being damped and is represented by

$$r = \frac{\omega_d}{\omega_s} \tag{2.3}$$

A tuning ratio of 1 is generally used but the optimum tuning ratio can depend on the properties of the primary system and excitation type. Typically a value of just less than 1 achieves an optimum tuning. Den Hartog (1985) derived the optimum tuning ratio for a TMD attached to a harmonically excited main system as

$$r_{opt} = \frac{1}{1+\mu} \tag{2.4}$$

However, as already stated this depends on the properties of the primary system and does not hold for a more complex system such as a continuous beam.

TMDs have been used widely throughout civil engineering applications, particularly in tall buildings subjected to wind and earthquake loading. The Citigroup Centre in New York and the John Hancock building in Boston were two of the first buildings to use a TMD to reduce

sway, details of which can be found in Kwok and Samali (1995). The Spire of Dublin is another more recent example of a structure with a TMD installed to mitigate its response during storm events.

As the success of early dampers was observed in practice, research into TMDs and other vibration mitigation devices grew considerably. Van de Vegte and de Silva (1976) performed an early study into passive vibration absorbers investigating their suitability for simply supported thin uniform beams. More recently, Hijmissen and Van Horssen (2007) investigated the wind induced vibrations of a tall building, modelled as a vertical Euler-Bernoulli beam. They found that the addition of a TMD at the top of the beam successfully reduced the response.

2.3.1.1 Multiple TMD system

Research has also been carried out considering the use of several TMDs for controlling the dynamic behaviour of structures, known as a Multiple Tuned Mass Damper (MTMD) system. Kareem and Kline (1995) examined the use of MTMDs comparing their effectiveness to that of a single TMD with the same overall mass ratio. The tuning of the TMDs was distributed evenly around the structure's dominant mode of vibration. Results showed the MTMD system achieved a more smoothed out transfer function than that of the single TMD, which resulted in two peaks either side of the original structures undamped natural frequency. They also stated the practicality of MTMDs, as a single large TMD may not be easily accounted for in terms of space requirements. Furthermore, failure of one damper in the MTMD system would not significantly compromise the effectiveness of the overall control system. Joshi and Jangid (1997) also found a MTMD system to be more effective than that of an equivalent single TMD. They looked at optimisation of the system with the aim of minimising the Root Mean Square (RMS) displacement response of the primary structure.

Rana and Soong (1998) also studied the use of MTMDs, considering the possibility of controlling multiple modes of a MDOF system by tuning each TMD to a separate resonant frequency of the primary structure. They studied the performance of TMDs under earthquake excitation using time histories from the El Centro and Mexican earthquakes in their analysis.

For a single TMD they showed that optimum damper parameters (frequency ratio and damping ratio of the TMD) found for the steady state harmonic analysis also held reasonably well for earthquake excitation. However, for multi-mode control they found a so-called 'modal contamination problem' whereby dampers tuned to the 2nd and 3rd modes of the structure resulted in a slight deterioration in the first mode response. Wu and Chen (2000) looked at optimisation of a MTMD system for multi-mode control of a structure experiencing seismic excitation. They considered the optimum placement of the TMDs with the aim of reducing the maximum acceleration response. Their results showed the MTMD system to be more effective than a single TMD. More recently, Li and Ni (2007) also considered optimisation of a MTMD system. Their study took errors in parameter estimation such as the natural frequency of the structure into account.

2.3.2 Tuned Liquid Damper

With the practicality of the TMD seen in practice, development into other vibration mitigation devices has rapidly gathered momentum. An early alternative to the TMD was the Tuned Liquid Damper or TLD.

A TLD consists of a tank partially filled with liquid (usually water), which is rigidly connected to the primary structure. The natural frequency of the TLD is determined by the length of the tank and the depth of the liquid. The TLD damps vibrations in the main structure through the sloshing forces generated from motion of the liquid inside the tank when the structure is experiencing an excitation. The damping provided by the TLD also depends on the liquid used but since this is usually water this parameter can be assumed constant. The simplest type of TLD is rectangular in shape. Lamb (1932) was the first to derive the natural frequency for shallow water motion in a rectangular container assuming linear wave water theory, expressed here in equation 2.5

$$f_w = \frac{1}{2\pi}\sqrt{\frac{\pi g}{L}\tanh\left(\frac{\pi h_0}{L}\right)} \tag{2.5}$$

where g is acceleration due to gravity, L is the length of the tank, h_0 is the water depth and π is the universal constant. The simple nature of TLDs make them particularly attractive for use in vibration suppression. They are easily installed and are low cost, have very little maintenance requirements and their damping effects kick in automatically even for very slight structural motion (i.e. what's known as a near zero trigger level).

Significant research into the dynamic behaviour of liquid motion in TLDs has been carried out. Li et al. (2002) studied the motion of fluid inside a rectangular TLD. By subjecting the TLD to a horizontal oscillation and analyzing the liquid behaviour using the continuity and momentum equations for fluids, they presented a formula for determining the control force produced by the TLD. Reed et al. (1998) investigated the behaviour of TLDs under large amplitude excitation through both experimental testing and numerical modelling. They identified the force due to liquid sloshing by subtracting the inertial force of the tank from the total force measured by a load cell. For large amplitude excitation they found the maximum wave height to peak at excitation frequencies much higher than the tank natural frequencies predicted by linear wave water theory. Just above this max wave height frequency a sudden drop in amplitude occurred, which they referred to as 'the jump phenomenon'. Further investigation into the effect of excitation amplitude on the TLD behaviour showed that as the amplitude of excitation increased, energy dissipation over a wider frequency range occurred. This property makes the TLD particularly suitable for large amplitude excitations. Good agreement was seen between their experimental and numerical results, however the numerical results failed to capture the so-called 'jump phenomenon'. Another formulation by Yu et al. (1999) modelled a TLD as an equivalent TMD with non-linear stiffness and damping. They found their equivalent TMD model to accurately predict the behaviour of the TLD for harmonic, white noise and seismic loading, giving their method merit for use as a design tool for TLDs.

Investigation into the use of TLDs for suppressing the dynamic response of structures has been widely researched. Fujino et al. (1992) studied the liquid motion inside a TLD when subjected to harmonic base excitation and stated the performance of an optimal TLD to be comparable to that of a TMD with the same mass ratio. Banerji et al. (2000) performed numerical simulations on a SDOF structure with a TLD attached which was subjected to real

and artificially generated earthquake ground motions. They considered a tuning ratio equal to one and investigated the TLD performance for three different mass ratios (1, 2 and 4%). They stated that the higher the damping inherently present in the structure, the higher the mass ratio required to achieve the same response reduction as for a more lightly damped system. They also found the higher the excitation the more effective the TLD becomes, which is in accordance with Reed et al's study (1998) into high amplitude excitation, mentioned above. Li et al. (2004) also studied the use of TLDs in reducing the seismic response of structures. They focused on the use of multiple TLDs for controlling more than one mode of the primary structure.

2.3.2.1 Sloped Bottom TLDs

Efforts to improve the damping properties of TLDs have been investigated by several researchers. Olsen and Reed (2001) carried out a study into the behaviour of sloped bottom TLDs. These are TLDs which have an incline built into the tank on both ends in the direction of liquid motion. The authors noted that this should give the tank the same dissipative properties as that of a beach. They developed a non-linear stiffness and damping model of the sloped bottom TLD and compared it to the equivalent standard TLD model developed by Yu et al. (1999). Their study showed that the sloped bottom TLD made more efficient use of the system mass during forced excitation than the comparable standard rectangular box TLD. Gardarsson et al. (2001) also studied sloped bottom TLDs carrying out an experimental investigation into their behaviour. Their experiments showed that the sloped bottom TLD had more liquid taking part in the control process than that of a standard rectangular TLD which had a certain amount of passive/inactive liquid. As a result, a sloped bottom TLD with a smaller mass ratio than that of a standard TLD could achieve the same response reduction. These results complemented those seen in the numerical study by Olsen and Reed (2001).

2.3.2.2 TLDs with Slat Screens

Other efforts to increase the effectiveness of TLDs looked at the use of slat screens. These are vertical screens placed inside the TLD to increase the damping provided by increasing the liquid sloshing forces. Tait et al. (2005b) developed a non-linear flow model to predict the

behaviour of TLDs with slat screens. Their model showed good agreement with experimental results and was capable of predicting the TLD behaviour for different numbers and locations of slat screens. Another study by the same authors considered a TLD equipped with slat screens in the two main directions under 2D excitation (Tait et al., 2005a). Their experimental results showed that the fundamental sloshing modes of a TLD in the two perpendicular (or principal) directions are uncoupled. They also demonstrated that a 1D non-linear model was capable of predicting the response of a 2D TLD by simply modeling the response along each principal axis separately. This is very practical from a design viewpoint as it allows the 2D TLD to be designed as two perpendicular 1D TLDs by simply choosing the appropriate tank dimensions.

2.3.2.3 Tuned Liquid Column Dampers

Perhaps the most successful adaptation of the TLD is the Tuned Liquid Column Damper or TLCD. This is a U-shaped tube which suppresses structural vibrations by motion of the liquid mass through an orifice installed in the U-shaped container. The opening ratio of the orifice can be used to control the damping ratio of the TLCD. Generally a smaller opening ratio results in a higher damping ratio. The use of TLCDs for controlling the dynamic responses of structures is a well researched area. Balendra et al. (1995) experimentally studied the characteristics of a TLCD and showed their effectiveness in controlling the dynamic response of towers with different fundamental frequencies. Shum and Xu (2004) looked at the use of multiple TLCDs in reducing the coupled lateral and torsional response of a long span bridge. Chang (1999) compared several different vibration absorbers, two of which were a TMD and a TLCD. While he found the TMD to be slightly more effective than the equivalent TLCD he acknowledged that liquid dampers may be more suitable in practice, as despite the slight compromise in performance they offer several advantages in terms of installation and maintenance. Colwell and Basu (2009) recently investigated the use of TLCDs for structural control of offshore wind turbines, one of the few published works on the use of vibration absorbers for dynamic control of these structures.

2.3.3 Smart Control Techniques

There are three main categories of vibration absorber: passive, active and semi-active. The vibration control techniques thus far discussed in this chapter have focused on passive devices. A passive damper is one with a fixed tuning, i.e. once the damper has been designed the tuning cannot be altered to account for changes in the behaviour of the primary system. Passive devices require no external energy and due to their low cost and simplicity they are a popular type of vibration absorber. Active devices make use of an external power source to directly apply a control force to the structure being damped. A real-time feedback algorithm is generally used to determine the control force needed to counteract the structures motion, hence reducing its dynamic response. Their adaptability is a big advantage over passive dampers as they are effective over a large frequency bandwidth as opposed to being tuned to a single frequency. However, due to the need for a large power source they are significantly more expensive to install and operate, often making their cost infeasible. Semi-active devices are a compromise between passive and active systems; the properties (i.e. stiffness/natural frequency) of the semi-active device itself can be adjusted in real-time with only a small amount of power required. This allows their tuning to be adjusted to cater for any change in the dynamic properties of the main structure. They are effective over a relatively large frequency bandwidth but require a lot less energy than their active counterparts.

As discussed in the previous sections, passive devices such as TMDs and TLDs have been widely used throughout many engineering disciplines. However, due to the non-linearity of nearly all engineering dynamical systems, research into semi-active control techniques has become an area of great interest and discussion due to their active capabilities without the need for a large power source.

2.3.3.1 Semi-active Dampers

Semi-active control methods have become the main focus of research into the area of control theory for flexible structures. As mentioned above the non-linearity of many engineering dynamical systems has led to the need for semi-active dampers. Furthermore damage occurring to flexible structures that can cause a loss in stiffness also raises the need for

adaptable control methods. Two of the most popular types of semi-active damper are the Magneto-Rheological Tuned Liquid Column Damper (MR-TLCD) and the Semi-active Tuned Mass Damper (STMD). An MR-TLCD is a TLCD which contains a Magneto-Rheological (MR) fluid instead of water. An MR fluid is one whose stiffness can be varied through the application of a magnetic field. This allows the tuning of the damper to be controlled by varying the strength of the magnetic field applied to the liquid. Investigation into the use of MR dampers for vibration control has been highlighted by many researchers. Wang et al. (2005) studied the use of MR-TLCDs in the control of tall buildings finding them to be more effective than a standard TLCD. Yoshioka et al. (2002) investigated the use of MR-TLCDs in base isolation systems, while Yang et al. (2002) looked at developing a numerical model to capture the behaviour of an MR-TLCD finding good agreement with experimental results. Zang and Roschke (1999) performed an experimental investigation into the dynamic control of a slender four storey building comparing an active control strategy to a semi-active MR damper. They found the MR damper to have a significant advantage over fully active systems as it requires a lot less power to provide the damping forces required.

An STMD is simply a TMD with a variable stiffness property which allows its natural frequency to be controlled. Pinkaew and Fujino (2001) looked at the effectiveness of STMDs under harmonic excitation and found substantial improvement in structural response over that achieved by passive TMDs. Ricciardelli et al. (2000) developed an iterative procedure to determine the ideal tuning and damping of an STMD under white noise excitation, while Nagarajaiah and Varadarajan (2005) investigated the semi-active control of a tall building excited by a wind load. They proposed a Short Time Fourier Transform (STFT) algorithm to control the tuning of the STMD. This algorithm makes use of Fourier analysis techniques to identify the dominant frequency in the response of the main system in real time. This will be discussed in more detail later in the thesis. Their model also took into account uncertainty in the stiffness of the building up to +/- 15%. Another study by Nagarajaiah and Sonmez (2007) looked at the use of single and multiple STMDs using a similar STFT control algorithm to track the excitation frequency. They found use of a single STMD led to the greatest reduction in response. However, they note that in practice multiple STMDs distributed around a small frequency range may be more effective due to small errors that may occur in identifying the excitation frequency.

2.3.4 Vibration Control of Wind Turbines

As highlighted in the previous sections, vibration absorbers have been used across a wide range of structures for controlling their dynamic responses. However, research into the use of dampers in wind turbines is noticeably scarce in published literature.

Murtagh et al. (2008) investigated the use of a passive TMD at the top of the turbine tower for controlling vibrations in the flapwise direction. Their dynamic model included the interaction between the blades and tower. When tuned to the predominant frequency of the coupled system good reduction in response was achieved. However, they noted that because in reality the system parameters are time-varying an active control strategy would probably be more appropriate. Colwell and Basu (2009) studied the use of a TLCD in the turbine tower for mitigating vibrations in the structure. They considered two models, one which assumed the blades to be lumped at the top of the tower; the other modelled the blades as discretised prismatic cantilever beams of rectangular hollow cross-section. This allowed the effect of the rotating blades to the analysed. In their rotating blade model they found the TLCD to achieve a maximum reduction of 60%.

The above studies both considered the use of dampers in the turbine tower. Due to their hollow nature wind turbine blades are automatically suitable for the installation of dynamic vibration absorbers such as those discussed throughout this chapter. However, little research exists in this area. Grabau (1999) developed a passive TLD control system for mitigation of edgewise vibrations in wind turbine blades on behalf of Danish company LM, details of which are given in the referred patent. The simple nature of the TLD makes it a particularly suitable damping device for controlling blade vibrations through liquid sloshing. Furthermore, once installed in the blade no maintenance is required. The damper hence exhibits a long design life and is thus a very cost effective control method. However, no analysis on the effectiveness of the device in mitigating vibrations in the blades was performed. The passive nature of the TLD is also unable to cater for changes in the dynamic behaviour of the turbine blades. Hence there is a need for smarter control devices such as a semi-active TLD which could adapt to changes in the dynamics of a turbine.

Some research has been carried out into counteracting the vibration problems seen in turbine blades by focusing on the actual design of the blades themselves. This has concentrated on increasing the structural damping inherently present in them or altering their aerodynamic characteristics (Chaviaropoutos et al., 2003, Chaviaropoutos et al., 2006).

However, no literature is known to exist which performs a detailed analysis on the effectiveness of vibration control devices in wind turbine blades. This thesis aims to address that knowledge gap through the numerical and experimental investigations carried out.

CHAPTER 3 - Theoretical Model of a Wind Turbine Including Blade-Tower Coupling

3.1 Introduction

This chapter details the theoretical model developed, which is used throughout this thesis in examining the structural dynamic behaviour of a wind turbine. A significant challenge in the modelling of these structures is inclusion of the blade-tower interaction which can have a major impact on the behaviour of the entire system. The model was developed from the ground up, first starting with just a single rotating blade including its dynamic coupling with the nacelle/tower. This was then extended to include all 3 blades, representative of a modern HAWT. Two separate models were derived; one looked at vibration in the flapwise direction, while the second considered edgewise vibration. Significant differences between the two models exist and have been highlighted over the course of the chapter.

3.2 Flapwise Model

As discussed in chapter 2, flapwise vibrations are vibrations occurring perpendicular to the direction of blade rotation. Most research into blade dynamics has thus far focussed on flapwise vibration as large displacements can lead to catastrophic failure of the turbine structure if a blade was to collide with the tower.

3.2.1 Dynamic Model Formulation

A lot of work into blade dynamics has focussed on aerodynamic behaviour such as that performed by Chaviaropoutos et al. (2003) and Snel (2003). Rasmussen (2003) provided an overview of the current state of the art knowledge in wind turbine aerodynamics and structural dynamics. The model formulated in this study considers purely the structural dynamic behaviour of the wind turbine system, allowing the coupling between the blades and tower to be captured accurately.

The dynamic model was derived using the Lagrangian formulation expressed in equation 3.1 below

$$\frac{d}{dt}\left(\frac{\delta T}{\delta \dot{q}_i}\right) - \frac{\delta T}{\delta q_i} + \frac{\delta V}{\delta q_i} = Q_i \tag{3.1}$$

where: T = kinetic energy of the system, V = potential energy of the system, q_i = displacement of degree of freedom i and Q_i = generalized loading corresponding to degree of freedom i. The overdot represents the first derivative with respect to time. The Lagrangian formulation was found to be particularly suited to this problem as it had the advantage of including all the dynamic coupling present in the system once the expressions for the kinetic and potential energies are found and substituted into equation 3.1. A schematic of the flapwise model is shown in figure 3.1 below.

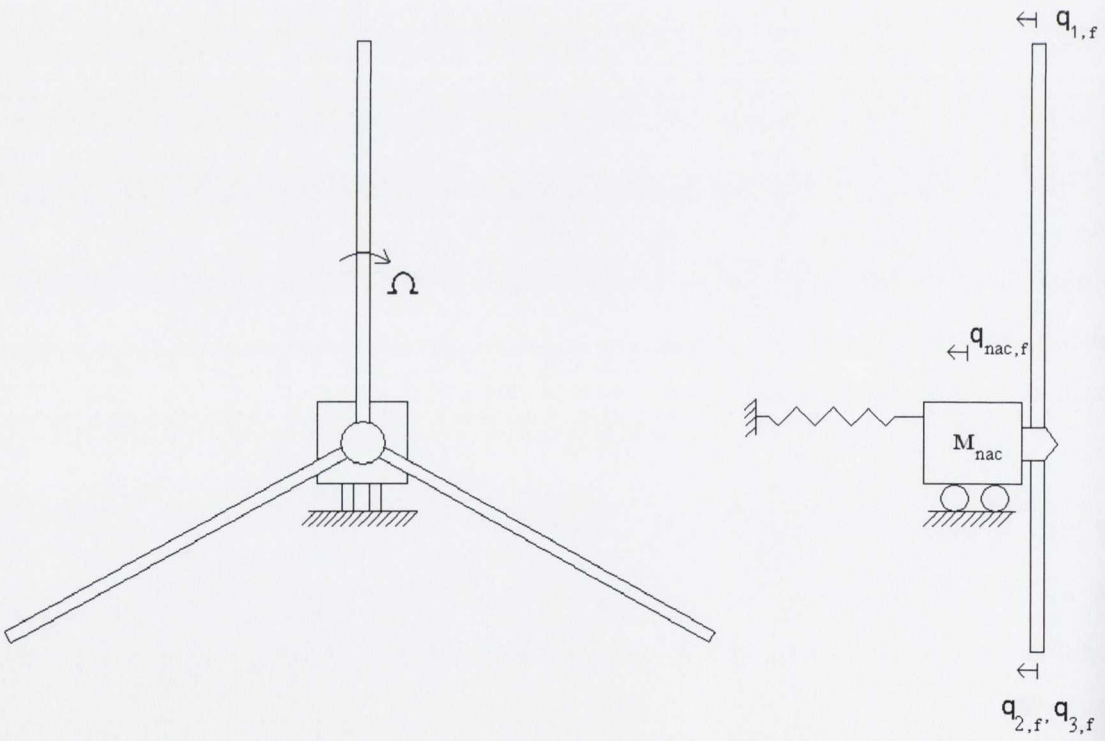

Figure 3.1: Schematic of flapwise model

The interaction between the blades and tower has been included through motion of the nacelle, modelled as the discrete mass M_{nac}, shown above in figure 3.1. Ω denotes the

rotational speed of the blades, while $q_{1,f}$, $q_{2,f}$, $q_{3,f}$ and $q_{nac,f}$ represent the flapwise motion of the blades and nacelle respectively. The blades were modelled as continuous cantilever beams of uniform cross section with their relative displacement expressed as the product of the assumed shape function (which is usually the fundamental modeshape) multiplied by the tip displacement, shown in equation 3.2 below.

$$u_{i,f}(x,t) = \phi(x) q_{i,f}(t) \tag{3.2}$$

where $\phi(x)$ = modeshape and $q_{i,f}(t)$ = relative tip displacement of blade i in the flapwise direction. The blades were assumed to be vibrating in their fundamental mode and a quadratic modeshape was assumed. This allowed reduction of the continuous beam to a single degree of freedom, a technique known as Raleigh's method (Clough and Penzien, 1993). As can be seen in equation 3.2, the relative displacement of the blade, $u_{i,f}(x,t)$, is a function of both the position on the blade, x, and time, t.

The total kinetic energy of blade i in the flapwise direction, $T_{bi,f}$ can therefore be represented by the integral expression

$$T_{bi,f} = \frac{1}{2}\bar{m}\int_0^L v_{bi,f}(x,t)^2\, dx \tag{3.3}$$

where $\bar{m}$ = mass per unit length of the blade, L = length of the blade (= 48m) and $v_{bi,f}$ is the total velocity of blade i including the nacelle motion that causes blade displacement. This ensures that the dynamic interaction between the blade and nacelle/tower is taken into account when applying the Lagrangian formulation in equation 3.1. The kinetic energy from the motion of the nacelle, $T_{nac,f}$ is simply given as

$$T_{nac,f} = \frac{1}{2} M_{nac} \dot{q}_{nac,f}^{\ 2} \tag{3.4}$$

The total kinetic energy in the system in the flapwise direction including the motion of all three blades and nacelle, T_f, is therefore represented by

$$T_f = \frac{1}{2}\overline{m}\sum_{i=1}^{3}\int_0^L v_{bi,f}(x,t)^2 dx + \frac{1}{2}M_{nac}\dot{q}_{nac,f}{}^2 \tag{3.5}$$

Similarly, the total flapwise potential energy can be shown to be

$$V_f = \frac{1}{2}EI_f\sum_{i=1}^{3}\int_0^L\left(\frac{\delta^2 u_{i,f}}{\delta x^2}\right)^2 dx + \frac{1}{2}K_{nac}q_{nac,f}{}^2 \tag{3.6}$$

where E = Young's modulus for the blades, I_f = second moment of area of the blades about the relevant axis and K_{nac} is the stiffness of the nacelle, which is equal to that of the tower. Due to the symmetric nature of the tower this will have the same value in both the flapwise and edgewise directions. This results in the motion of the nacelle accurately representing the motion of the top of the tower and hence capturing the coupling between it and the blades.

3.2.1.1 Centrifugal Stiffening

To accurately model the structural dynamic behaviour of a wind turbine the centrifugal stiffening of the blades must also be included. This results in the stiffness of the blades increasing as the rotational speed increases. The centrifugal force on blade i, F_{ci}, acting at the point x is expressed as

$$F_{ci} = \Omega^2\int_x^L m(\zeta)\zeta d\zeta \tag{3.7}$$

where ζ is the distance from x to the current point considered and $m(\zeta)$ is the mass distribution. The resulting potential energy due to centrifugal stiffening of blade i, V_{ci}, was expressed by Hansen (2003) as

$$V_{ci} = \frac{1}{2}\Omega^2 \int_0^L \left(q_i \frac{d\phi(x)}{dx} \right)^2 \int_x^L m(\zeta)\zeta d\zeta dx \tag{3.8}$$

This was added to the potential energy in equation 3.6 above.

3.2.1.2 Flapwise Equations of Motion

Substituting the expressions for the kinetic and potential energies into the Lagrangian formulation in equation 3.1 allowed the equations of motion for vibration in the flapwise direction to be derived. These can be expressed in the general form of equation 3.9 below

$$\begin{bmatrix} \frac{m_b}{5} & 0 & 0 & \frac{m_b}{3} \\ 0 & \frac{m_b}{5} & 0 & \frac{m_b}{3} \\ 0 & 0 & \frac{m_b}{5} & \frac{m_b}{3} \\ \frac{m_b}{3} & \frac{m_b}{3} & \frac{m_b}{3} & M_{nac} + 3m_b \end{bmatrix} \begin{Bmatrix} \ddot{q}_{1,f} \\ \ddot{q}_{2,f} \\ \ddot{q}_{3,f} \\ \ddot{q}_{nac,f} \end{Bmatrix} + \begin{bmatrix} c_{st,b} & 0 & 0 & 0 \\ 0 & c_{st,b} & 0 & 0 \\ 0 & 0 & c_{st,b} & 0 \\ 0 & 0 & 0 & c_{st,nac} \end{bmatrix} \begin{Bmatrix} \dot{q}_{1,f} \\ \dot{q}_{2,f} \\ \dot{q}_{3,f} \\ \dot{q}_{nac,f} \end{Bmatrix} +$$
$$\begin{bmatrix} \frac{4EI_f}{L^3} + \frac{4\Omega^2 m_b}{15} & 0 & 0 & 0 \\ 0 & \frac{4EI_f}{L^3} + \frac{4\Omega^2 m_b}{15} & 0 & 0 \\ 0 & 0 & \frac{4EI_f}{L^3} + \frac{4\Omega^2 m_b}{15} & 0 \\ 0 & 0 & 0 & K_{nac} \end{bmatrix} \begin{Bmatrix} q_{1,f} \\ q_{2,f} \\ q_{3,f} \\ q_{nac,f} \end{Bmatrix} = \{Q_f\} \tag{3.9}$$

where m_b is the total blade mass. As can be seen in equation 3.9 the system matrices are all constant in nature (i.e. time invariant). The terms in the damping matrix, marked $c_{st,b}$ and $c_{st,nac}$, arise due to the structural damping included in the blades and nacelle respectively. This was assumed to be in the form of stiffness proportional damping. The vector of displacements of each dof in the flapwise direction is denoted as $q_{i,f}$ with the single and double overdot representing the first and second derivatives with respect to time. This results in a system with

four dofs; one for each of the three blades and one for the nacelle. Finally, Q_f is the generalised loading in the flapwise direction.

3.2.2 Model Validation

In assessing the behaviour of the dynamic model described a comparison was made between the cantilever blade model and a rotating Euler-Bernoulli beam. The Frobenius method was initially used to determine the natural frequency of a stationary Euler Bernoulli beam. This natural frequency was then assumed for the stationary blades in the proposed rotating cantilever model. The natural frequencies of the Euler Bernoulli beam were then determined for different rotational speeds (again using the Frobenius technique), and compared to those calculated from an eigenvalue analysis of the cantilever blade model outlined above. This allowed the effect of centrifugal stiffening in the two models to be compared.

3.2.2.1 Euler Bernoulli Rotating Beam

The governing differential equation for a rotating Euler Bernoulli beam with rigid support under flapwise vibration is

$$\rho A \frac{\partial^2 w}{\partial t^2} + \frac{\partial^2}{\partial x^2}\left(EI \frac{\partial^2 w}{\partial x^2} \right) - \frac{\partial}{\partial x}\left(T \frac{\partial w}{\partial x} \right) = f(x,t) \tag{3.10}$$

where ρ is the density of the beam (taken as 1300kg/m^3 for a flexible blade), A is the cross sectional area, w is the relative displacement of a point with respect to its static deflected position, E is the Young's modulus of elasticity of the material of the beam, I is the moment of inertia of the beam about its relevant axis, T is the centrifugal tension force on the beam at a point x with respect to the origin and f is the applied force per unit length on the beam. The cross sectional area, A, and bending rigidity, EI, are assumed to be constant along the length of the beam, x. Both w and f are dependent on the location on the beam with respect to the origin, x, and time, t. The centrifugal tension T is expressed as

$$T(x) = \int_{x}^{L} \rho A \Omega^2 (r + x) dx \tag{3.11}$$

where L is the length of the beam, r is the radius of the rigid hub to which the flexible beam is attached and Ω is the angular velocity of rotation of the beam, which is assumed to be constant. The effect of gravity on the rotation of the beam is assumed negligible compared to the centrifugal effect.

The non-dimensional rotational speed parameter and natural frequency parameters are defined as

$$\nu = \eta^2 = \frac{\rho A \Omega^2 L^4}{EI} \tag{3.12}$$

and

$$\mu = \overline{\Omega}^2 = \frac{\rho A \omega^2 L^4}{EI} \tag{3.13}$$

respectively, where ω is the natural frequency of the beam. After setting $f(x,t) = 0$ in equation 3.10, substituting in the non-dimensional parameters, and separating the time and space dependent ordinary differential equations, the modeshape equation is obtained in a dimensionless form as

$$D^4 W(X) - 0.5\nu(1 + 2\rho_0) D^2 W(X) + \nu\rho_0 D[XDW(X)] + 0.5\upsilon D\left(X^2 DW(X) - \mu W(X)\right) = 0 \tag{3.14}$$

where

$$D = \frac{d}{dX},\ X = \frac{x}{L},\ W(X,t) = \frac{w(x,t)}{L} \text{ and } \rho_0 = \frac{r}{L} \tag{3.15}$$

Employing the Frobenius method of series solution of differential equations as in Naguleswaran (1994) and considering ideal clamped-free boundary conditions for a cantilever, the natural frequency equation is obtained to be

$$D^2F(1,2)D^3F(1,3)-D^3F(1,2)D^2F(1,3)=0 \tag{3.16}$$

where

$$F(X,c)=\sum a_{n+1}(c)X^{c+n} \tag{3.17}$$

By choosing

$$a_1(c)=1,\ a_2(c)=0,\ a_3(c)=\frac{0.5\nu(1+2\rho_0)}{(c+2)(c+1)} \text{ and } a_4(c)=\frac{-\nu\rho_0 c}{(c+3)(c+2)(c+1)} \tag{3.18}$$

the recurrence relation is obtained as

$$\begin{aligned}&(c+n+4)(c+n+3)(c+n+2)(c+n+1)a_{n+5}(c)-0.5\nu(1+2\rho_0)(c+n+2)(c+n+1)a_{n+3}(c)\\&+\nu\rho_0(c+n+1)^2a_{n+2}(c)+[0.5\nu(c+n)(c+n+1)-\mu]a_{n+1}(c)=0\end{aligned} \tag{3.19}$$

The normalised modeshape equation can be derived as

$$\Phi_n(X)=\frac{[D^2F(1,3)F(X,2)-D^2F(1,2)F(X,3)]}{[D^2F(1,3)F(1,2)-D^2F(1,2)F(1,3)]} \tag{3.20}$$

3.2.2.2 Comparison to Eigenvalue Analysis of Cantilever Model

The Frobenius method results for the Bernoulli Euler beam were compared to two different cases from Lagrangian analysis. The first was a single rotating uniform cantilever beam assuming the nacelle motion to be zero. The second was a 3 blade turbine model which

included blade-nacelle/tower interaction. A 14^{th} term expansion was deemed sufficient for the Frobenius results. All natural frequencies calculated are for the first mode of vibration. Three rotational speeds were compared, the results of which are shown in table 3.1. It can be seen that there is a good agreement between the Frobenius results and the Lagrangian single blade model. For the full 3 blade model including nacelle coupling four eigenvalues are present from the 4 dof. The lowest of these frequencies corresponding to the nacelle has been omitted, with the other three eigenvalues listed in table 3.1. One of these is significantly higher than the other two, arising from the interaction between the blades and nacelle. Omission of the nacelle coupling results in 3 identical eigenvalues which are in close agreement with the Lagrangian single blade and Frobenius results.

Ω (Revs/min)	Bernoulli-Euler Frobenius results (Hz)	Lagrangian 1-blade (no coupling) Eigenvalues (Hz)	Lagrangian 3-blades (nacelle coupled) Eigenvalues (Hz)
0	1.5588	1.5588	1.5588, 1.5588, 1.5588
10	1.5703	1.5700	1.5700, 1.5700, 1.9207
60	1.9274	1.9399	1.9394, 1.9394, 2.3649
120	2.8010	2.7863	2.7859, 2.7859, 3.3867

Table 3.1: Comparison of Bernoulli-Euler and Lagrangian dynamic models

3.2.3 Loading

Two loading scenarios were derived for studying the response of the turbine model. The first considered a steady wind speed, while the second added a turbulent component to the steady wind flow.

3.2.3.1 Steady Load

A simple load case was first assumed, namely a constant wind speed that varied linearly with height. Rotation of the blades through this wind field results in a time varying load on each of the blades with a period corresponding to the rotational speed, Ω. Equation 3.21 shows the expression for the load per unit length on blade one.

$$Q_{1f} = \left(\frac{v_{nac}{}^2 A}{3} + \frac{\partial v_{nac+L}{}^2 A}{10} \right) + \left(\frac{v_{nac} \partial v_{nac+L} A}{2} \right) \cos(\Omega t) \tag{3.21}$$

where v_{nac} is the wind speed at the nacelle height, and ∂v_{nac+L} is the increase in wind speed between the nacelle and maximum blade tip height, i.e. when the blade is in the vertical upright position. This was determined from the logarithmic law described in section 1.3.2 of this thesis. Finally, A is the area of the blade on which the load acts. Higher harmonics also arise in this expression but are several orders of magnitude lower than the first harmonic and have therefore been ignored. The loads on blades two and three are similar to that expressed for blade one but with phase shifts of $2\pi/3$ and $4\pi/3$ representing the angles between the blades. The load on the nacelle has been taken as zero to allow the coupling between the blades and nacelle to be analysed. Any motion of the nacelle is therefore due to dynamic interaction from the blades.

3.2.3.2 Turbulent Load

The second loading scenario considered the same load case as the first but with an added random component modelling turbulent wind. This turbulent velocity component was generated at a height equal to that of the nacelle using a Kaimal spectrum (1972) defined by equations 3.22, 3.23 and 3.24 below. Uniform turbulence was assumed for the blades.

$$\frac{f S_{vv}(H,f)}{v_*{}^2} = \frac{200c}{(1+50c)^{\frac{5}{3}}} \tag{3.22}$$

where: H = nacelle height, $S_{vv}(H, f)$ is the PSDF (Power Spectral Density Function) of the fluctuating wind velocity as a function of the hub elevation and frequency, v_* is the friction velocity from equation 3.23, and c is known as the Monin coordinate which is defined in equation 3.24.

$$\bar{v}(H) = \frac{1}{k} v_* \ln \frac{H}{z_0} \tag{3.23}$$

$$c = \frac{fH}{\bar{v}(H)} \tag{3.24}$$

where k is Von-Karman's constant (typically around 0.4 (Simiu and Scanlan, 1996)), z_0 = 0.005 (the roughness length), and $\bar{v}(H)$ is the mean wind speed. This results in a turbulence intensity of 0.115 in the generated spectrum. Figure 3.2 shows a plot of a sample turbulent wind flow generated using the above technique.

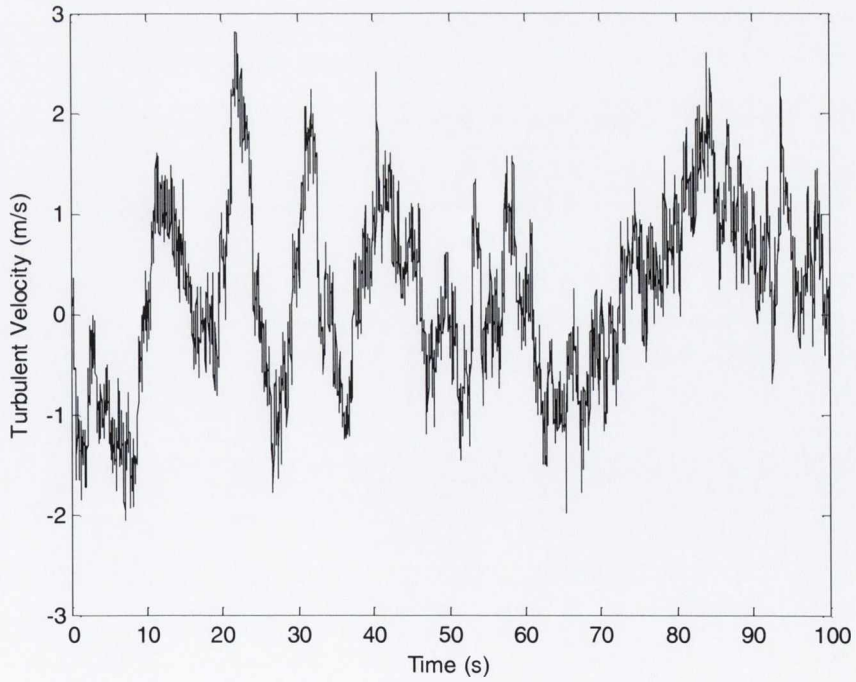

Figure 3.2: Sample turbulent wind flow

3.2.4 Numerical Simulations

Simulations were carried out in Matlab to examine the time history response of the dynamic model. Fourier analysis was also carried out to determine the frequency spectrum of the system.

3.2.4.1 Steady Wind Load

Most modern wind turbines operate at relatively slow rotational speeds. Figure 3.3 shows the simulated time history response of blade one for a rotational speed, Ω = 3.14rad/s (0.5Hz), typical of a large multi-megawatt turbine. The loading on the system is a steady wind load as described in section 3.2.3.1. The response is seen to decay over time due to the structural damping assumed in the model.

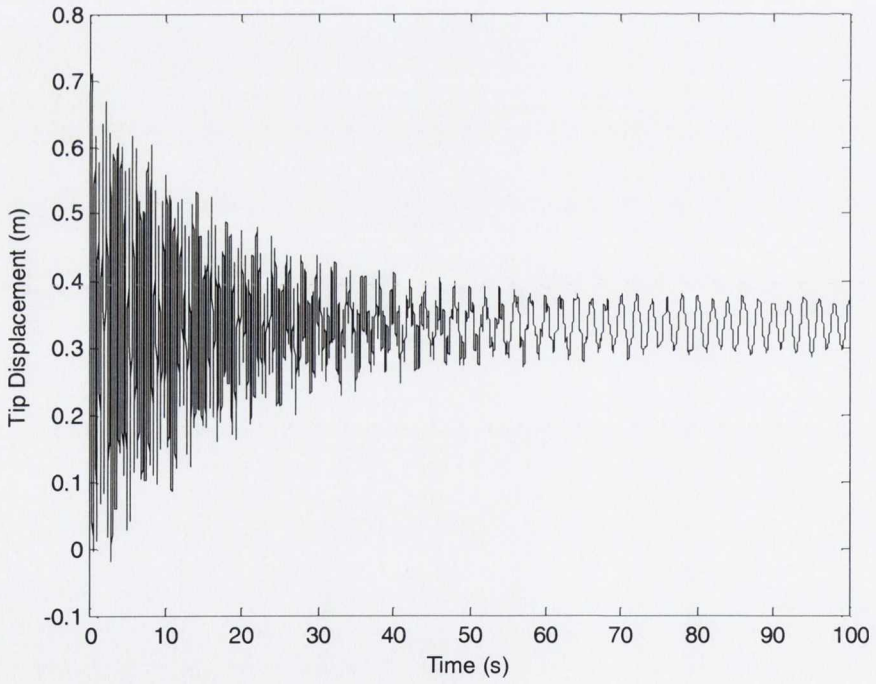

Figure 3.3: Flapwise response of blade 1, steady load, Ω = 3.14rad/s

The non-zero mean in the blade response seen in figures 3.3 above can be attributed to the nature of the loading which itself has a non-zero mean. The response of the blade was then transformed to the frequency domain by means of a Fast Fourier Transform (FFT). This

allowed identification of the frequency peaks in the blade. Figure 3.4 below shows a plot of the frequency spectrum of blade one corresponding to the time history response in figure 3.3.

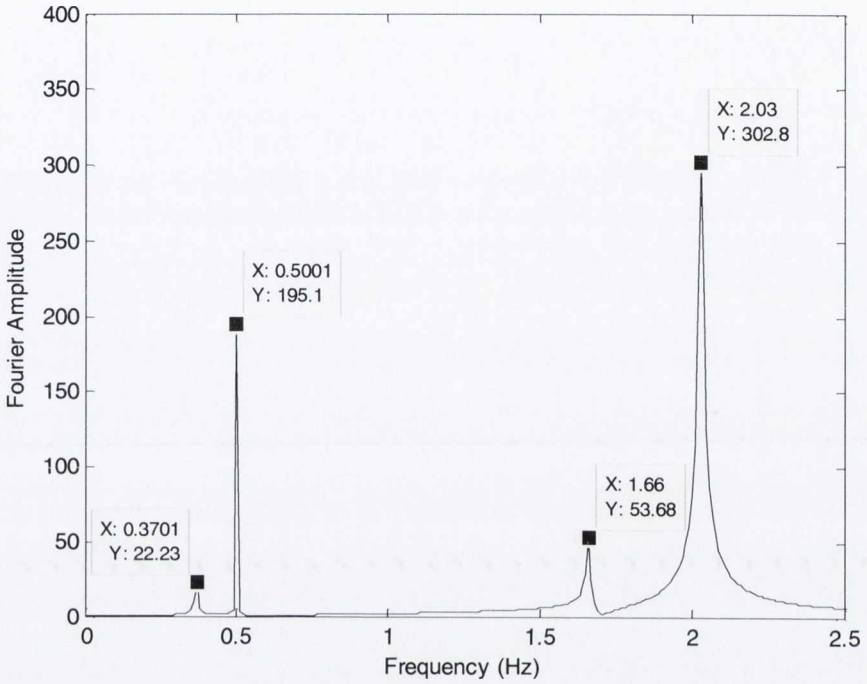

Figure 3.4: Blade 1 flapwise frequency spectrum, steady load, $\Omega = 3.14$rad/s

As can be observed in figure 3.4, three main peaks occur in the response of the blade. The first peak occurs at 0.5Hz (3.14rad/s) which is equal to the rotational speed of the blades and forcing function frequency (equation 3.21). Two more significant peaks exist, one at 1.66Hz and the largest at 2.03Hz, close to the natural frequency of the blades. A small peak is also seen at 0.37Hz.

As expected the displacement responses of blades two and three are similar in nature to that of the first blade with a phase difference due to the angle between the blades. Furthermore the same frequency peaks were observed as for blade one in figure 3.4, emphasising the identical dynamic properties of each of the individual blades.

The displacement response of the nacelle over the first 100s is plotted in figure 3.5. As stated in section 3.2.3.1 a loading of zero has been assumed on the nacelle meaning any motion is

therefore a result of the load transfer from the blades. This gives a good indication as to the amount of movement that can be induced in the turbine tower solely due to the dynamic coupling with the blades.

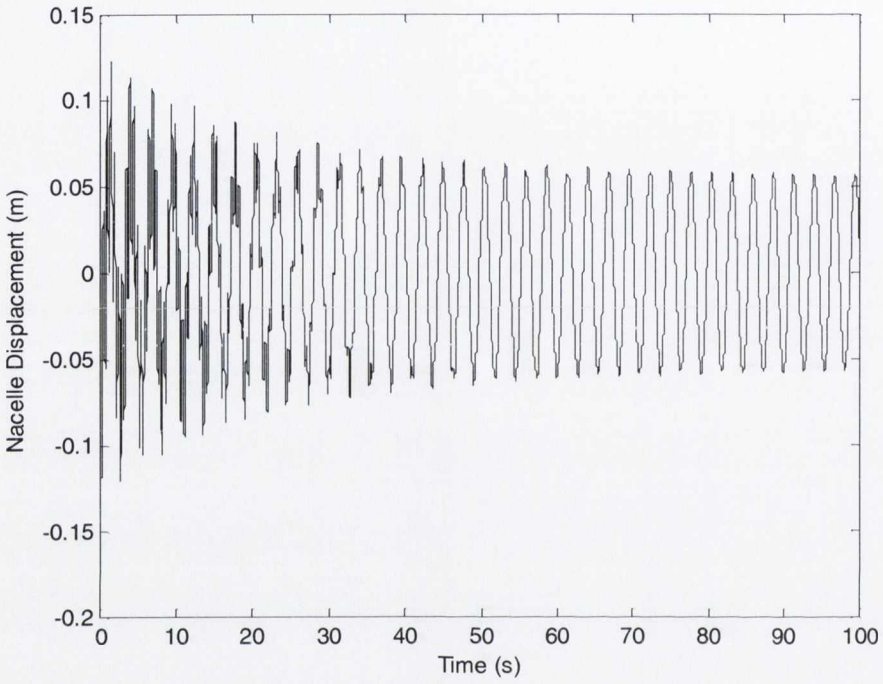

Figure 3.5: Flapwise response of the nacelle, steady load, Ω = 3.14rad/s

Comparing the magnitude of the nacelle displacement to that of the blades at t = 100s shows the peak to peak value of the nacelle to be of a similar magnitude to that of the blades. Due to the flexible nature of turbine blades, tip displacements of the order of several metres are not uncommon during high wind events. Therefore it can be concluded that significant motion can be induced in the tower through the coupling with the blades.

The frequency response of the nacelle was also plotted and is shown in figure 3.6. Two frequency peaks are seen in the response. The first, at 0.37Hz, is reasonably close to the operational speed of the turbine and the nacelle natural frequency of 0.56Hz. This frequency corresponds to the smallest of the four peaks seen in the blade response (figure 3.5). The second occurs at 2.03Hz corresponding to the largest peak seen in the frequency spectrum of

the blades. Further study into these peaks will be performed in the control chapters of this thesis.

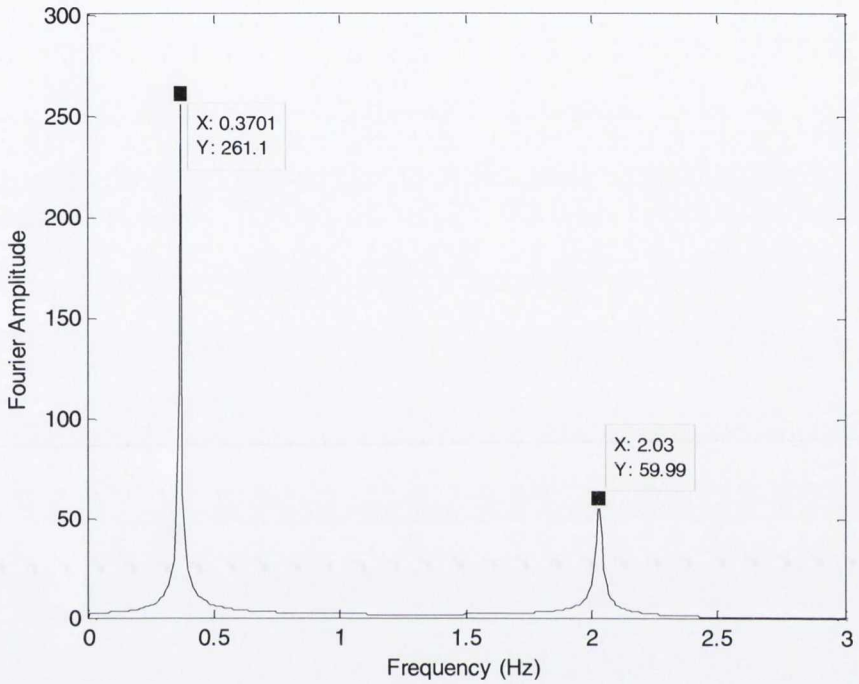

Figure 3.6: Nacelle flapwise frequency spectrum, steady load, Ω = 3.14rads/s

3.2.4.2 Turbulent Wind Load

The response of the system to the turbulent load described in section 3.2.3.2 was also studied. This represents a more realistic load experienced by an operating wind turbine. Figure 3.7 shows the time history response of blade one for 100s of turbulent loading. The corresponding frequency spectrum is plotted in figure 3.8. A rotational speed of 0.5Hz was again assumed for the blades. As expected, the frequency peaks are seen at the same locations as for the steady wind load as the dynamic characteristics of the system have not altered. Similar plots were also seen for the other two blades.

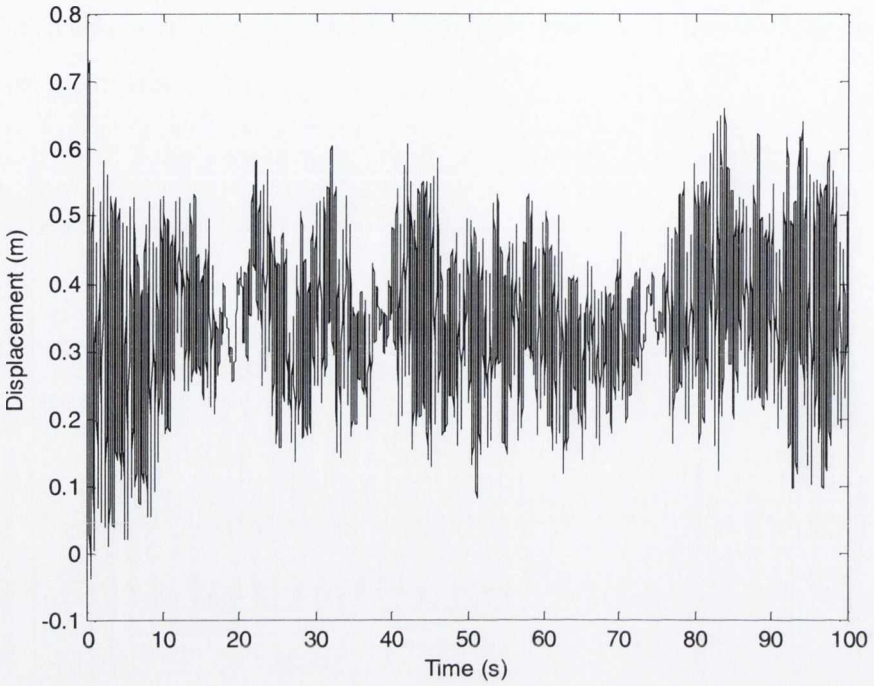

Figure 3.7: Blade 1 flapwise response, turbulent load, Ω = 3.14rad/s

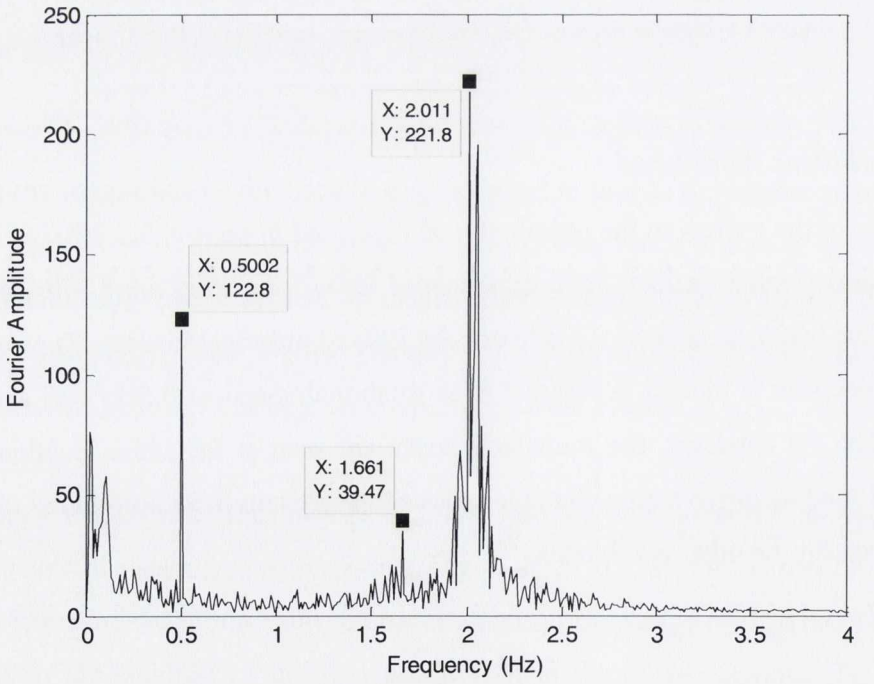

Figure 3.8: Blade 1 flapwise frequency spectrum, turbulent load, Ω = 3.14rad/s

Similarly, the response of the nacelle and its frequency spectrum are illustrated in figures 3.9 and 3.10. Again the resonant frequencies occur at the same points as for the steady wind load plots. A larger blade displacement is seen due to the broad banded nature of the turbulent load. This results in no reduction in the blade response to a steady state as seen in the steady wind load plots previously. The nacelle displacement also has a larger magnitude through the coupling in the model.

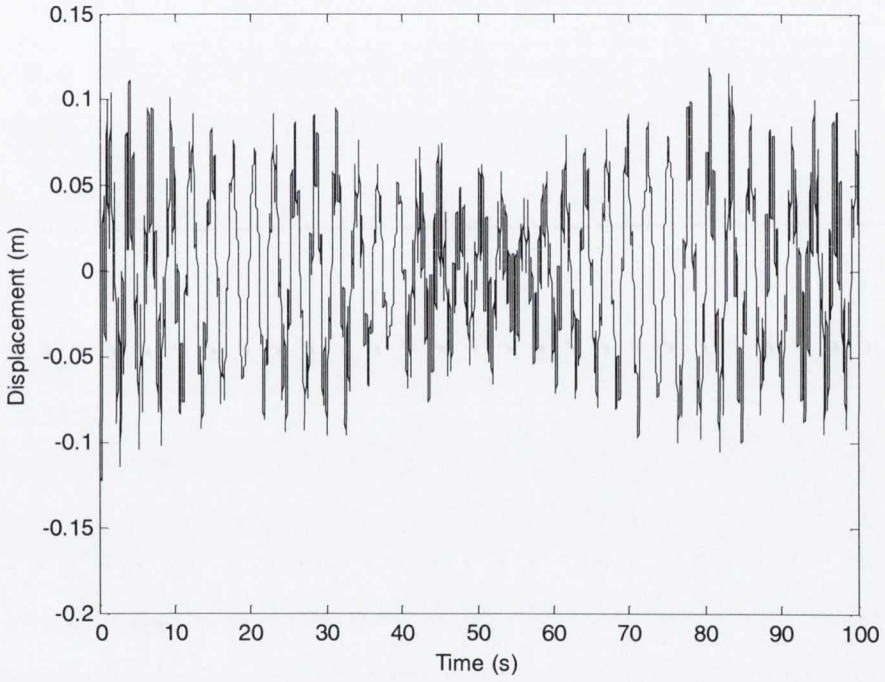

Figure 3.9: Nacelle flapwise time history response, turbulent load, Ω = 3.14rad/s

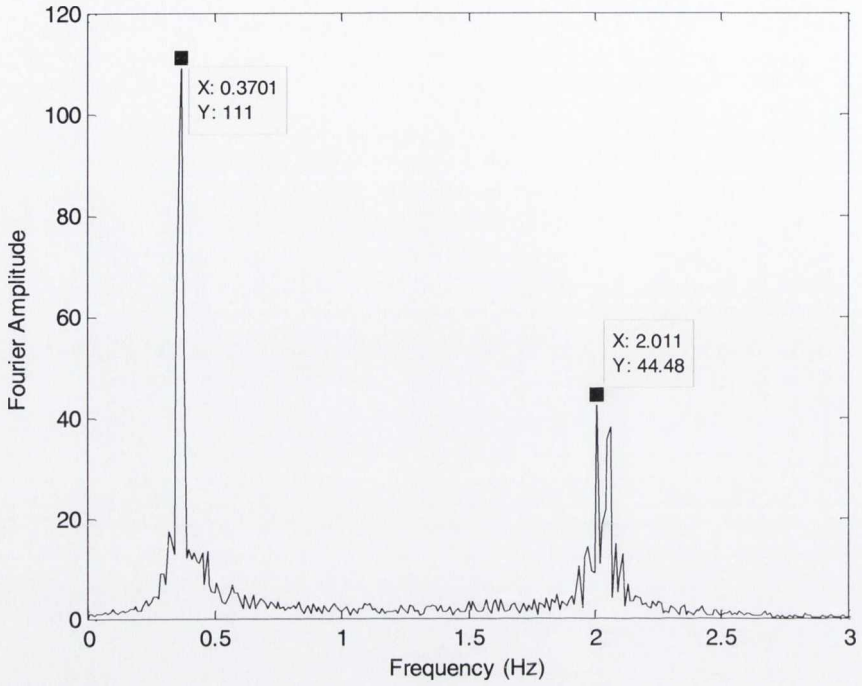

Figure 3.10: Nacelle flapwise frequency spectrum, turbulent load, Ω = 3.14rad/s

3.3 Edgewise Model

Edgewise vibrations are those occurring in the plane of blade rotation. The issue of edgewise vibrations in wind turbine blades is recently becoming a more prominent problem than that of flapwise. Investigation into the phenomenon has been carried out by Thomson et al. (2000) and Chaviaropoutos (2001).

3.3.1 Model Formulation

The edgewise model was formulated by the same Lagrangian method as that used for the flapwise model described previously. Coupling between the blades and nacelle/tower was again included. A schematic of the model is shown in figure 3.11.

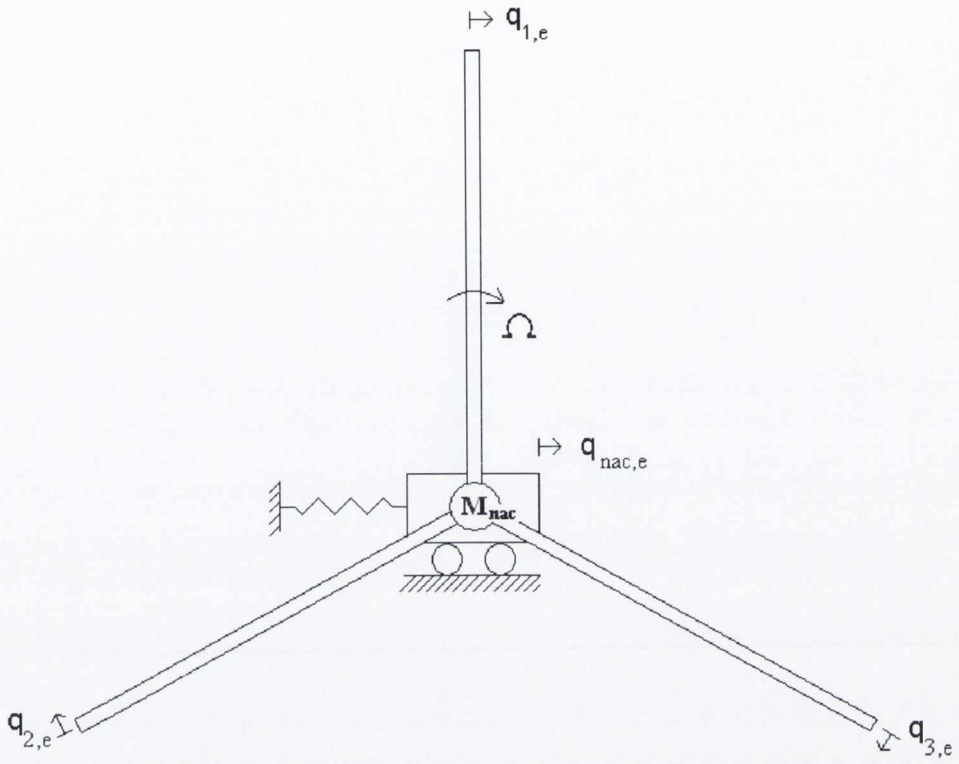

Figure 3.11: Schematic of edgewise model

The kinetic and potential energies of the edgewise model are similar in nature to those of the flapwise model (equations 3.5 and 3.6) and are expressed in equations 3.25 and 3.26.

$$T_e = \frac{1}{2}\overline{m}\sum_{i=1}^{3}\int_0^L v_{bi,e}(x,t)^2 dx + \frac{1}{2}M_{nac}\dot{q}_{nac,e}{}^2 \tag{3.25}$$

$$V_e = \frac{1}{2}EI_e\sum_{i=1}^{3}\int_0^L\left(\frac{\delta^2 u_{i,e}}{\delta x^2}\right)^2 dx + \frac{1}{2}K_{nac}q_{nac,e}{}^2 \tag{3.26}$$

where the subscript, e, represents the edgewise direction with the other variables as defined previously. Centrifugal stiffening was again added as expressed in equation 3.8. The effect of gravity on the system was not considered as this has no effect on the analysis or control strategy proposed in this thesis. The equations of motion were then derived using the Lagrangian formulation from equation 3.1. These are expressed in equation 3.27.

$$
\begin{bmatrix}
\frac{m_b}{5} & 0 & 0 & \frac{m_b}{3}\cos(\Omega t) \\
0 & \frac{m_b}{5} & 0 & \frac{m_b}{3}\cos\left(\Omega t+\frac{2}{3}\pi\right) \\
0 & 0 & \frac{m_b}{5} & \frac{m_b}{3}\cos\left(\Omega t+\frac{4}{3}\pi\right) \\
\frac{m_b}{3}\cos(\Omega t) & \frac{m_b}{3}\cos\left(\Omega t+\frac{2}{3}\pi\right) & \frac{m_b}{3}\cos\left(\Omega t+\frac{4}{3}\pi\right) & M_{nac}+3m_b
\end{bmatrix}
\begin{Bmatrix} \ddot{q}_{1,e} \\ \ddot{q}_{2,e} \\ \ddot{q}_{3,e} \\ \ddot{q}_{nac,e} \end{Bmatrix} +
$$

$$
\begin{bmatrix}
c_{st,b} & 0 & 0 & 0 \\
0 & c_{st,b} & 0 & 0 \\
0 & 0 & c_{st,b} & 0 \\
-\frac{2}{3}m_b\Omega\sin(\Omega t) & -\frac{2}{3}m_b\Omega\sin\left(\Omega t+\frac{2}{3}\pi\right) & -\frac{2}{3}m_b\Omega\sin\left(\Omega t+\frac{4}{3}\pi\right) & c_{st,nac}
\end{bmatrix}
\begin{Bmatrix} \dot{q}_{1,e} \\ \dot{q}_{2,e} \\ \dot{q}_{3,e} \\ \dot{q}_{nac,e} \end{Bmatrix} +
$$

$$
\begin{bmatrix}
\frac{4EI_e}{L^3}+\frac{\Omega^2 m_b}{15} & 0 & 0 & 0 \\
0 & \frac{4EI_e}{L^3}+\frac{\Omega^2 m_b}{15} & 0 & 0 \\
0 & 0 & \frac{4EI_e}{L^3}+\frac{\Omega^2 m_b}{15} & 0 \\
-\frac{m_b}{3}\Omega^2\cos(\Omega t) & -\frac{m_b}{3}\Omega^2\cos\left(\Omega t+\frac{2}{3}\pi\right) & -\frac{m_b}{3}\Omega^2\cos\left(\Omega t+\frac{4}{3}\pi\right) & K_{nac}
\end{bmatrix}
\begin{Bmatrix} q_{1,e} \\ q_{2,e} \\ q_{3,e} \\ q_{nac,e} \end{Bmatrix} =
\begin{Bmatrix} Q_{1,e} \\ Q_{2,e} \\ Q_{3,e} \\ Q_{nac,e} \end{Bmatrix}
\qquad (3.27)
$$

The most important feature in these equations is the time varying nature of the mass, stiffness and damping matrices. This makes the behaviour of the edgewise model significantly more complicated than that of the flapwise model which contains no time varying terms. The damping matrix is of particular interest due to the negative time varying terms that occur in the fourth row. These are purely a result of the coupling between the nacelle and blades as omission of the nacelle motion in the formulation results in no such terms arising in the final equations. The negative damping that arises in the model is in accordance with the study of Thomson et al. (2000) who noted that total damping in the edgewise direction may become negative.

The addition of structural damping for the edgewise model is a complicated issue as in time varying systems it is something which is not well understood. Indeed in normal time invariant systems such as the flapwise model described previously structural damping is something that can only be estimated. For the stationary turbine ($\Omega = 0$), time varying terms are eliminated in equation 3.27 so the presence of some structural damping can be assumed as in the case of the flapwise model. Therefore the structural damping assumed in the edgewise model is taken as

stiffness proportional damping for the stationary turbine, i.e., proportional to the stiffness matrix for $\Omega = 0$.

3.3.2 Edgewise Loading

The edgewise loading on wind turbine blades arises due to the lift forces induced on the blades when the wind flows over them. Since the aerodynamic behaviour has not been considered in this study the wind is assumed to be flowing in the edgewise direction, thus exerting a load on the blades.

3.3.2.1 Steady Load

With this in mind a simple load case similar to that used in the flapwise model was studied. This assumed the generalized loading on the blades, Q_1, Q_2 and Q_3 to be a result of a steady wind-load which varied with height and acted in the edgewise direction. The rotation of the blades meant that the magnitude of this load acting on the blades varied with time. Due to the complex harmonic nature of the loading, Q_1, Q_2 and Q_3 were taken as the first harmonic term of the generalized load, expressed as

$$Q_1 = \left(\frac{v_{nac}{}^2 A}{6} + \frac{3\partial v_{nac+L}{}^2 A}{40} \right) + \left(\frac{3 v_{nac} \partial v_{nac+L} A}{8} \right) \cos(\Omega t) \tag{3.28}$$

where as before v_{nac} = wind speed at nacelle height, ∂v_{nac+L} = the increase in wind speed between the nacelle and maximum blade tip height, i.e. when blade is in upright vertical position. Q_2 and Q_3 are worked out similarly with phase lags of $2\pi/3$ and $4\pi/3$ respectively due to the angles between the blades. The load on the nacelle, Q_{nac}, was again taken as zero. All motion of the nacelle was again a result of the dynamic coupling with the blades. As can be seen in equation 3.28 the frequency of the loading is equal to the rotational speed of the blades as for the flapwise case.

3.3.2.2 Turbulent Load

A second loading scenario was also studied, again considering an added turbulent component to the steady wind flow of equation 3.28. This was formulated using the same technique as for the flapwise loading and was described previously in section 3.2.3.2.

3.3.3 Numerical Simulations

Time histories were again generated in Matlab for the edgewise model considering steady and turbulent wind loading.

3.3.3.1 Steady Wind Load

Figure 3.12 shows the time history response of blade one to the steady wind load outlined in section 3.3.2.1. A blade rotational speed of 3.14rad/s (0.5Hz) was once more assumed. Figure 3.13 plots the corresponding frequency spectrum of the blade. As can be seen in this graph a peak again occurs at the rotational speed of the blades and forcing function frequency. Another peak arises just under 2Hz, close to the natural frequency of the blades. Blades two and three again exhibited similar time history responses and frequency spectra.

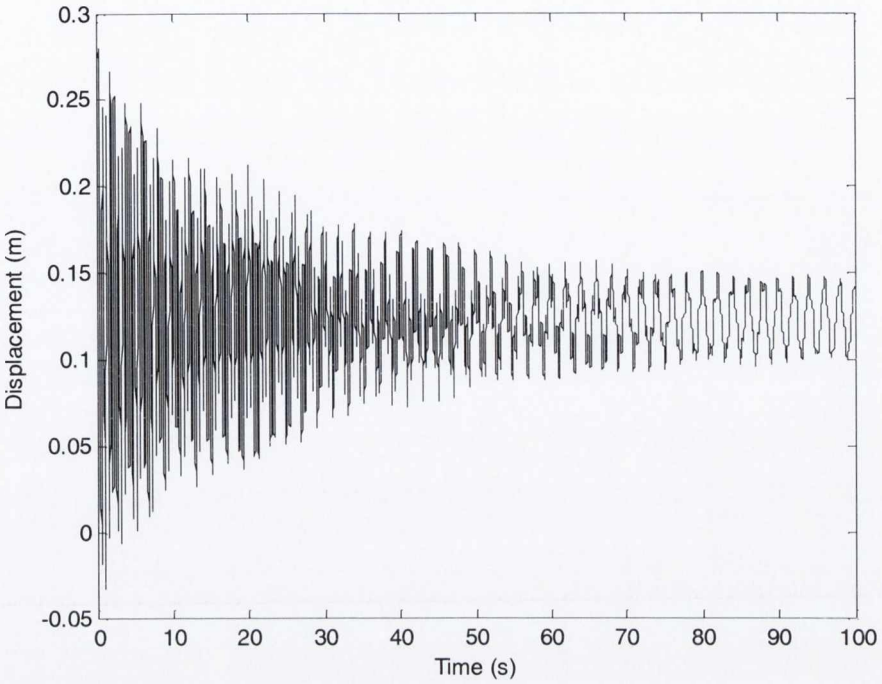

Figure 3.12: Blade 1 edgewise response, steady load, Ω = 3.14rad/s

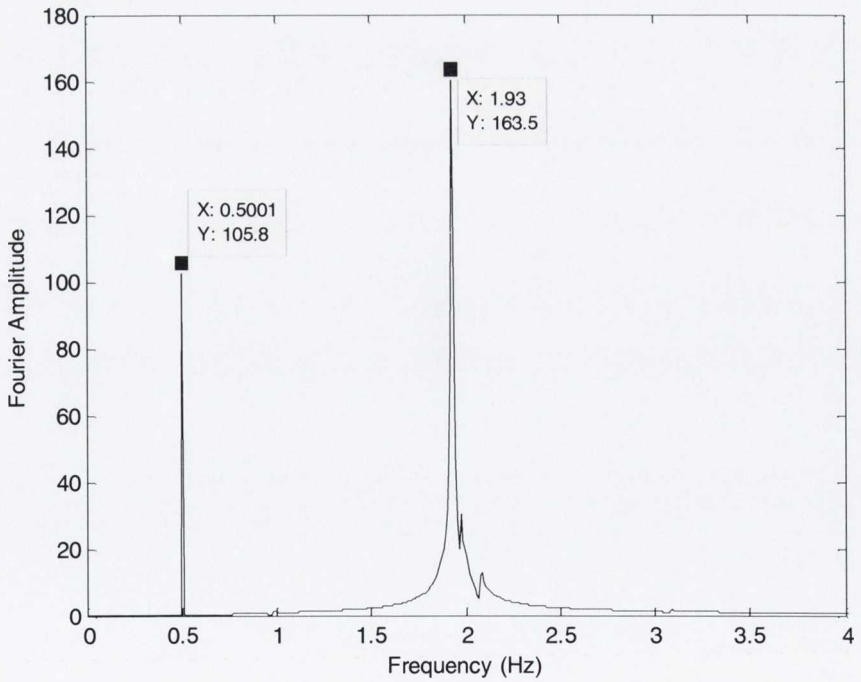

Figure 3.13: Blade 1 edgewise frequency spectrum, steady load, Ω = 3.14rad/s

Figure 3.14 shows a plot of the nacelle time history response for the steady wind loading over the first 100s. As can be seen, the amplitude of nacelle motion after 100s is approximately 10% of the amplitude of blade motion highlighting the coupling seen between the components of the turbine under edgewise vibration. This is significantly weaker than the coupling seen in the flapwise model which resulted in nacelle motion similar in magnitude to that of the blade once steady state had been reached.

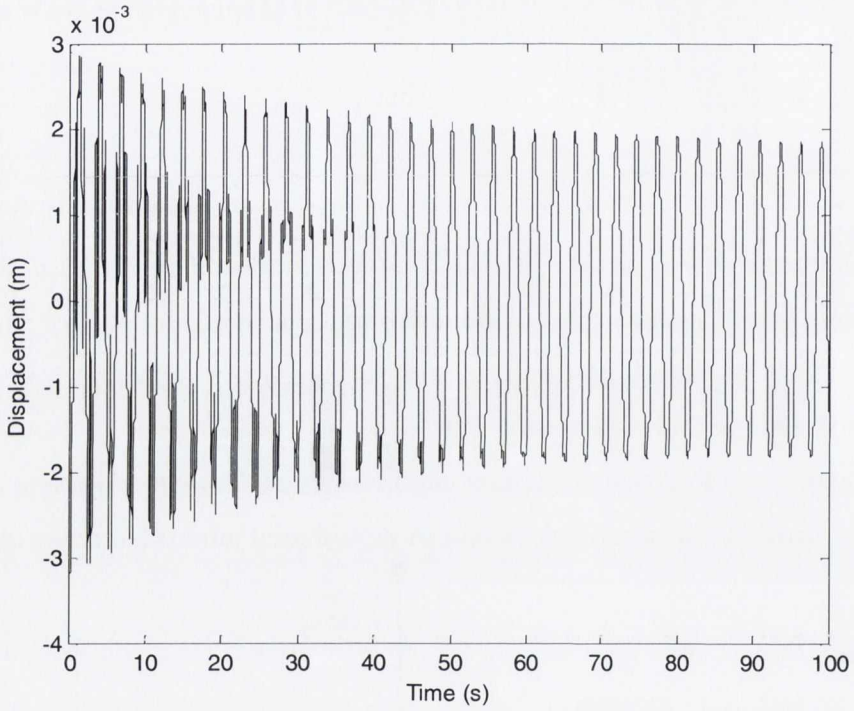

Figure 3.14: Nacelle edgewise response, steady load, Ω = 3.14rad/s

The resulting frequency spectrum is again shown below in figure 3.15 with one significant frequency peak at 0.37Hz and two small peaks at 1.48Hz and 2.58Hz respectively. Again, further study into these frequency peaks will be performed in the control chapters of this thesis.

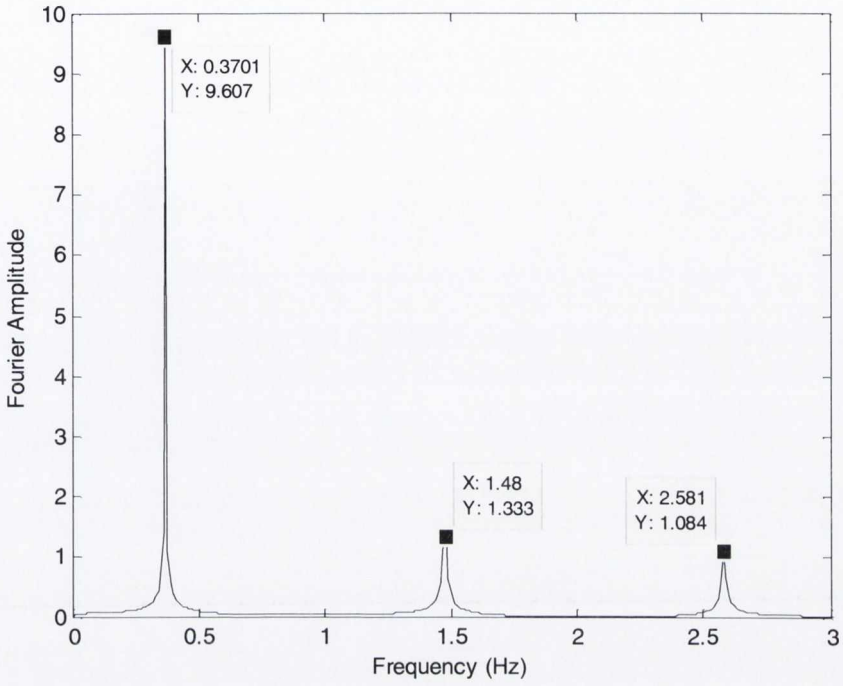

Figure 3.15: Nacelle edgewise frequency spectrum, steady load, Ω = 3.14rad/s

3.3.3.2 Turbulent Wind Load

The response of the edgewise model to the turbulent load previously outlined was also analysed. Figure 3.16 and 3.17 below show the time history response for blade one and the resulting frequency spectrum when subjected to the turbulent loading scenario. As before and as seen in the flapwise model, the frequency peaks occur at approximately the same values as for the steady wind load results.

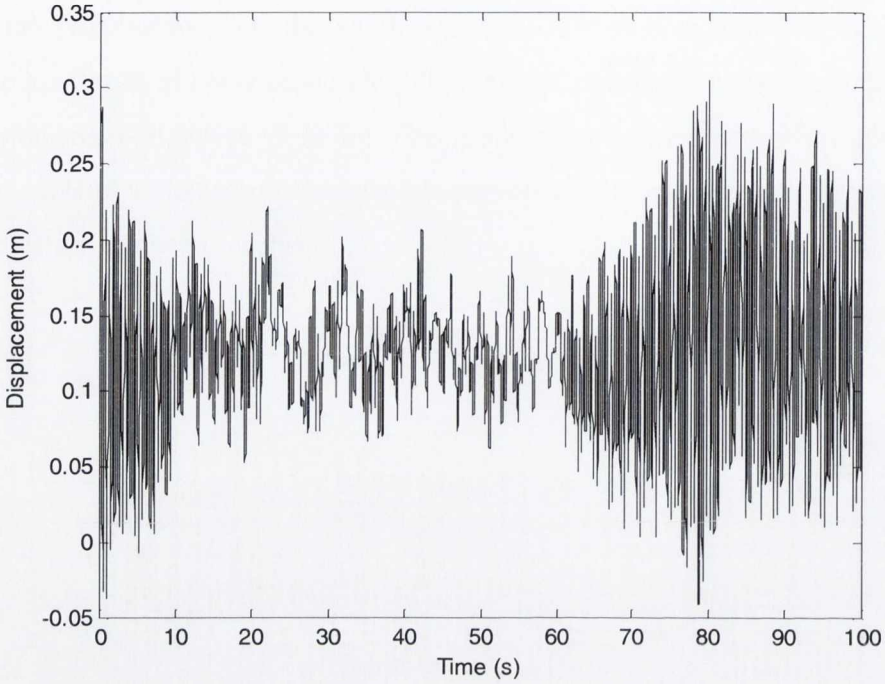

Figure 3.16: Blade 1 edgewise response, turbulent load, Ω = 3.14rad/s

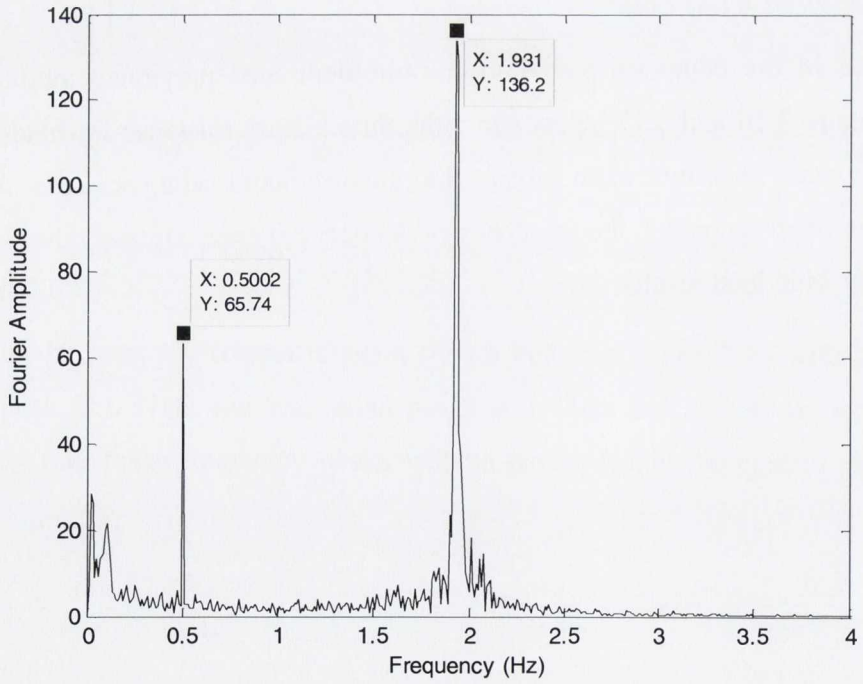

Figure 3.17: Blade 1 edgewise response, turbulent load, Ω = 3.14rad/s

Figures 3.18 and 3.19 plot the time history response and frequency spectrum for the nacelle under the same turbulent loading. A similar degree of coupling was seen as for the steady wind load results plotted previously.

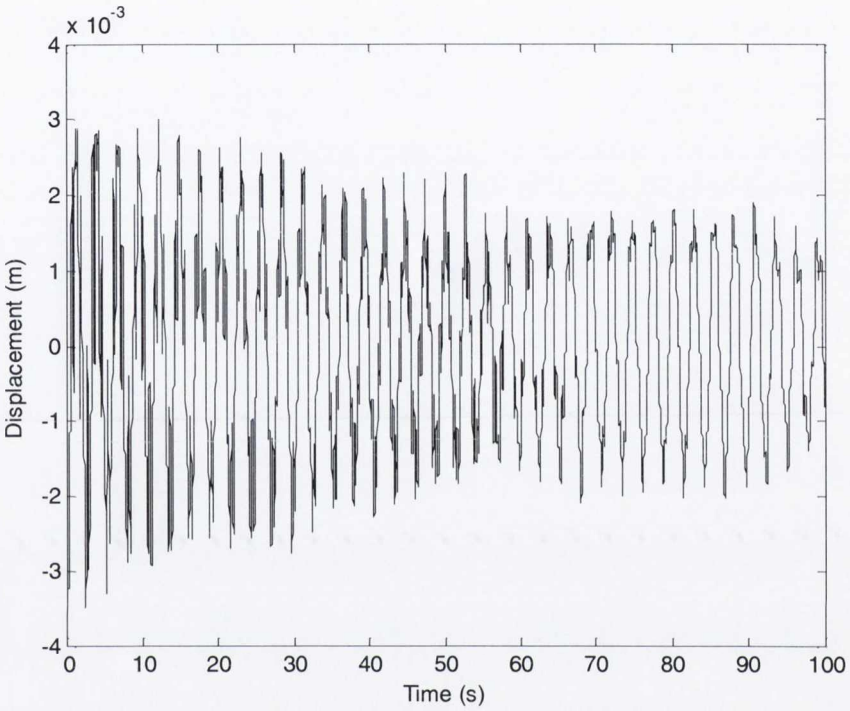

Figure 3.18: Nacelle edgewise response, turbulent load, Ω = 3.14rad/s

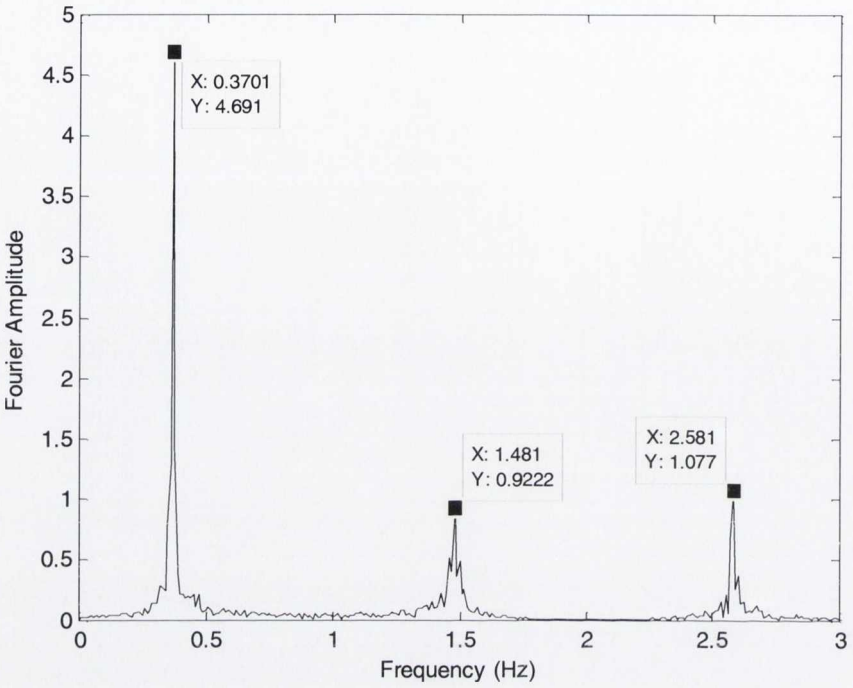

Figure 3.19: Nacelle edgewise frequency spectrum, turbulent load, Ω = 3.14rad/s

3.4 Conclusions

This chapter outlined the formulation of the structural dynamic model developed for analysis of the dynamic behaviour of a wind turbine. Models for both flapwise and edgewise vibrations were derived and their responses studied for both steady and turbulent wind loads. The coupling between the blades and nacelle of the system was included. The results showed that significant nacelle motion could be induced through the dynamic interaction with the blades. This was observed to be stronger in the flapwise model than in the edgewise. Furthermore, the coupling in the edgewise model resulted in the occurrence of time varying terms throughout the equations of motion of the system. No such time varying behaviour arose in the flapwise model.

CHAPTER 4 - Passive Control Using TMDs

4.1 Introduction

This chapter introduces the aspect of structural vibration control, which aims to develop a method for mitigating vibrations in wind turbine structures. As outlined in section 2.3.4 little investigation has been done into this area using structural control strategies. Research performed into controlling the dynamic behaviour of wind turbines has largely focussed on the design of the blades themselves by trying to increase the structural damping inherently present in them or alter their aerodynamic characteristics (Chaviaropoutos et al., 2003, Chaviaropoutos et al., 2006). A couple of studies have investigated the use of dampers in the turbine tower (Murtagh et al., 2008, Colwell and Basu, 2009). However, use of dampers in the blades has yet to be investigated in any great detail.

The flapwise and edgewise models developed in Chapter 3 are extended to include damping devices in both the blades and nacelle of the turbine. Their effectiveness in controlling the dynamic response of the system is analysed in this chapter, specifically highlighting the coupling seen between the blades and nacelle.

4.2 Flapwise Model

4.2.1 Addition of TMDs

The hollow nature of wind turbine blades makes them automatically suitable for the installation of vibration mitigation devices such as TMDs. Despite this, little or no research has been carried out on the effectiveness of dampers in reducing vibrations in a wind turbine system. In the model developed in this section four dampers have been added to the flapwise model derived in Chapter 3, one at each blade tip and one at the nacelle. These have been modelled as mass-spring-dashpot systems, representative of a TMD (or equivalent TLD) as described is section 2.3.1 of this thesis. Figure 4.1 shows the flapwise model with attached TMDs. As can be seen in the figure, the relative displacements of the dampers are labelled $d_{i,f}$,

where, as before 'i' indicates the degree of freedom and 'f' signifies the flapwise direction. The effectiveness of the nacelle and blade TMDs have been studied separately. Any coupling in the system can therefore be seen clearly, e.g. when tuning the nacelle TMD to a resonant frequency of the nacelle/tower, a reduction in blade displacement can also be achieved due to the dynamic interaction present in the structure. This will be evident later in this chapter.

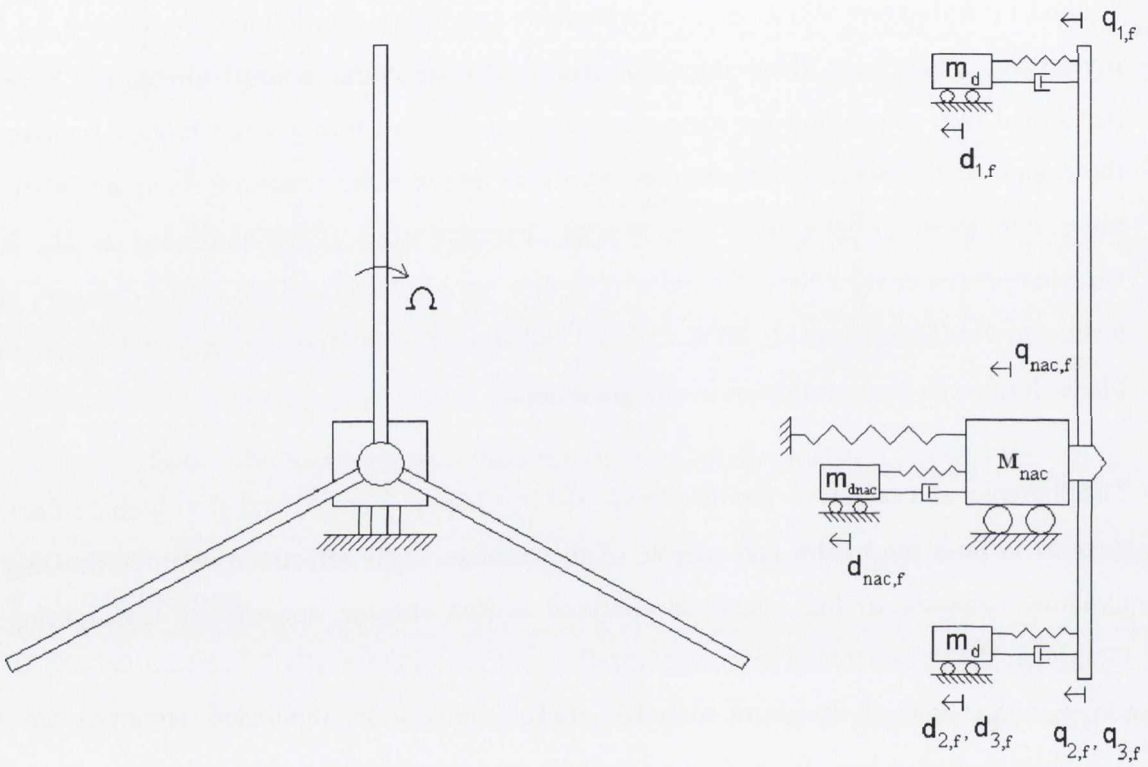

Figure 4.1: Flapwise model with TMDs attached

Equations of motion were formulated for the system with dampers attached using the Lagrangian formulation. This technique was outlined in Chapter 3 for the model with no dampers attached, henceforth referred to as the undamped model. Equation 4.1 below gives the equations of motion for the damped system where $M_{f,damp}$, $C_{f,damp}$ and $K_{f,damp}$ represent the mass, damping and stiffness matrices respectively for the damped model (model with TMDS included). The vector of displacements is given by $q_{f,damp}$, with the overdots signifying the first and second derivatives with respect to time, i.e. the velocity and acceleration vectors. The final model consists of 8 dofs with a TMD at each blade tip and at the nacelle.

$$[M_{f,damp}]\{\ddot{q}_{f,damp}\}+[C_{f,damp}]\{\dot{q}_{f,damp}\}+[K_{f,damp}]\{q_{f,damp}\}=\{Q_f\} \tag{4.1}$$

where the system matrices are defined below in equations 4.2, 4.3 and 4.4.

$$M_{f,damp}=\begin{bmatrix}
\frac{m_b}{5}+m_{db} & m_{db} & 0 & 0 & 0 & 0 & \frac{m_b}{3}+m_{db} & 0 \\
m_{db} & m_{db} & 0 & 0 & 0 & 0 & m_{db} & 0 \\
0 & 0 & \frac{m_b}{5}+m_{db} & m_{db} & 0 & 0 & \frac{m_b}{3}+m_{db} & 0 \\
0 & 0 & m_{db} & m_{db} & 0 & 0 & m_{db} & 0 \\
0 & 0 & 0 & 0 & \frac{m_b}{5}+m_{db} & m_{db} & \frac{m_b}{3}+m_{db} & 0 \\
0 & 0 & 0 & 0 & m_{db} & m_{db} & m_{db} & 0 \\
\frac{m_b}{3}+m_{db} & m_{db} & \frac{m_b}{3}+m_{db} & m_{db} & \frac{m_b}{3}+m_{db} & m_{db} & M_{nac}+3m_b+3m_{db}+m_{dnac} & m_{dnac} \\
0 & 0 & 0 & 0 & 0 & 0 & m_{dnac} & m_{dnac}
\end{bmatrix} \tag{4.2}$$

$$C_{f,damp}=\begin{bmatrix}
c_{st,b} & 0 & 0 & 0 & 0 & 0 & 0 & 0 \\
0 & c_{db,f} & 0 & 0 & 0 & 0 & 0 & 0 \\
0 & 0 & c_{st,b} & 0 & 0 & 0 & 0 & 0 \\
0 & 0 & 0 & c_{db,f} & 0 & 0 & 0 & 0 \\
0 & 0 & 0 & 0 & c_{st,b} & 0 & 0 & 0 \\
0 & 0 & 0 & 0 & 0 & c_{db,f} & 0 & 0 \\
0 & 0 & 0 & 0 & 0 & 0 & c_{st,nac} & 0 \\
0 & 0 & 0 & 0 & 0 & 0 & 0 & c_{dnac,f}
\end{bmatrix} \tag{4.3}$$

$$K_{f,damp}=\begin{bmatrix}
\frac{4EI_f}{L^3}+\frac{4\Omega^2 m_b}{15} & 0 & 0 & 0 & 0 & 0 & 0 & 0 & 0 \\
0 & k_{db,f} & 0 & 0 & 0 & 0 & 0 & 0 & 0 \\
0 & 0 & \frac{4EI_f}{L^3}+\frac{4\Omega^2 m_b}{15} & 0 & 0 & 0 & 0 & 0 & 0 \\
0 & 0 & 0 & k_{db,f} & 0 & 0 & 0 & 0 & 0 \\
0 & 0 & 0 & 0 & \frac{4EI_f}{L^3}+\frac{4\Omega^2 m_b}{15} & 0 & 0 & 0 & 0 \\
0 & 0 & 0 & 0 & 0 & k_{db,f} & 0 & 0 & 0 \\
0 & 0 & 0 & 0 & 0 & 0 & K_{nac} & 0 & 0 \\
0 & 0 & 0 & 0 & 0 & 0 & 0 & k_{dnac,f} & 0
\end{bmatrix} \tag{4.4}$$

with m_{db} and m_{dnac} representing the mass of the dampers in the blades and nacelle respectively, $c_{db,f}$ and $c_{dnac,f}$ equal to the damping in the blade and nacelle dampers in the flapwise direction, and $k_{db,f}$ and $k_{dnac,f}$ equal to the stiffness of the blade and nacelle dampers in the flapwise direction.

Simulations were run for both the undamped and damped systems to allow the vibration mitigation effect of the TMDs to be analysed. The tuning of the TMDs was determined by transforming the time history response of the undamped system to the frequency domain by means of an FFT, which allows easy identification of the resonant frequencies present in the system. This technique was described in Chapter 3 of the thesis.

4.2.2 Effectiveness of TMDs

As mentioned previously the effectiveness of the nacelle and blade TMDs were studied separately to allow dynamic coupling in the system to be clearly identifiable. A steady wind load was used for the following results, as outlined in section 3.2.3.1 of this thesis.

4.2.2.1 TMD at the nacelle

The first control scheme studied looked at the effectiveness of a TMD installed at the nacelle of the turbine. A mass ratio, μ = 1% was assumed for the TMD. The damping present in the TMD was conservatively estimated as 1%. Figure 4.2 and 4.3 show the time history and corresponding frequency response of the nacelle for a steady wind load and a blade rotational speed of 3.14rad/s. These were previously plotted in chapter 3.

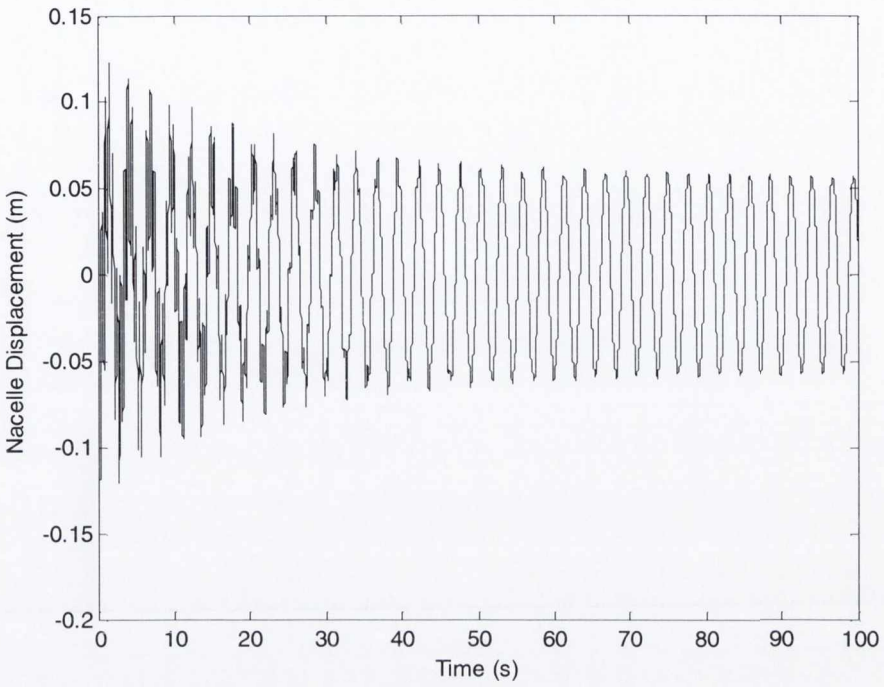

Figure 4.2: Flapwise response of the nacelle, steady load, Ω = 3.14rad/s

As can be seen in figure 4.3 below, two distinct frequency peaks exist in the system, at 0.37Hz and 2.03Hz. The peak at 0.37Hz has the largest amplitude and is hence the dominant frequency in the response of the nacelle.

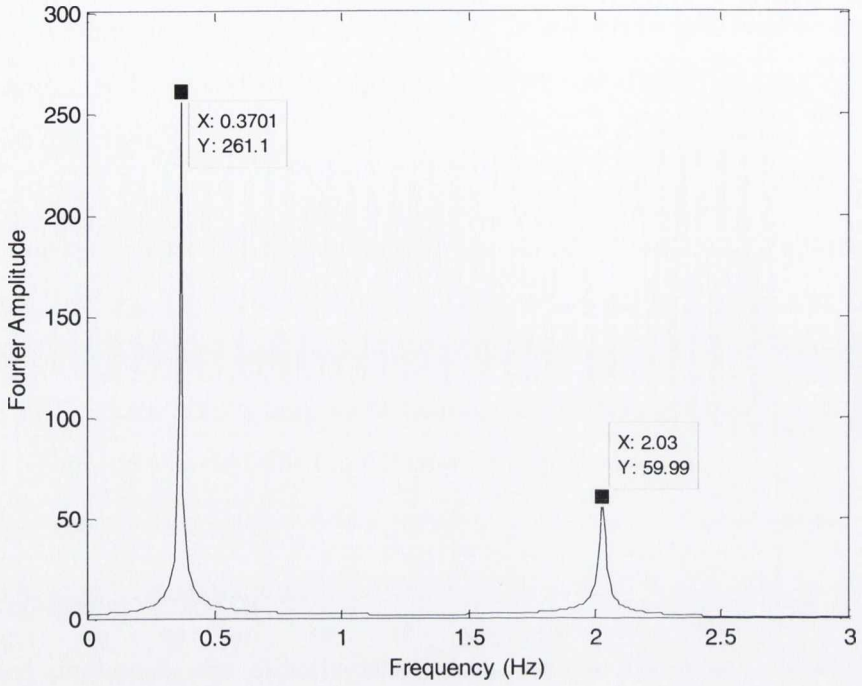

Figure 4.3: Nacelle flapwise frequency spectrum, steady load, Ω = 3.14rads/s

The nacelle TMD was first tuned to this larger peak at 0.37Hz. Effective tuning of a TMD to a resonant frequency of the primary structure (such as that at 0.37Hz in figure 4.3), results in the single undamped peak being reduced to two smaller peaks, one either side of the original frequency. Optimal tuning of the damper is achieved when the two peaks in the damped frequency spectrum are of equal height. This is also dependent on the damping in the TMD.

Figure 4.4 compares the time history response of the damped structure to the undamped structure over a time period of 100 seconds, while figure 4.5 compares the undamped and damped frequency plots. As can be observed in figure 4.4 the TMD achieves a significant reduction in the displacement response of the nacelle as the excitation frequency of 0.5Hz is close to the peak at 0.37Hz in the nacelle frequency plot, to which the TMD is tuned. A tuning ratio of unity was applied. In the frequency spectrum plotted in figure 4.5, the x-axis scale has been changed to allow the double peak to be seen clearly. The small peak in the blade response at 0.37Hz also experienced a reduction due to the coupling in the system. However, due to the tiny amplitude of this peak, negligible reduction was seen in the displacement response of the blade.

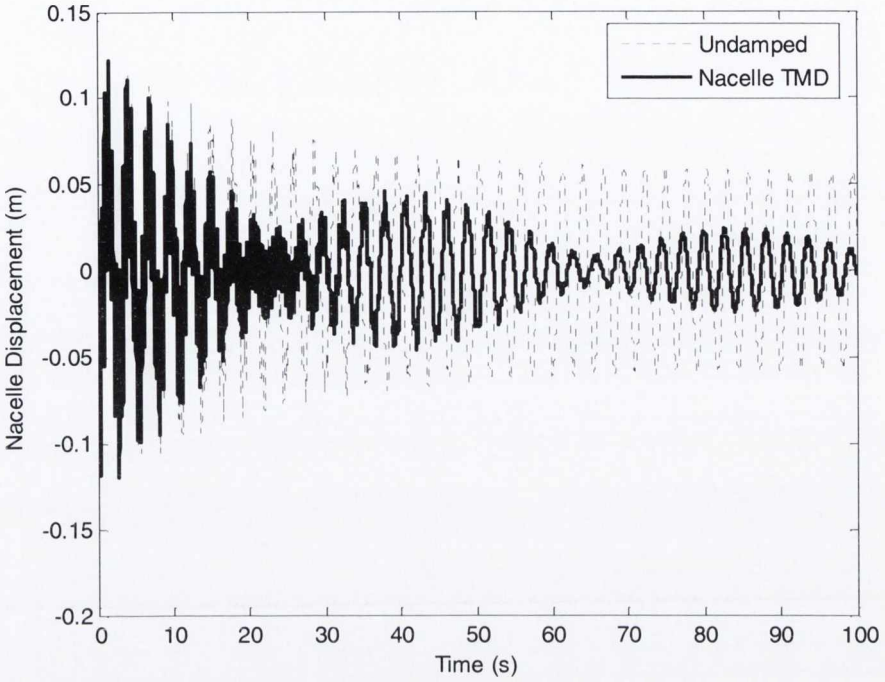

Figure 4.4: Flapwise response of nacelle, steady load, $\Omega = 3.14$rads/s, $\omega_{dnac} = 0.37$Hz.

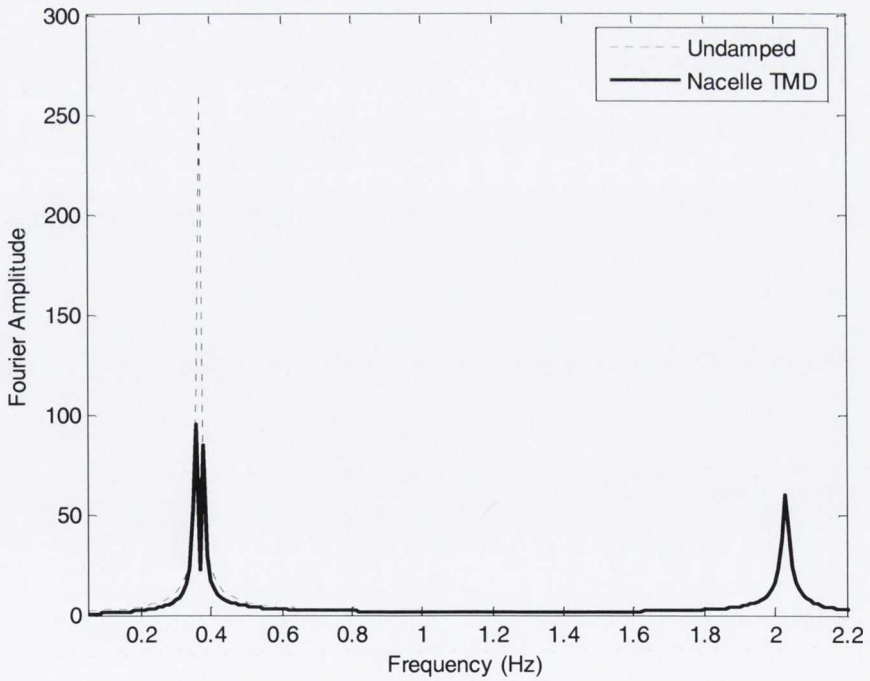

Figure 4.5: Nacelle flapwise frequency spectrum, steady load, $\Omega = 3.14$rads/s, $\omega_{dnac} = 0.37$Hz

The tuning of the TMD at the nacelle was then changed to the second peak, seen at 2.03Hz in figure 4.3 and the results plotted. Figure 4.6 shows the displacement response of the nacelle. As can be seen a reduction is achieved during the transient phase of the response. When steady state is reached no improvement is seen with the damper attached. This is due to the fact that the structure is being excited at 0.5Hz, significantly far away from the resonant peak at 2.03Hz to which the TMD is tuned. The frequency spectrum is shown in figure 4.7. The reduced double peak around 2.03Hz is clearly observable.

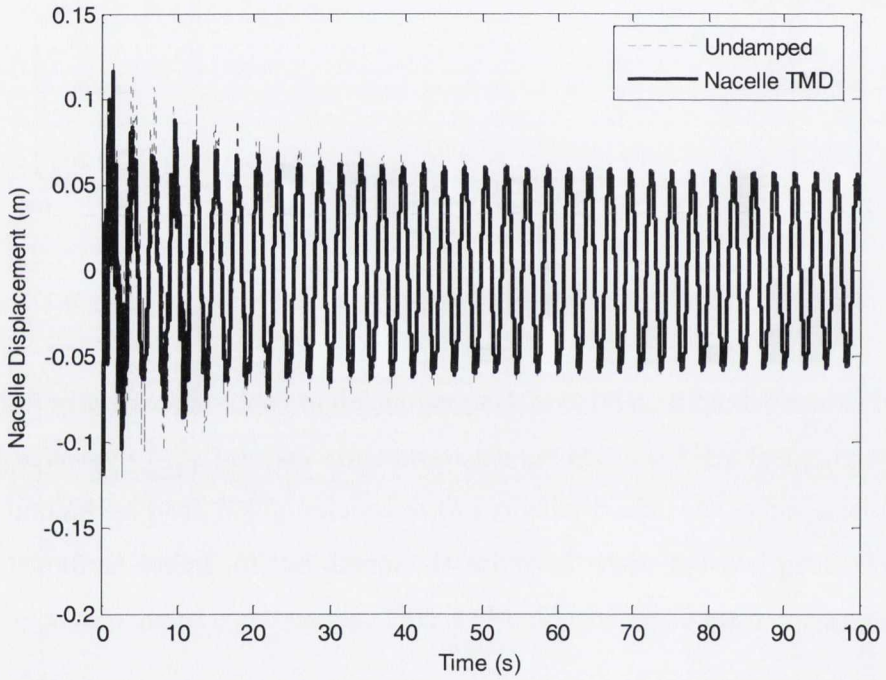

Figure 4.6: Flapwise response of nacelle, constant load, $\Omega = 3.14$rads/s, $\omega_{dnac} = 2.03$Hz

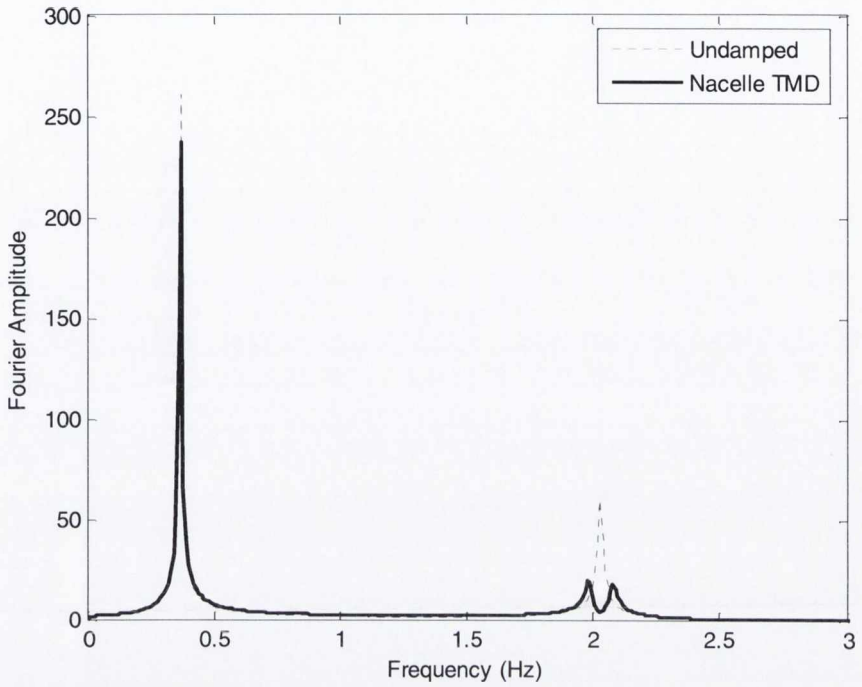

Figure 4.7: Nacelle flapwise frequency spectrum, steady load, $\Omega = 3.14$rads/s, $\omega_{dnac} = 2.03$Hz

It is important to note a reduction in the response of the blades was also achieved for this tuning frequency of the nacelle TMD. Figures 4.8 and 4.9 illustrate the time history response and frequency spectrum for one of the blades. As can be seen in figure 4.9, a peak also exists at 2.03Hz in the blade frequency spectrum. This is the largest peak in the response of the blade. As mentioned in the previous chapter significant coupling between the blades and nacelle is present in the system. As a result the peak at 2.03Hz in the blade frequency response has been replaced by two peaks of lower amplitude, highlighted in figure 4.9. Hence, a reduction is also achieved in the transient phase of the blade displacement through the dynamic interaction with the nacelle. Again, no reduction is seen in the steady state response as the system is being excited at 0.5Hz.

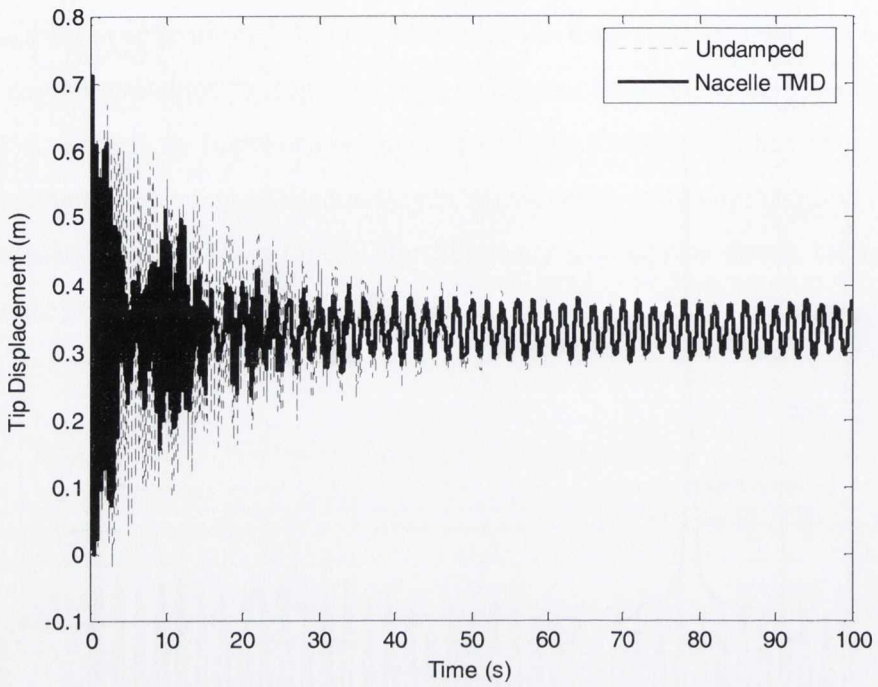

Figure 4.8: Flapwise response of blade 1, steady load, $\Omega = 3.14$rads/s, $\omega_{dnac} = 2.03$Hz

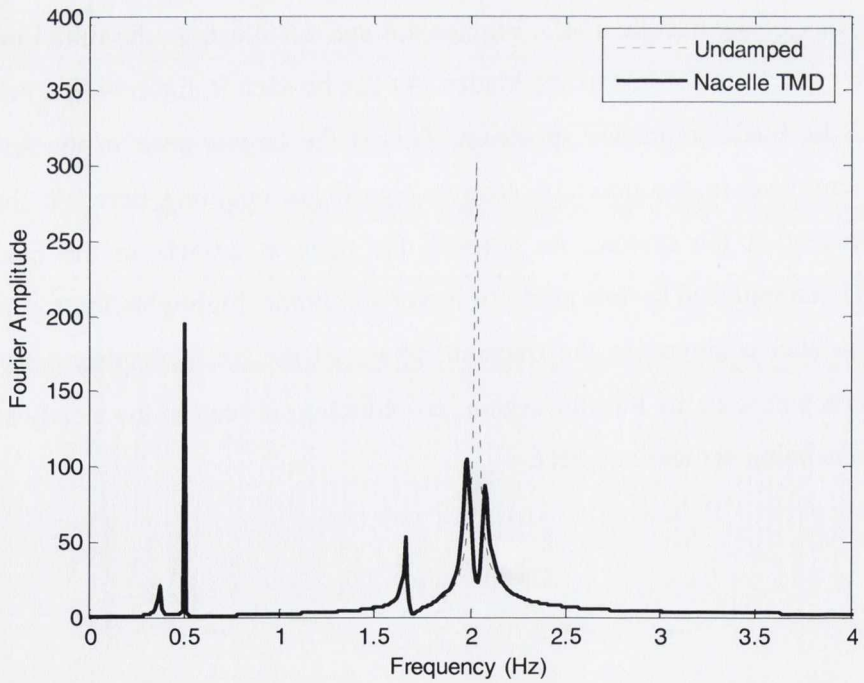

Figure 4.9: Blade 1 flapwise frequency spectrum, steady load, $\Omega = 3.14$rads/s, $\omega_{dnac} = 2.03$Hz

4.2.2.2 TMDs in the Blades

The effect of the TMDs in the blades in mitigating vibrations in the turbine model was then studied. Figures 4.10 and 4.11 below show the displacement response and corresponding frequency response plot of blade one respectively. These were previously plotted in chapter 3 of this thesis. Identical plots are seen for the other two blades.

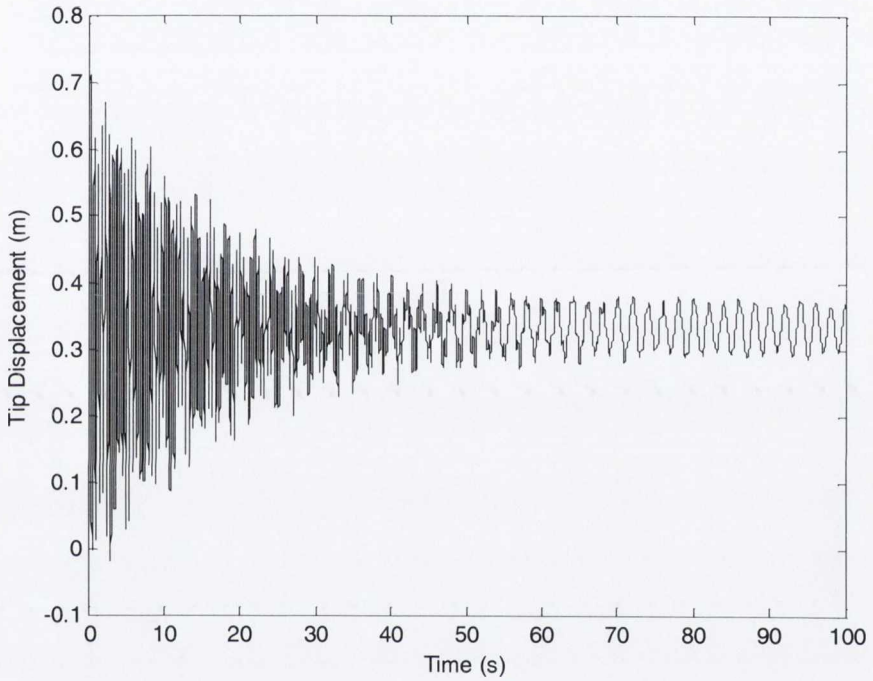

Figure 4.10: Flapwise response of blade 1, steady load, Ω = 3.14rad/s

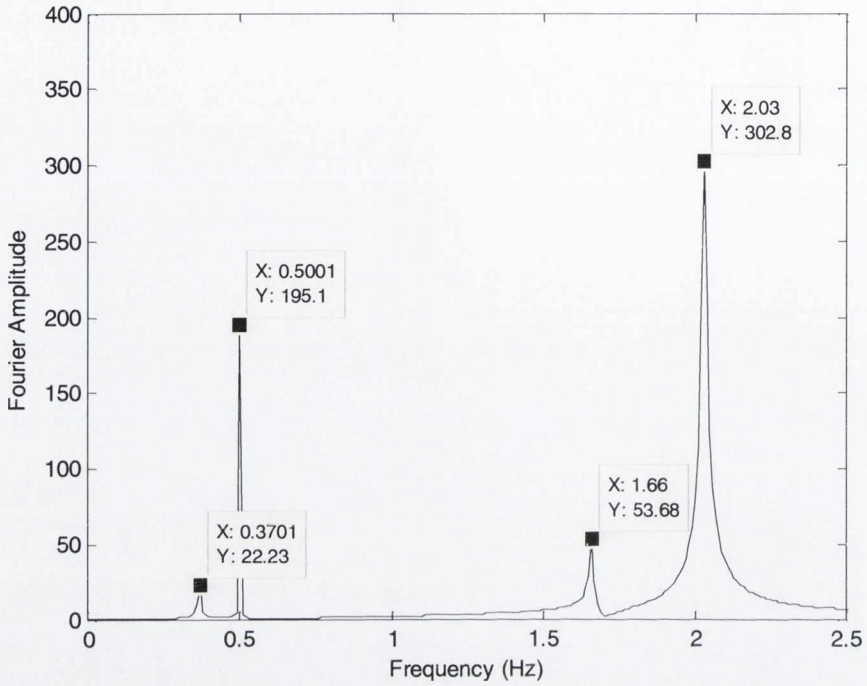

Figure 4.11: Blade 1 flapwise frequency spectrum, steady load, $\Omega = 3.14$rad/s

Tuning the TMDs to the smallest peak at 0.37Hz was first investigated but as expected negligible reduction was achieved in the displacement due to the tiny amplitude of this peak. The TMDs were then tuned to the next peak at 0.5Hz which corresponded to the rotational speed of the blades and forcing function frequency (see equation 3.22). However, despite the larger magnitude of this peak negligible reduction was seen in the response of the system. This highlights that tuning the TMD to the forcing function frequency is ineffective in controlling vibrations in the turbine. This holds true unless the forcing frequency corresponds to a frequency peak in the primary structure itself, i.e. when the structure is in resonance. This will be illustrated later in this chapter.

The tuning of the TMDs was then shifted to the higher peaks near the natural frequency of the blades. The dampers were first tuned to 1.66Hz. Figure 4.12 shows the displacement response of blade one, while figure 4.13 shows the corresponding frequency spectrum.

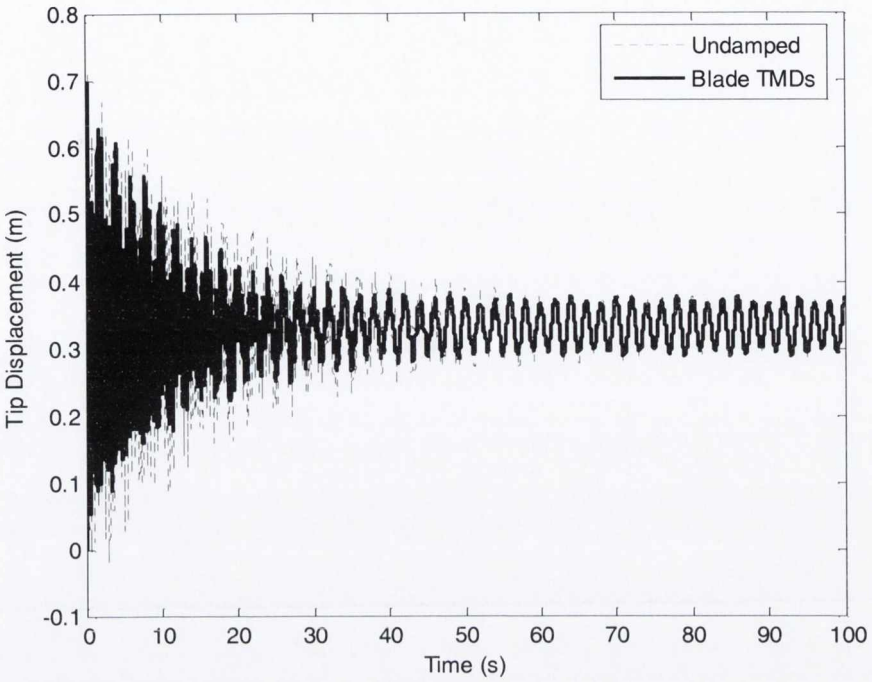

Figure 4.12: Flapwise response of blade 1, steady load, $\Omega = 3.14$rad/s, $\omega_{db} = 1.66$Hz

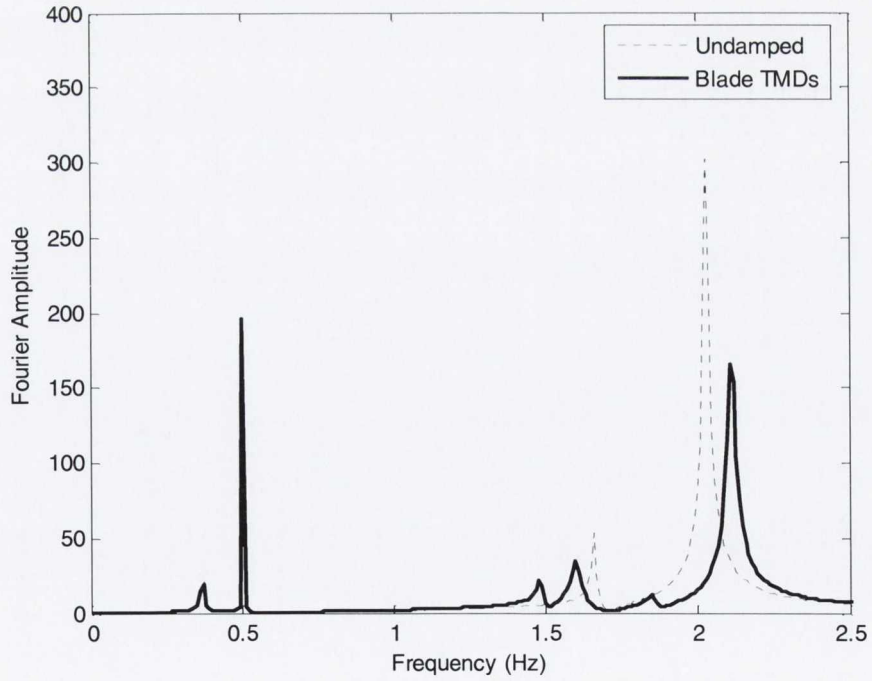

Figure 4.13: Blade 1 flapwise frequency spectrum, steady load, $\Omega = 3.14$rad/s, $\omega_{db} = 1.66$Hz

As can be observed in figure 4.13 tuning the damper to the peak at 1.66Hz results in a significant reduction not only in that peak, but also in the one seen at 2.03Hz. Due to the two peaks being in close proximity, an optimal reduction with peaks of equal height is difficult to achieve. However, the tuning shown achieves a good reduction during transience in the flapwise displacement response of the blade, plotted above in figure 4.12. The dynamic coupling between the blade and nacelle at the frequency of 2.03Hz highlighted in the previous section also comes into effect, with a small reduction seen in the transient displacement of the nacelle. This has been plotted in figure 4.14 with the corresponding frequency spectrum illustrated in figure 4.15. The double peak seen in the nacelle frequency spectrum is not indicative of optimal tuning for the nacelle response as the two peaks aren't of equal height. No reduction in blade or nacelle displacement is seen during steady state again due to the excitation frequency.

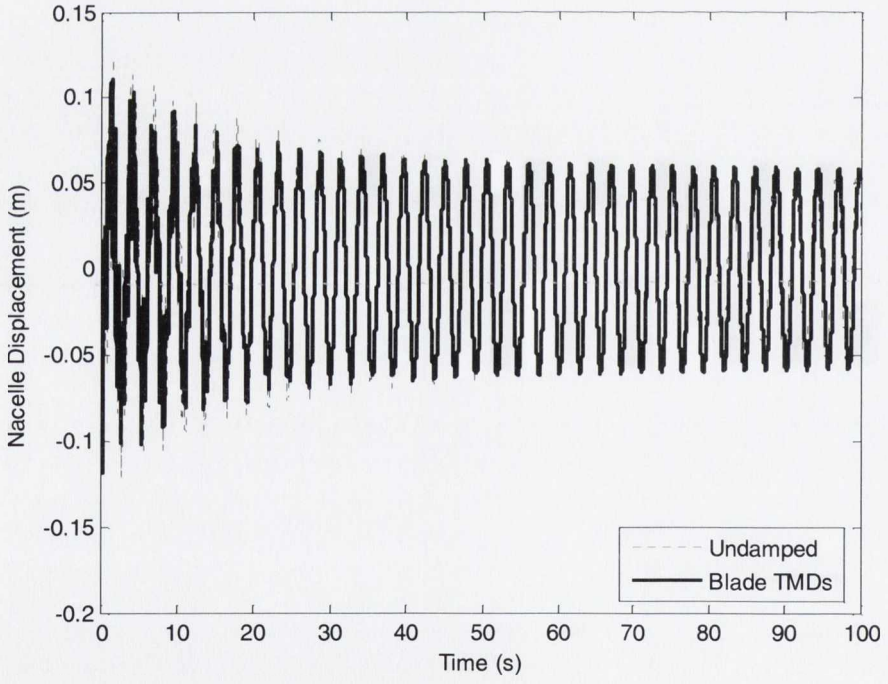

Figure 4.14: Flapwise response of nacelle, steady load, $\Omega = 3.14$rad/s, $\omega_{db} = 1.66$Hz

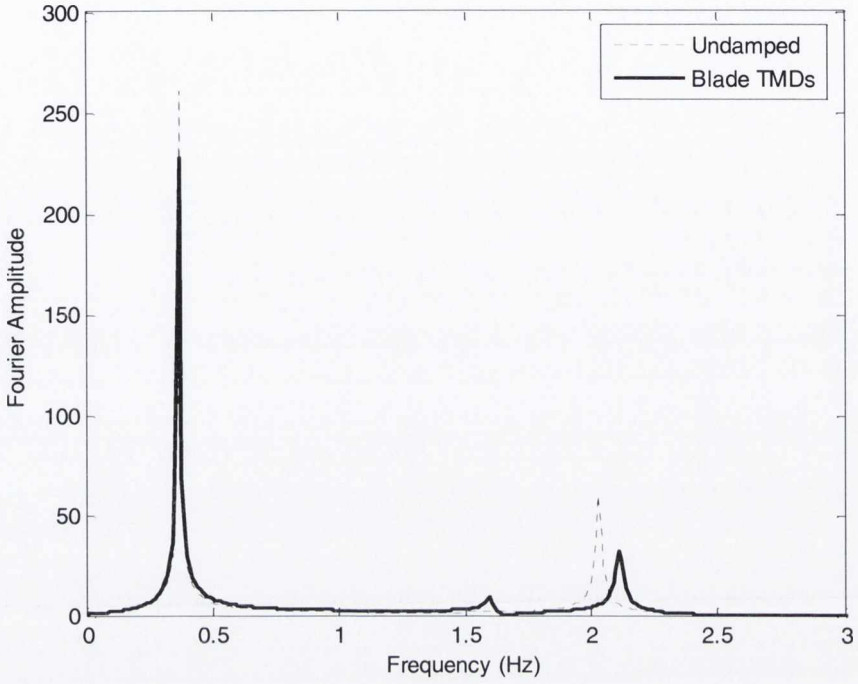

Figure 4.15: Nacelle flapwise frequency spectrum, steady load, $\Omega = 3.14$rad/s, $\omega_{db} = 1.66$Hz

Finally the blade TMDs were tuned to the largest of the peaks at 2.03Hz. As expected a large reduction in response occurs during the transient phase as can be seen in figure 4.16. Due to the larger amplitude of this peak the reduction in the transient response of the blade was greater than that seen for tuning the TMDs to the peak at 1.66Hz. The blade frequency spectrum is plotted in figure 4.17. Due to the dynamic coupling previously seen in the system when the nacelle TMD was tuned to the peak at 2.03Hz, the reverse is also true, with a small reduction achieved in the nacelle transient response when the blade TMDs are tuned to this peak. The nacelle displacement response and frequency spectrum are plotted in figures 4.18 and 4.19 respectively.

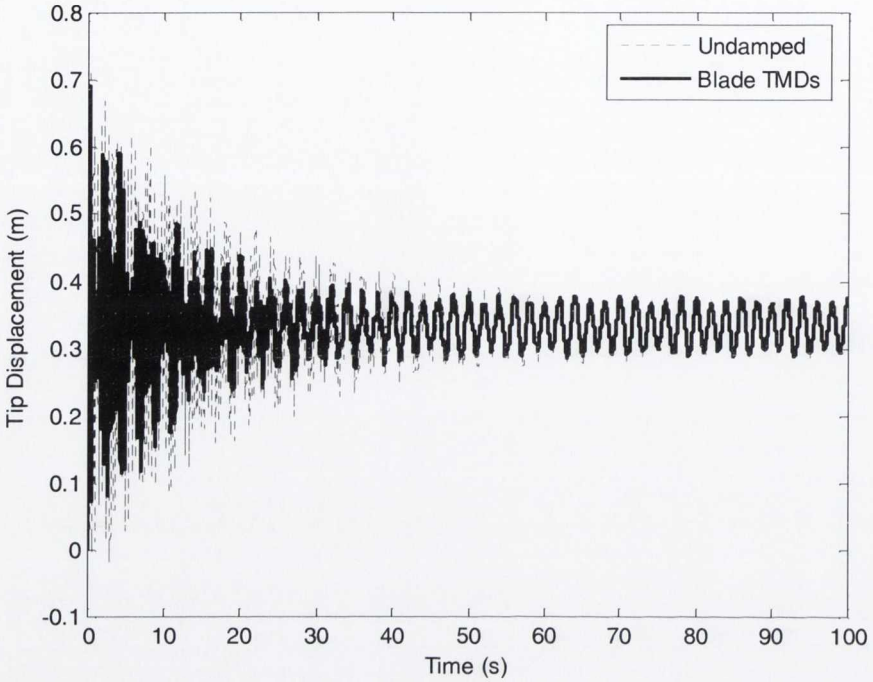

Figure 4.16: Flapwise response of blade 1, steady load, $\Omega = 3.14$rad/s, $\omega_{db} = 2.03$Hz

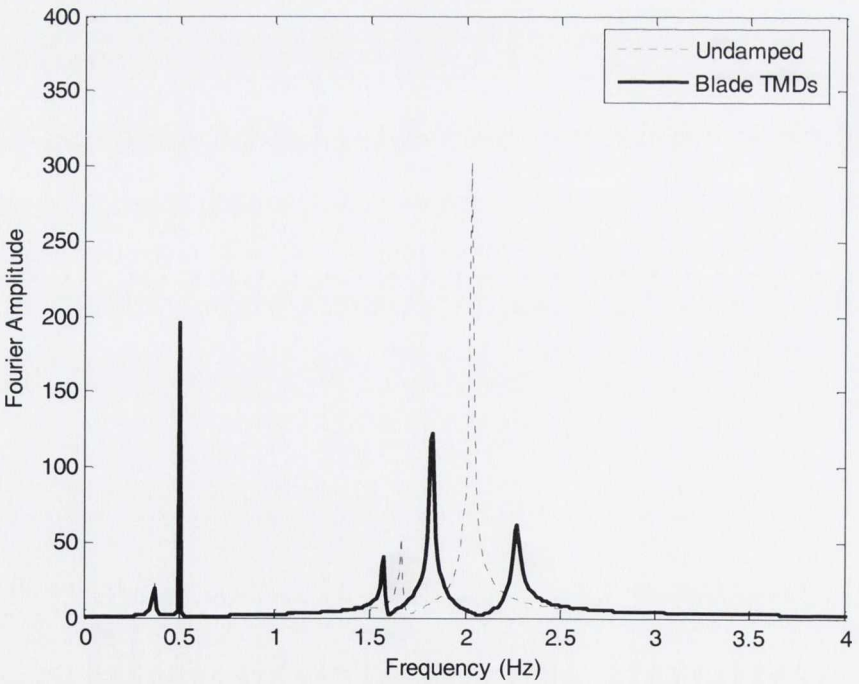

Figure 4.17: Blade 1 flapwise frequency spectrum, steady load, $\Omega = 3.14$rad/s, $\omega_{db} = 2.03$Hz

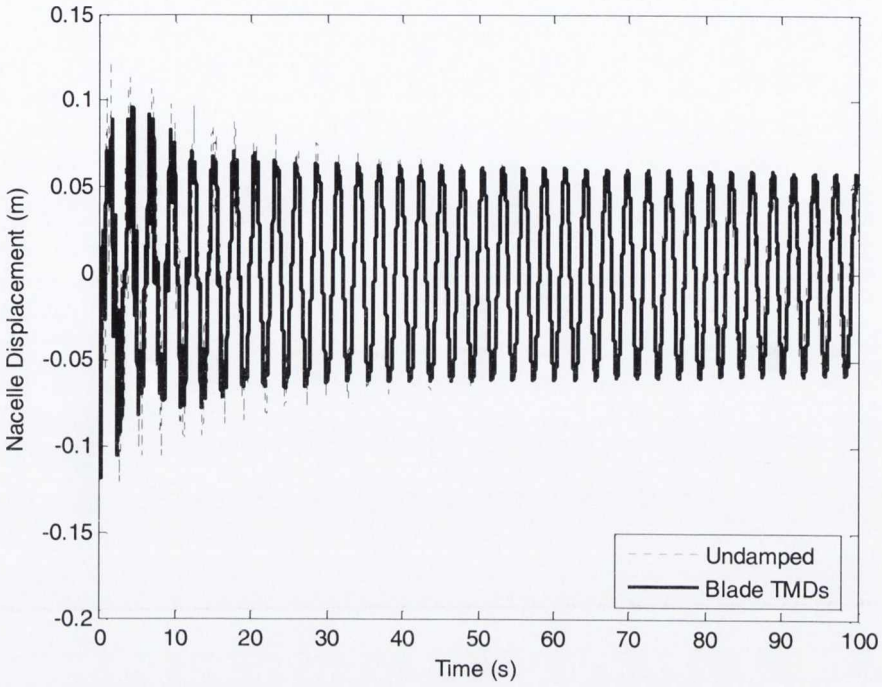

Figure 4.18: Flapwise response of nacelle, steady load, $\Omega = 3.14$rad/s, $\omega_{db} = 2.03$Hz

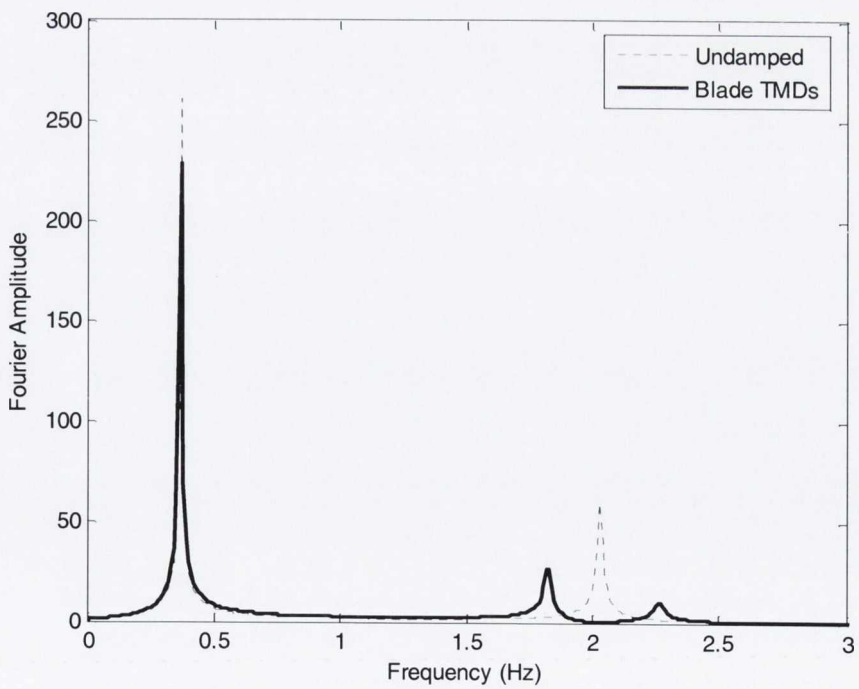

Figure 4.19: Nacelle flapwise frequency spectrum, steady load, $\Omega = 3.14$rad/s, $\omega_{db} = 2.03$Hz

The above results highlight the coupled peaks seen in the flapwise turbine model. As can be seen no reduction was achieved in the steady state response of the blades as the excitation frequency is sufficiently far from the frequency peaks in the blade response.

The rotational speed of the blades was then increased to look at the performance of the blade TMDs when the blades are excited at resonance. A rotational speed of 2Hz (12.5rad/s) was applied to the system. The blade TMDs were tuned to this frequency with the resulting time history response shown in figure 4.20. As can be seen a reduction of over two thirds is achieved by the TMDs at steady state as the blades are being excited at their resonant frequency.

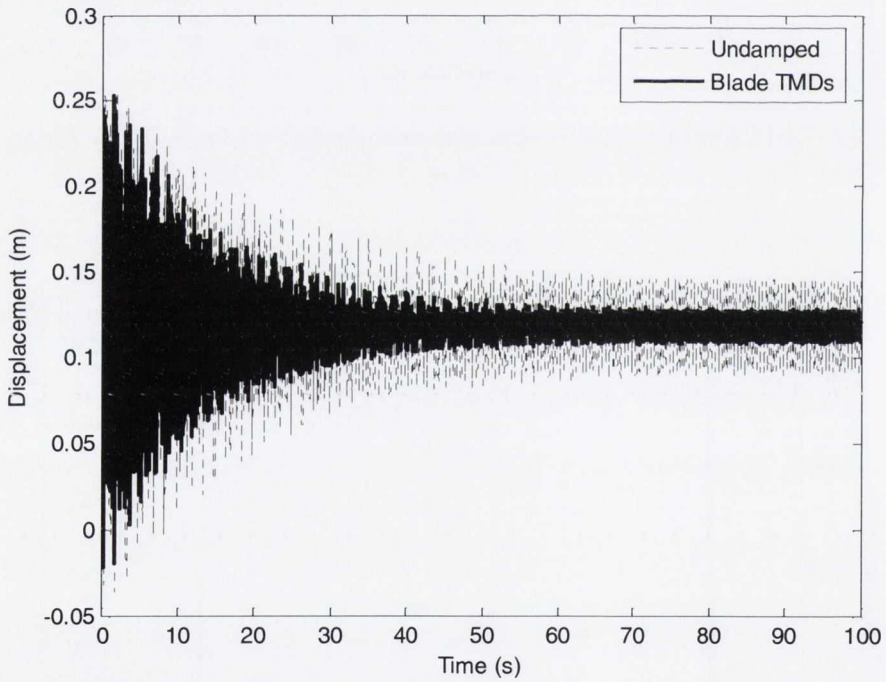

Figure 4.20: Flapwise response of blade 1, steady load, Ω = 13.5rad/s, ω_{db} = 2.15Hz

4.3 Edgewise Model

4.3.1 Addition of TMDs

As for the flapwise model TMDs were again added to the blades and nacelle, this time in the edgewise direction. Figure 4.21 below shows the edgewise model with the dampers attached.

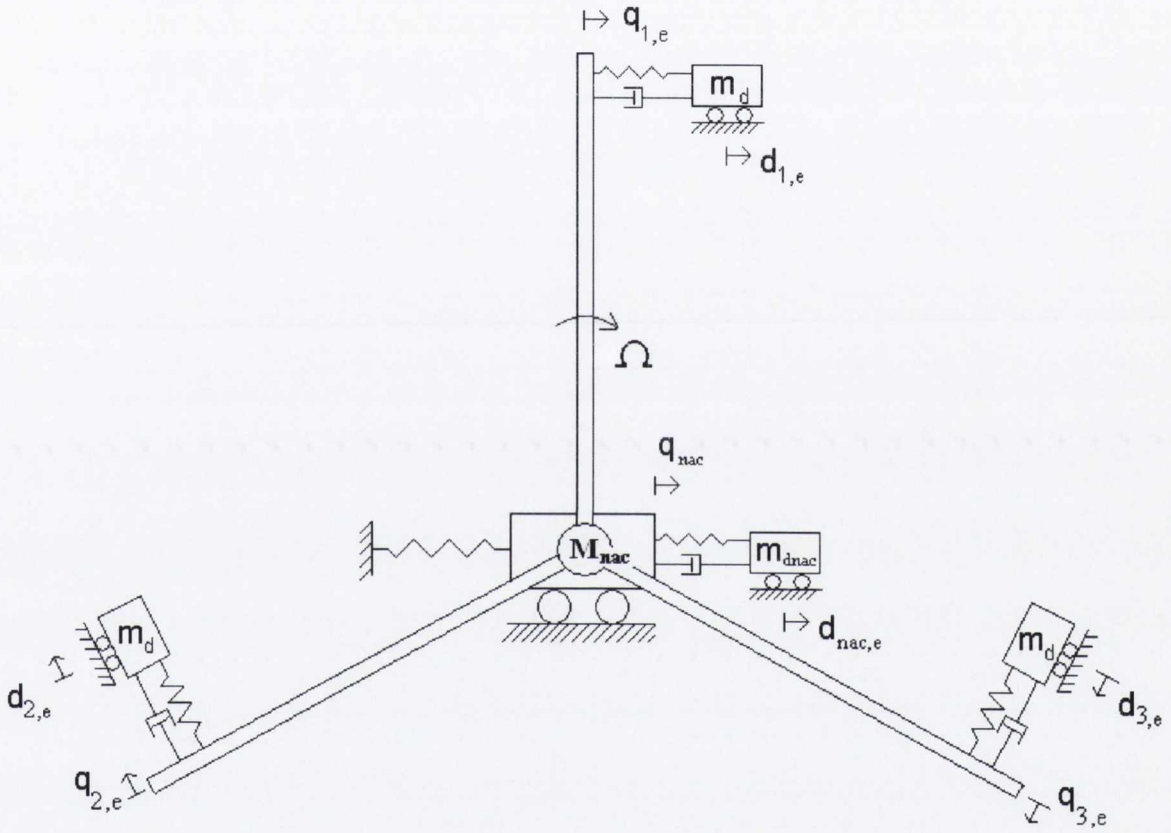

Figure 4.21: Edgewise model with TMDs attached

The relative displacements of the dampers are labelled $d_{i,e}$, where, as before 'i' indicates the degree of freedom and 'e' signifies the flapwise direction. Equations of motion were once more formulated for the edgewise model with the TMDs attached, which can be expressed in the form

$$[M_{e,damp}]\{\ddot{q}_{e,damp}\}+[C_{e,damp}]\{\dot{q}_{e,damp}\}+[K_{e,damp}]\{q_{e,damp}\}=\{Q_e\} \tag{4.5}$$

where $M_{e,damp}$, $C_{e,damp}$ and $K_{e,damp}$ represent the system matrices. The vector of displacements is given by $q_{e,damp}$, with the overdots signifying the first and second derivatives with respect to time, i.e. the velocity and acceleration vectors.

As detailed in Chapter 3, the edgewise model consists of time varying system matrices as can be seen in equations 4.6 to 4.13. As the damper is moving in the plane of blade rotation its motion may need to be restricted due to effects from the blade rotation. The effect of the bending of the blade on the damper deformation has not been considered. The damper displacement is therefore assumed to be transverse with respect to the blade at all times during the rotation. The final model consists of 8 dofs with a TMD at each blade tip and at the nacelle. As for the flapwise model, a mass ratio, μ, of 1% was assumed for the TMDs. The resulting system matrices are defined as shown with $c_{db,e}$ and $k_{db,e}$, and $c_{dnac,e}$ and $k_{dnac,e}$ representing the damping and stiffness present in the blade and nacelle dampers respectively.

$$M_{e,damp} = \begin{bmatrix} \frac{m_b}{3}+m_{db} & m_{db} & 0 & 0 & 0 & 0 & A_1 & 0 \\ m_{db} & m_{db} & 0 & 0 & 0 & 0 & B_1 & 0 \\ 0 & 0 & \frac{m_b}{3}+m_{db} & m_{db} & 0 & 0 & A_2 & 0 \\ 0 & 0 & m_{db} & m_{db} & 0 & 0 & B_2 & 0 \\ 0 & 0 & 0 & 0 & \frac{m_b}{3}+m_{db} & m_{db} & A_3 & 0 \\ 0 & 0 & 0 & 0 & m_{db} & m_{db} & B_3 & 0 \\ A_1 & B_1 & A_2 & B_2 & A_3 & B_3 & M_{nac}+3m_b+3m_{db}+m_{dnac} & m_{dnac} \\ 0 & 0 & 0 & 0 & 0 & 0 & m_{dnac} & m_{dnac} \end{bmatrix} \tag{4.6}$$

$$\text{with } A_i = \left(\frac{m_b}{3}+m_{db}\right)\cos\left(\Omega t+\frac{2\pi}{3}(i-1)\right) \tag{4.7}$$

$$\text{and } B_i = m_{db}\cos\left(\Omega t+\frac{2\pi}{3}(i-1)\right) \tag{4.8}$$

$$C_{e,damp} = \begin{bmatrix} c_{st,b} & 0 & 0 & 0 & 0 & 0 & 0 & 0 \\ 0 & c_{db,e} & 0 & 0 & 0 & 0 & C_1 & 0 \\ 0 & 0 & c_{st,b} & 0 & 0 & 0 & 0 & 0 \\ 0 & 0 & 0 & c_{db,e} & 0 & 0 & C_2 & 0 \\ 0 & 0 & 0 & 0 & c_{st,b} & 0 & 0 & 0 \\ 0 & 0 & 0 & 0 & 0 & c_{db,e} & C_3 & 0 \\ D_1 & C_1 & D_2 & C_2 & D_3 & C_3 & c_{st,nac} & 0 \\ 0 & 0 & 0 & 0 & 0 & 0 & 0 & c_{dnac,e} \end{bmatrix} \tag{4.9}$$

$$\text{with } C_i = -m_{db}\Omega \sin\left(\Omega t + \frac{2\pi}{3}(i-1)\right) \tag{4.10}$$

$$\text{and } D_i = \left(\frac{-2m_b}{3} - 2m_{db}\right)\sin\left(\Omega t + \frac{2\pi}{3}(i-1)\right) \tag{4.11}$$

$$K_{e,damp} = \begin{bmatrix} \frac{4EI_e}{L^3} + \frac{\Omega^2 m_b}{15} - m_{db}\Omega^2 & 0 & 0 & 0 & 0 & 0 & 0 & 0 \\ 0 & k_{db,e} & 0 & 0 & 0 & 0 & 0 & 0 \\ 0 & 0 & \frac{4EI_e}{L^3} + \frac{\Omega^2 m_b}{15} - m_{db}\Omega^2 & 0 & 0 & 0 & 0 & 0 \\ 0 & 0 & 0 & k_{db,e} & 0 & 0 & 0 & 0 \\ 0 & 0 & 0 & 0 & \frac{4EI_e}{L^3} + \frac{\Omega^2 m_b}{15} - m_{db}\Omega^2 & 0 & 0 & 0 \\ 0 & 0 & 0 & 0 & 0 & k_{db,e} & 0 & 0 \\ E_1 & 0 & E_2 & 0 & E_3 & 0 & K_{nac} & 0 \\ 0 & 0 & 0 & 0 & 0 & 0 & 0 & k_{dnac,e} \end{bmatrix} \tag{4.12}$$

$$\text{where } E_i = \left(\frac{-m_b}{3} - m_{db}\right)\Omega^2 \cos\left(\Omega t + \frac{2\pi}{3}(i-1)\right) \tag{4.13}$$

As before '*i*' denotes the blade under consideration.

4.3.2 Effectiveness of TMDs

As for the flapwise model results above a steady wind load in the edgewise direction was used to assess the behaviour of the TMDs (equation 3.29). The vibration mitigating effects of the nacelle and blade TMDs were again considered separately.

4.3.2.1 TMD at the Nacelle

A TMD was added to the nacelle in the plane of blade rotation to reduce vibrations in the edgewise direction. Figures 4.22 and 4.23 show the displacement response and corresponding frequency spectrum of the nacelle for a constant rotational speed of 3.14rad/s. These were plotted previously in section 3.3.3.1 of this thesis. As can be observed in figure 4.23, three peaks are seen in the frequency response. The dominant peak at 0.37Hz is close to the natural frequency of the nacelle/tower, while the other two peaks are closer to the blade natural frequency.

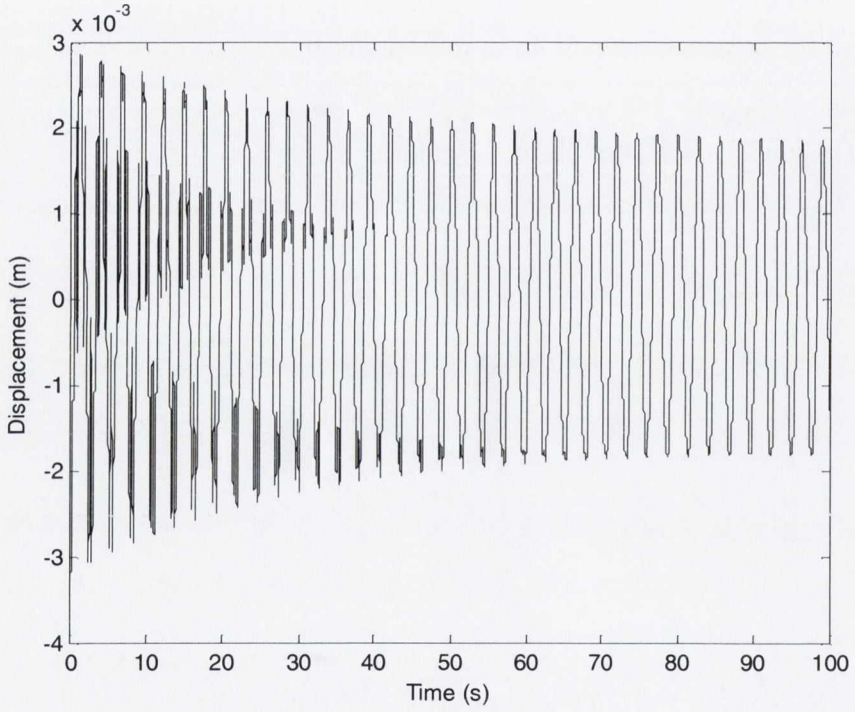

Figure 4.22: Edgewise response of the nacelle, steady load, Ω = 3.14rad/s

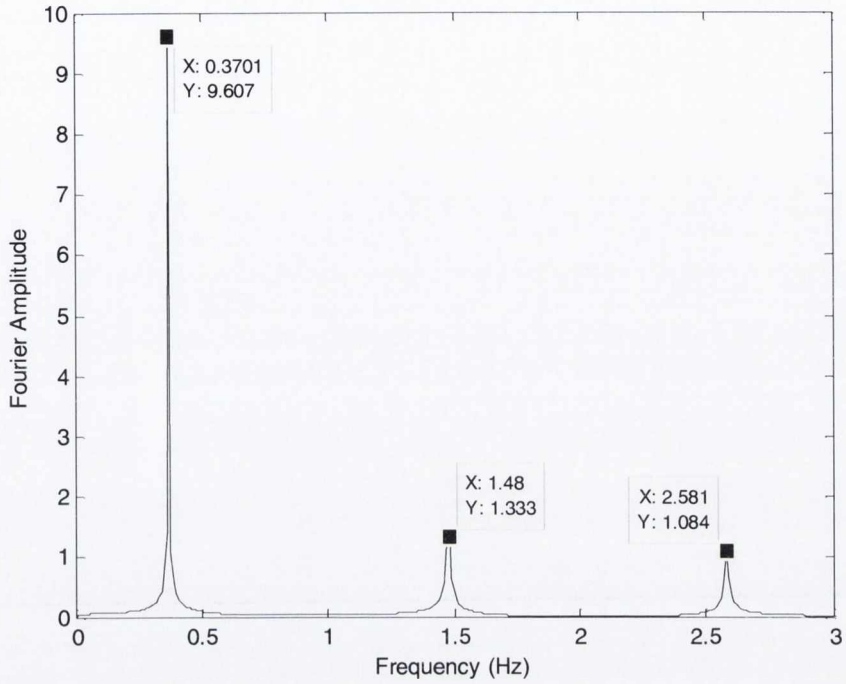

Figure 4.23: Nacelle edgewise frequency spectrum, steady load, Ω = 3.14rad/s

The TMD was first tuned to the dominant peak at 0.37Hz. A large reduction was seen in the response of the nacelle, shown in figure 4.24. As before a tuning ratio of 1 achieves a near optimal reduction. This is confirmed by the near equal height peaks either side of the original undamped peak in the corresponding frequency spectrum. This is plotted in figure 4.25. No reduction was seen in the response of the blades indicating that this peak is uncoupled to any of the blade resonant frequencies.

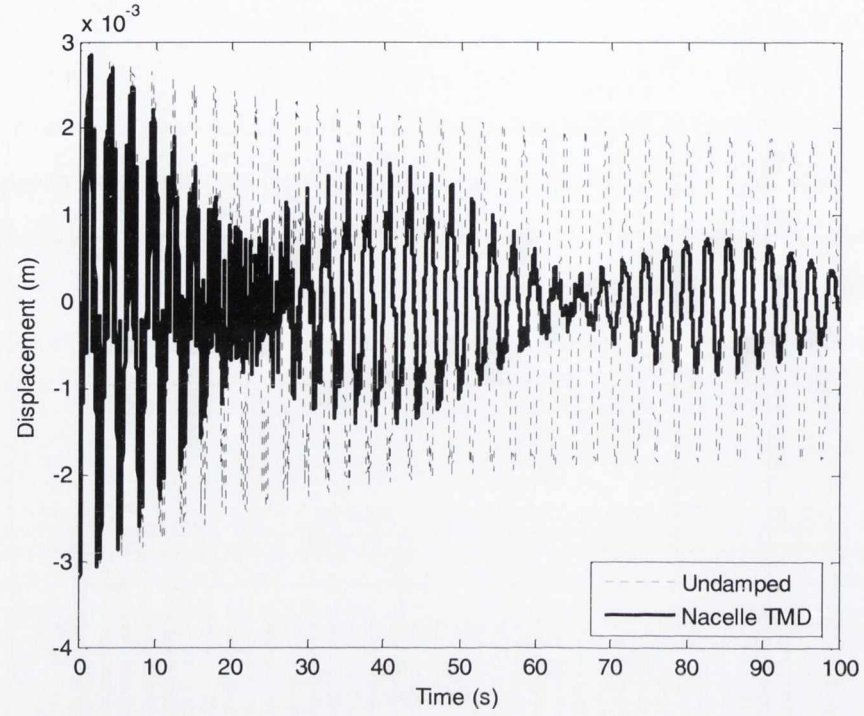

Figure 4.24: Edgewise response of nacelle, steady load, $\Omega = 3.14$rads/s, $\omega_{dnac} = 0.37$Hz

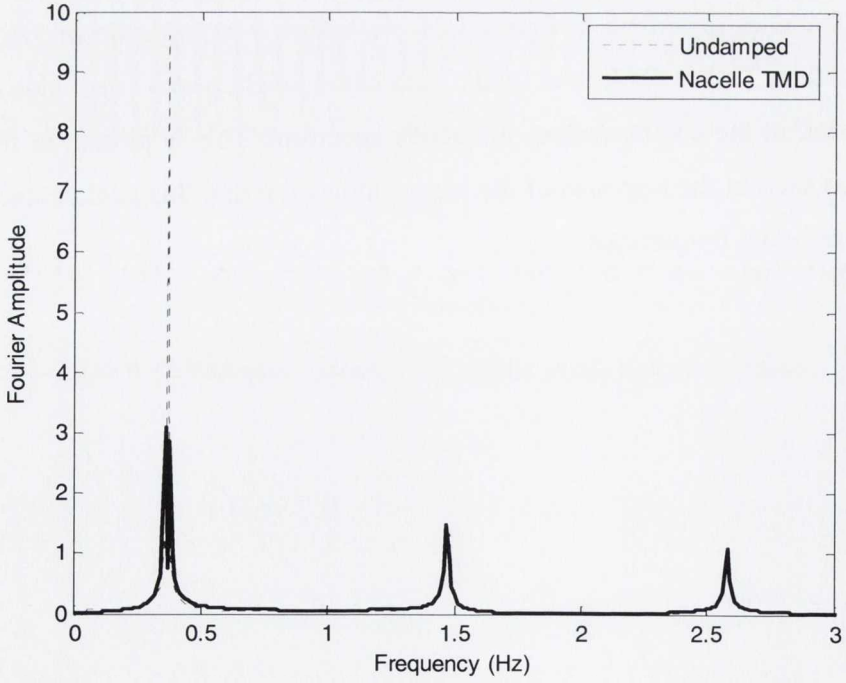

Figure 4.25: Nacelle edgewise frequency spectrum, steady load, $\Omega = 3.14$rads/s, $\omega_{dnac} = 0.37$Hz

The simulations were then repeated with the TMD tuned to the second frequency peak at 1.48Hz in figure 4.23. A small reduction is initially achieved in the transient response of the nacelle, illustrated in figure 4.26. This is a result of the lower amplitude of this peak. The frequency response of the nacelle is shown in figure 4.27.

A negligible reduction was also achieved in the blades. The displacement response of blade one is plotted in figure 4.28 with the corresponding frequency spectrum shown in figure 4.29. As can be seen in the frequency spectrum, no real reduction is achieved with the nacelle TMD.

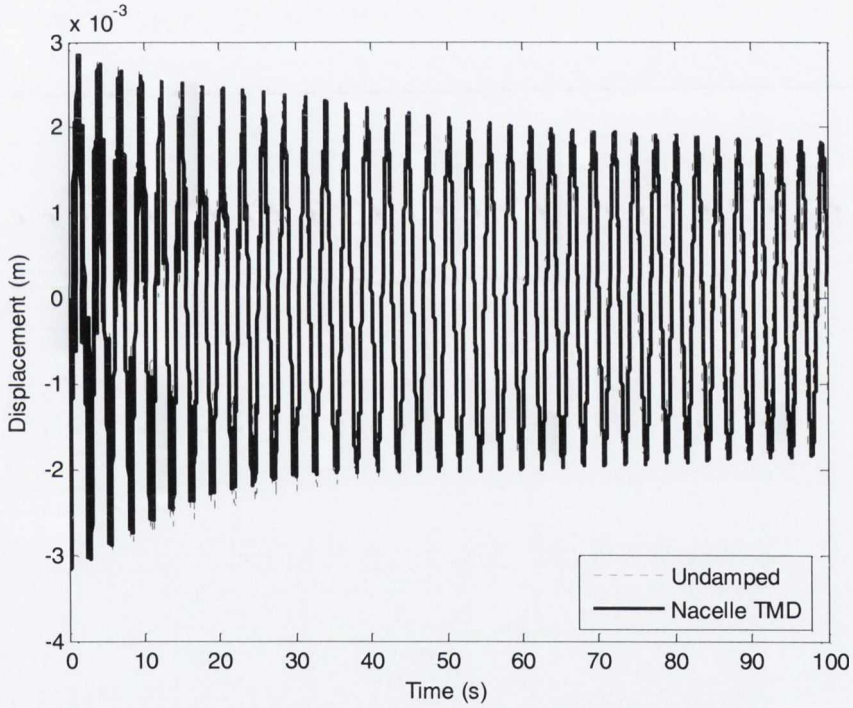

Figure 4.26: Edgewise response of nacelle, steady load, $\Omega = 3.14$rads/s, $\omega_{dnac} = 1.48$Hz

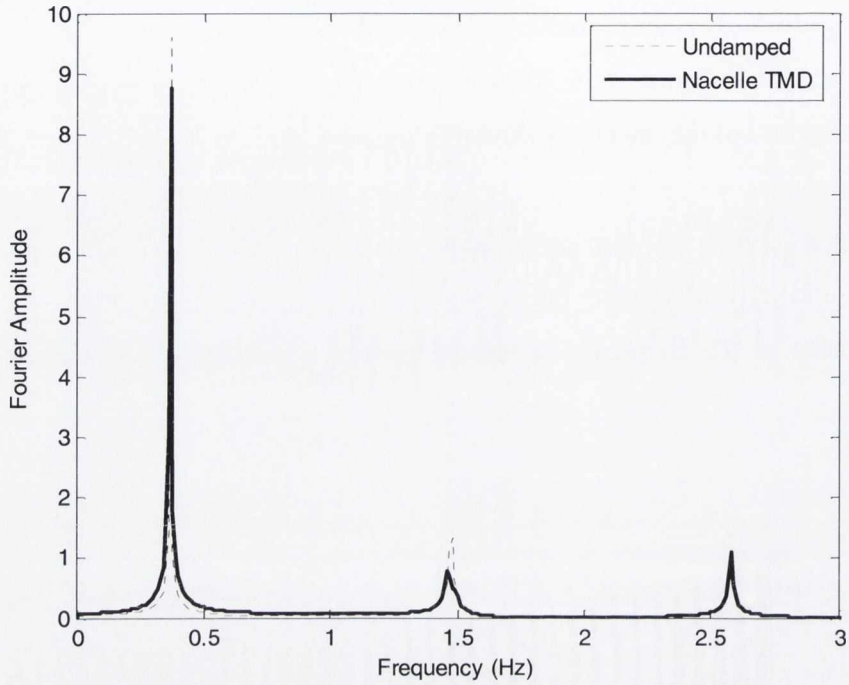

Figure 4.27: Nacelle edgewise frequency spectrum, steady load, $\Omega = 3.14$rads/s, $\omega_{dnac} = 1.48$Hz

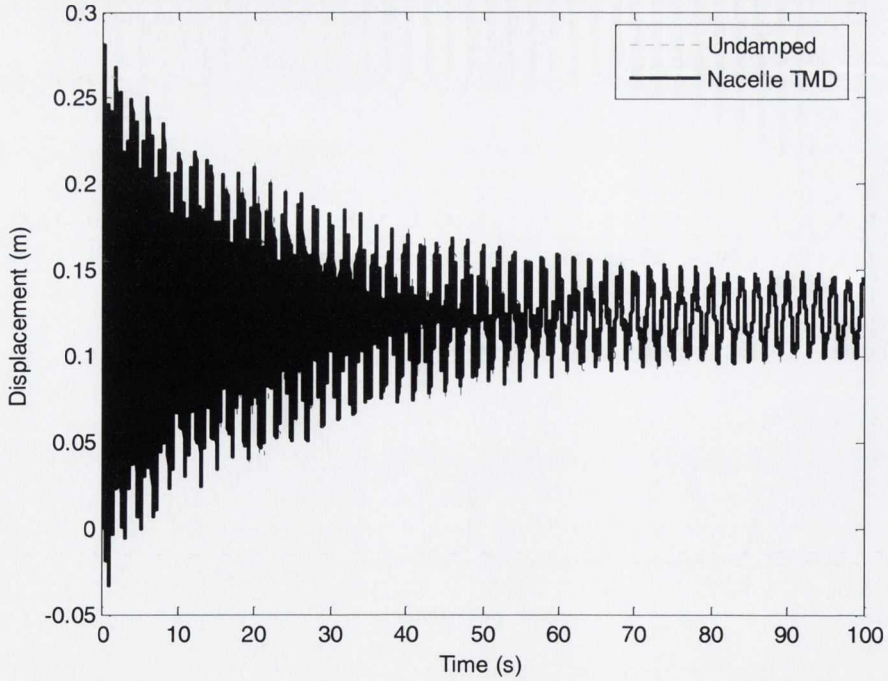

Figure 4.28: Edgewise response of blade 1, steady load, $\Omega = 3.14$rads/s, $\omega_{dnac} = 1.48$Hz

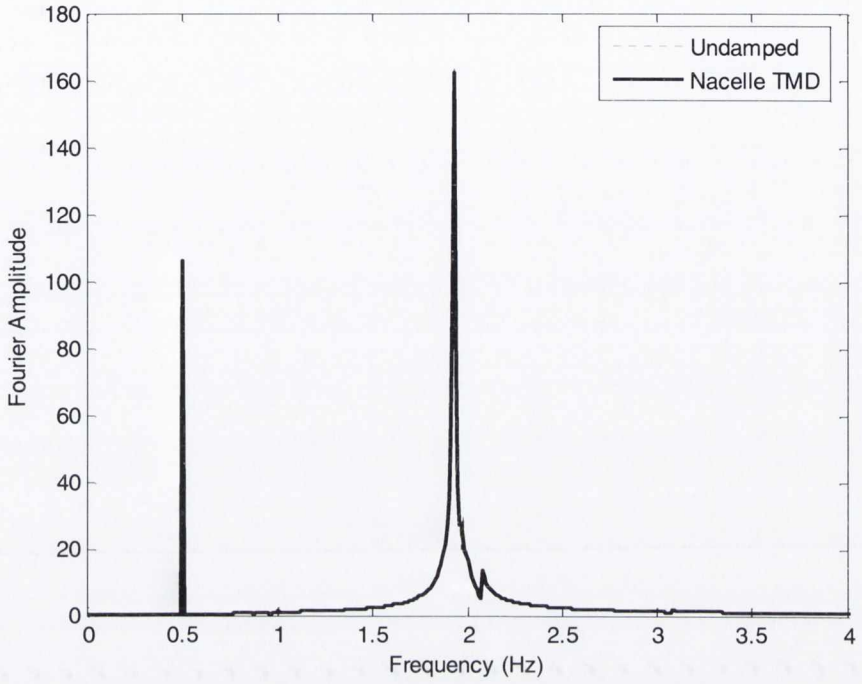

Figure 4.29: Blade 1 edgewise frequency spectrum, steady load, $\Omega = 3.14$rads/s, $\omega_{dnac} = 1.48$Hz

Finally, tuning to the third peak in the nacelle frequency spectrum was also analysed. This occurs at a frequency of 2.58Hz as previously seen. Due to the similar amplitude of this peak to the peak at 1.48Hz almost identical results were seen for both the nacelle and blades.

4.3.2.2 TMDs in the Blades

As for the flapwise model in section 4.2.2.2 TMDs were also added to the blades to mitigate vibrations in the edgewise direction. Figures 4.30 and 4.31 show the displacement response and corresponding frequency spectrum of blade one, again for a constant rotational speed of 3.14rad/s. As for the flapwise model, a peak is seen at 0.5Hz which corresponds to the forcing function frequency and rotational speed of the blades. Tuning the TMDs to this peak was once more found to be ineffective as it doesn't correspond to a resonant frequency in the blades. The tuning of the blade TMDs were therefore focussed on the peak seen near 2Hz, which is close to the natural frequency of the blades.

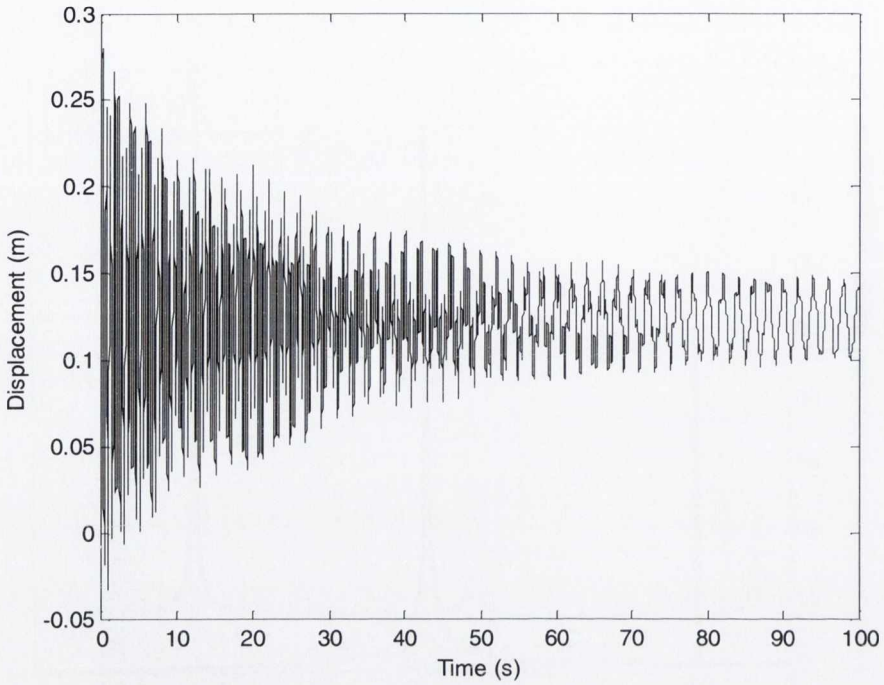

Figure 4.30: Blade 1 edgewise response, steady load, Ω = 3.14rad/s

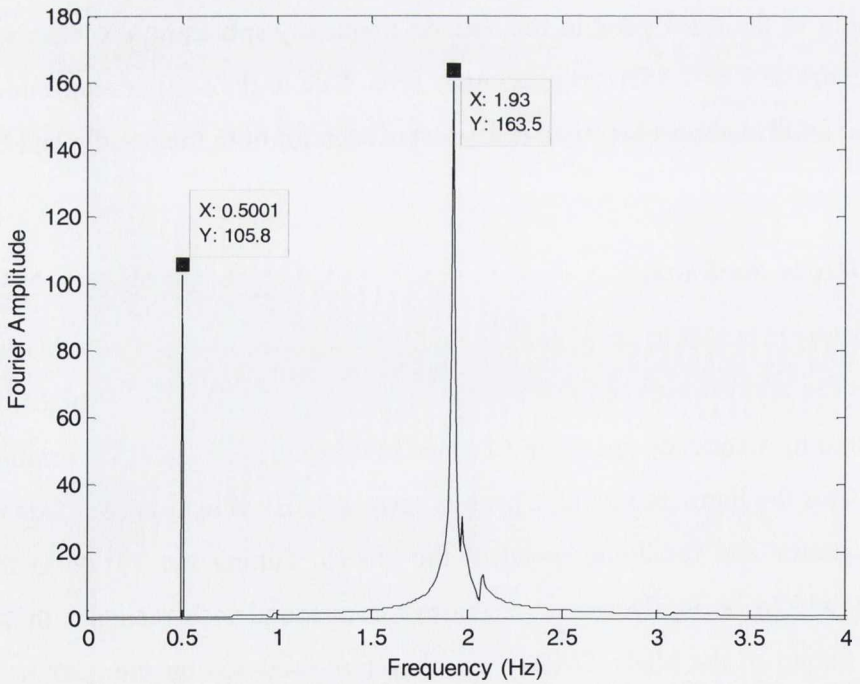

Figure 4.31: Blade 1 edgewise frequency spectrum, steady load, Ω = 3.14rad/s

As expected a good reduction is seen in the transient response of the blades plotted in figure 4.32. As for the flapwise results no reduction is seen at steady state as the excitation frequency doesn't correspond to any of the turbine frequency peaks. The corresponding frequency spectrum in figure 4.33 shows the peak at 1.93Hz to be significantly reduced in magnitude. The nacelle displacement is plotted in figure 4.34. The frequency response plot in figure 4.35 shows that the peaks at 1.48Hz and 2.58Hz have both been suppressed through the coupling between the blades and nacelle. A small reduction results during transience in the nacelle displacement response as seen in figure 4.34. No reduction is achieved at steady state as the loading frequency again doesn't correspond to any of the resonant frequencies in the system.

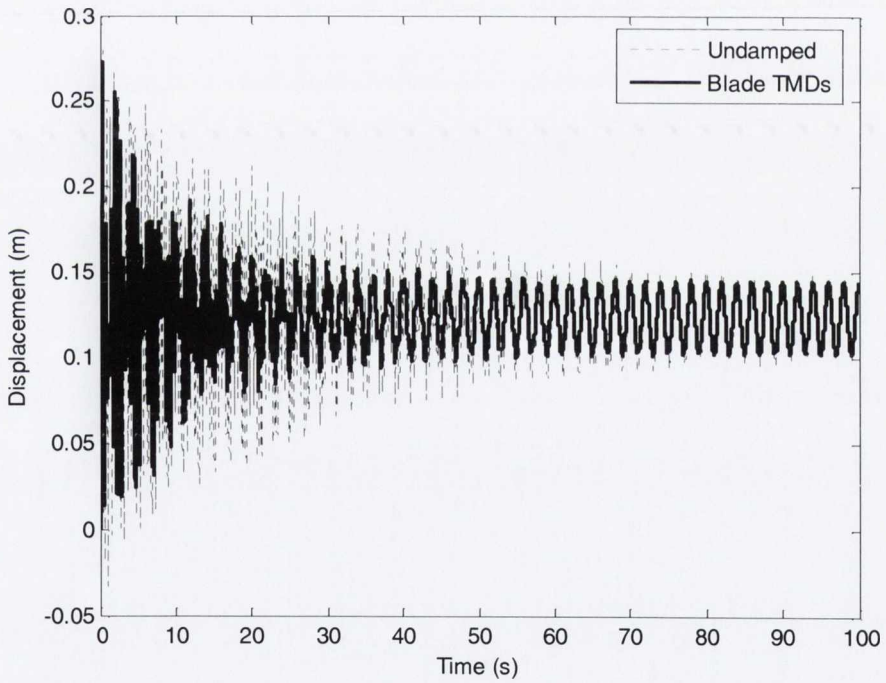

Figure 4.32: Edgewise response of blade 1, steady load, Ω = 3.14rads/s, ω_b = 1.93Hz

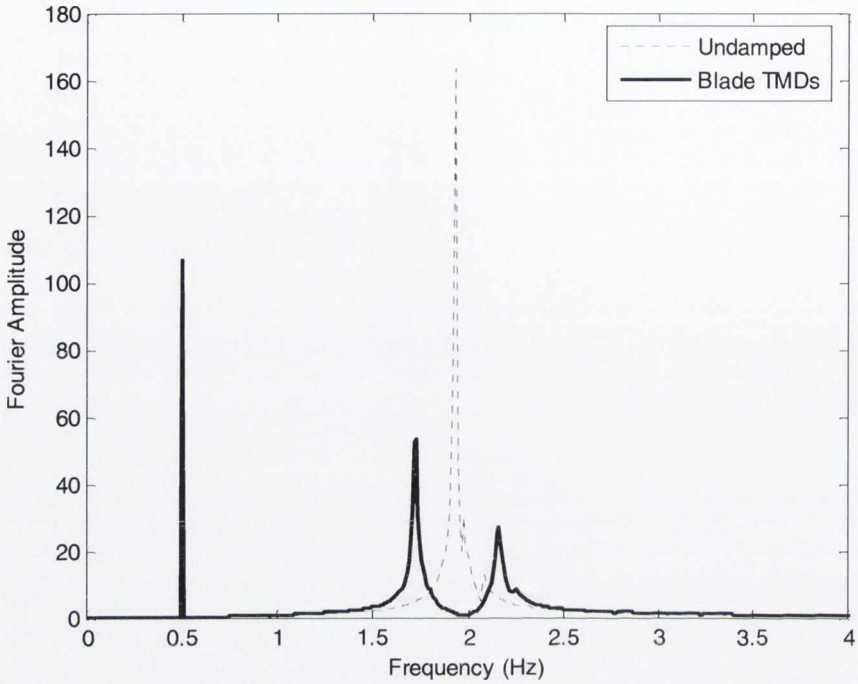

Figure 4.33: Blade 1 edgewise frequency spectrum, steady load, $\Omega = 3.14$rads/s, $\omega_b = 1.93$Hz

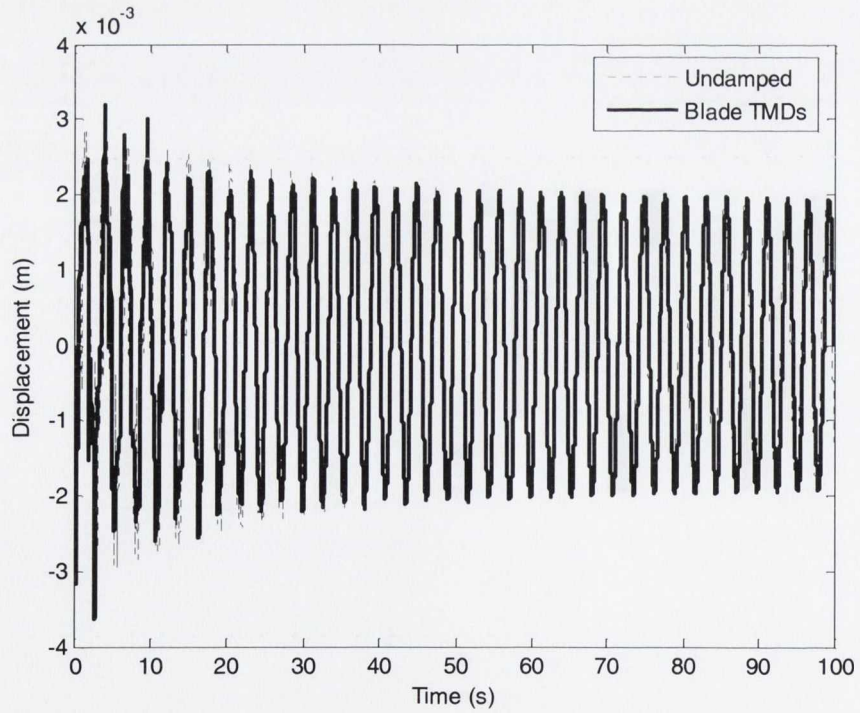

Figure 4.34: Edgewise response of nacelle, steady load, $\Omega = 3.14$rads/s, $\omega_b = 1.93$Hz

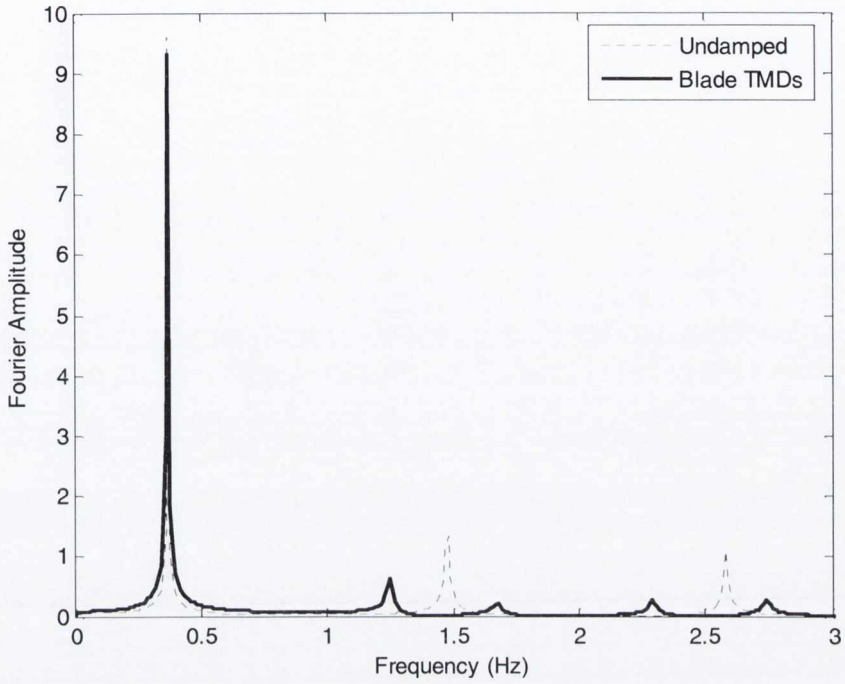

Figure 4.35: Nacelle edgewise frequency spectrum, steady load, $\Omega = 3.14$rads/s, $\omega_b = 1.93$Hz

As for the flapwise model, the rotational speed of the turbine was increased to allow the system to be excited at resonance. A rotational speed of 12.5 rad/s or 2Hz once more achieved this. The blade TMDs were tuned to this frequency. The response of blade one is shown in figure 4.36. A huge reduction of approximately 90% is achieved during steady state as the blades are being excited near their resonant frequency highlighting the effectiveness of the TMDs.

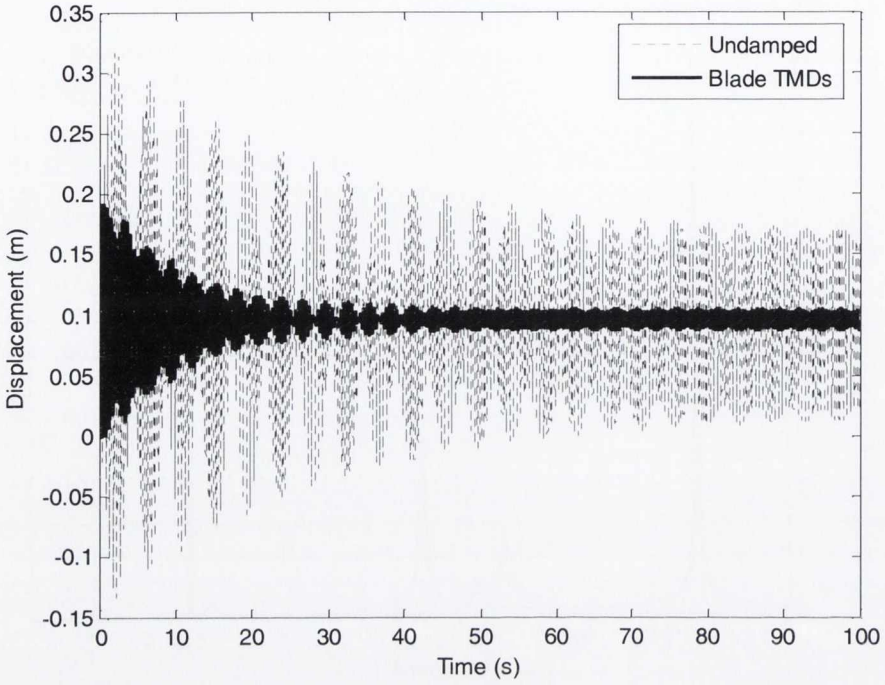

Figure 4.36: Flapwise response of blade 1, steady load, $\Omega = 13.5$rad/s, $\omega_{db} = 2.15$Hz

4.4 Conclusions

This chapter detailed the inclusion of vibration mitigating devices to study their effectiveness in reducing the response of the dynamic model developed in chapter 3. Passive dampers were added to the nacelle and blades of the turbine as outlined above. These were modelled as mass-spring-dashpot systems, representative of a TMD or equivalent TLD. A simple steady wind load was assumed to excite the blades. Tuning to each of the frequency peaks in the system was investigated in turn for both the flapwise and edgewise models. This allowed the coupled peaks in the model to be observed. The rotational speed of the blades dictated the frequency of the loading. For a slow rotational speed, typical of a modern operating wind turbine, it was found that the blades were not excited at resonance. Hence, no reduction was seen once steady state was achieved. However, the TMDs did mitigate the blade displacement during the transient phase of the response.

The blades were also excited at resonance by increasing their rotational speed so the frequency of the steady wind load corresponded to the largest frequency peak in the blades.

As expected good reduction was achieved at steady state by inclusion of the TMDs. For the flapwise model a reduction of over two thirds was seen while for the edgewise model a reduction of 90% was observed.

Furthermore, while passive dampers have been shown to effectively reduce the response of both the blades and nacelle/tower, their main limitation arises from their inability to cater for changes in the dynamic parameters of the primary system. As a result, smart control methods are needed to effectively mitigate the response of the turbine structure while catering for changes in the system dynamics. The following chapter presents a semi-active control algorithm which can cater for such changes and successfully control the behaviour of the structure. The steady wind load considered in this chapter is replaced by a turbulent wind load, more representative of a loading scenario experienced by a real life wind turbine.

CHAPTER 5 - Semi-Active Control Algorithm Using a Short Time Fourier Transform Method

5.1 Introduction

In chapter 4, passive dampers in the form of TMDs were added to the flapwise and edgewise models. These were represented by mass-spring-dashpot systems. Accurate tuning of the TMDs was found to successfully mitigate the dynamic response of the turbine for the steady wind load considered. However, with modern wind turbines operating at variable rotational speeds and experiencing more complex loading scenarios, the need for intelligent control methods to cater for changes in the dynamic parameters of the system due to changes in operational and environmental conditions has become apparent.

In this chapter STMDs have been proposed for structural vibration control and a smart control algorithm has been presented, allowing real time tuning of these dampers to the resonant frequencies of the turbine structure. The algorithm controls the tuning of the dampers in the blades and the nacelle, and has been applied to both the flapwise and edgewise models. Variations in the dynamic parameters of the system were investigated to determine if the algorithm could successfully cater for changes in the behaviour of the turbine. Its effectiveness in mitigating vibrations was studied for a turbulent wind load, typical of that experienced by an operational wind turbine.

5.2 Semi Active Control Strategy

5.2.1 Short Time Fourier Transform

The semi-active control algorithm developed was based on a Short Time Fourier Transform (STFT) technique as outlined by Nagarajaiah and Basu (2009). The Fourier Transform of a signal $s(t)$ is given by

$$s(\omega) = \frac{1}{\sqrt{2\pi}} \int s(t) e^{-j\omega t} dt \tag{5.1}$$

However, a disadvantage of the Fourier transform is that it calculates the frequency distribution of the entire signal. To counteract this, the STFT was devised which splits the signal up into small time segments. Each one is then analyzed by a Fourier Transform to ascertain the frequencies present. By combining each of these frequency spectra the time frequency distribution of the system can be attained. The STFT can be formulated as

$$s_t(\omega) = \frac{1}{\sqrt{2\pi}} \int_{-\infty}^{\infty} s(\tau) h(\tau - t) e^{-j\omega t} dt \tag{5.2}$$

where $s(\tau)$ is the short time segment and $h(\tau - t)$ is a window function that emphasizes the signal around the time, *t*.

5.2.2 STFT Control Algorithm

Significant research has been carried out into the use of STFT techniques for development of semi-active control algorithms (Nagarajaiah and Varadarajan, 2005, Nagarajaiah and Sonmez, 2007). The STFT algorithm presented in this study allows the STMDs to be tuned in real-time to the dominant frequencies in the system. Before each segment is Fourier analysed it is multiplied by a window function as outlined in equation 5.2. A Hanning window function was chosen which emphasized the local frequencies near the current time to allow real-time tuning of the dampers. The dominant frequencies in each time segment are then identified and the STMDs tuned to these frequencies. The process is repeated every second allowing the tuning of the STMDs to be adjusted in real-time as the frequencies of the system change. The semi-active algorithm is illustrated in the flow chart in figure 5.1.

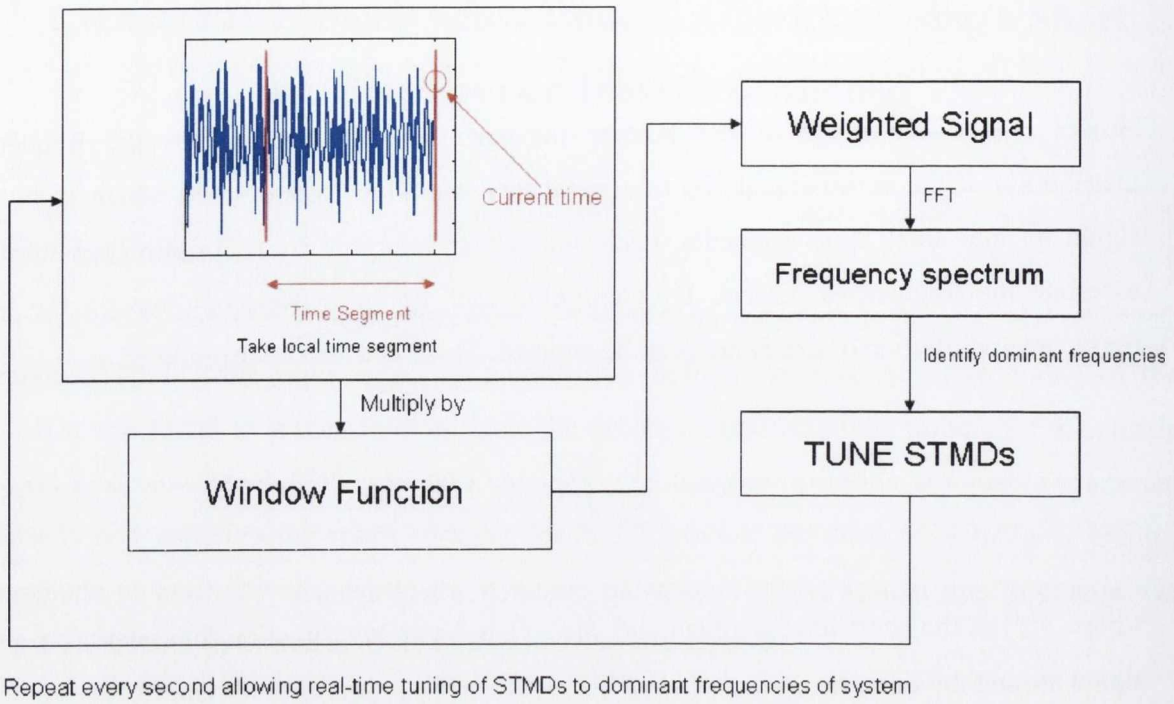

Figure 5.1: Semi-active control algorithm

In order to assess the effectiveness of the semi-active algorithm, some parameters of the turbine model were varied over time to see if the STMDs could adjust for these changes in the behaviour of the system. The parameters considered were:

- the rotational speed of the blades, Ω
- the natural frequency of the blades, ω_b
- the natural frequency of the nacelle, ω_{nac}

In each set of results, the undamped and damped responses are plotted to highlight the effectiveness of the STFT algorithm. The simulations run for an initial period of 41 seconds and the STFT algorithm is then activated. This facilitates the collection of data for the first time segment of 40 seconds, needed for the STFT computations. Every second this window is subsequently updated allowing real-time tracking of the dominant frequencies in the response of the turbine. This results in a frequency step of 0.025Hz. Use of a smaller window means a larger sampling frequency and can result in mistuning of the STMDs, i.e. not been tuned close

enough to the dominant frequencies to have a significant vibration mitigation effect. During the passive phase, the TMDs are detuned so the real-time tuning of the dampers can be seen when the semi-active algorithm is initiated.

5.3 Flapwise Model Results

The semi-active control strategy as outlined in the previous section was first applied to the flapwise model.

5.3.1 Turbulent Wind load

The effectiveness of the algorithm in controlling the response of the system when subjected to the turbulent loading outlined in section 3.2.3.2 is presented in this section. This represents a more realistic loading scenario than the steady wind load considered in chapter 4 of this thesis.

Simulations were first run with all parameters constant. A rotational speed of 3.14rad/s (0.5Hz), typical of a modern wind turbine, was considered. Figure 5.2 shows the displacement response of blade one. The STFT algorithm initiates at t = 41s due to the window size of 40s. As can be seen a good reduction is achieved in the blade tip displacement from t = 41s for this broad banded turbulent load. While no reduction is seen in the maximum blade displacement a reduction of over 50% is frequently achieved throughout the response. Figure 5.3 outlines the behaviour of the blade STMD, plotting the blade displacement, the STMD displacement and the STMD tuning. At t = 41s the STMD is seen to tune to the dominant frequency in the blade response and adjusts in real-time throughout the remainder of the time history, hence achieving the reduction seen in the blade displacement in figure 5.2. Similar results were achieved for blades 2 and 3.

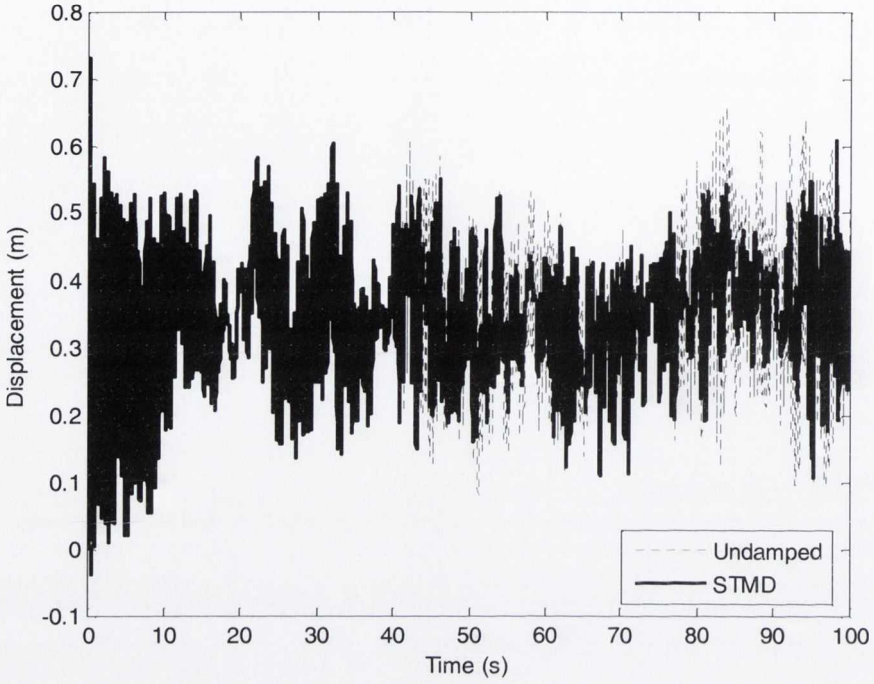

Figure 5.2: Flapwise response of blade 1, turbulent load, Ω = 3.14rad/s

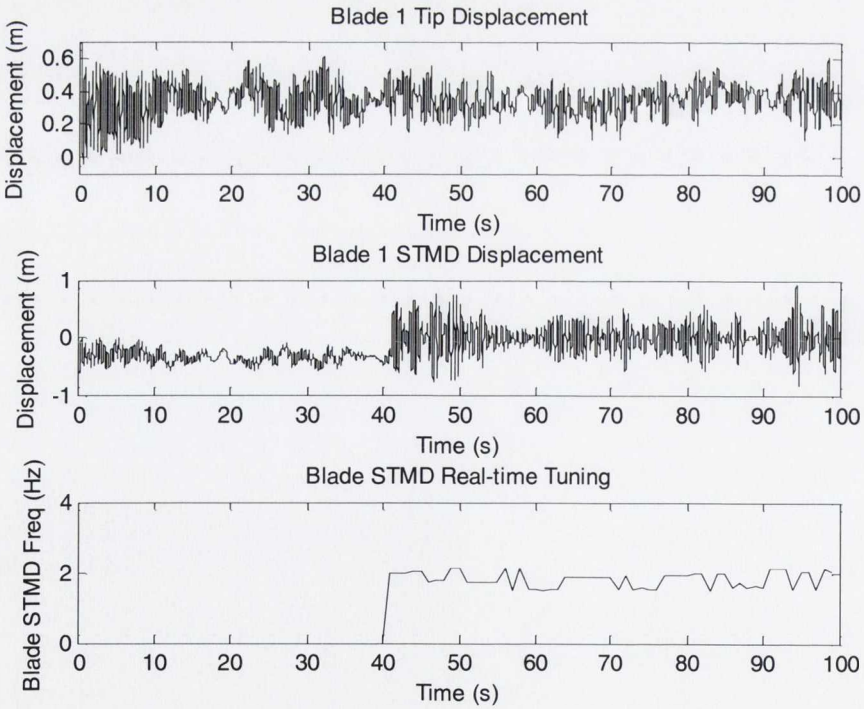

Figure 5.3: Blade flapwise STMD behaviour, turbulent load, Ω = 3.14rad/s

Figure 5.4 shows the response of the nacelle. Once more, the STMD is observed to initiate at t = 41s achieving a reduction in nacelle displacement throughout the remainder of the time history. A reduction of 50% is achieved in the maximum nacelle displacement with a reduction of up to two thirds seen throughout the response once the semi-active algorithm kicks in.

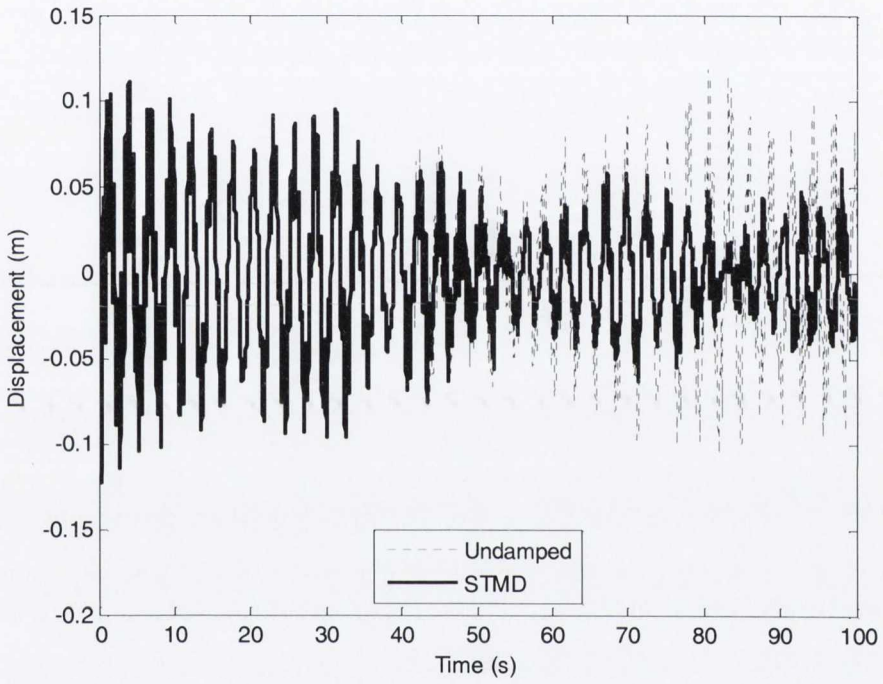

Figure 5.4: Flapwise response of the nacelle, turbulent load, Ω = 3.14rad/s

Figure 5.5 plots the behaviour of the nacelle STMD. The damper is once more seen to tune in real-time to the dominant frequency in the response of the nacelle once the control algorithm initiates at t = 41s.

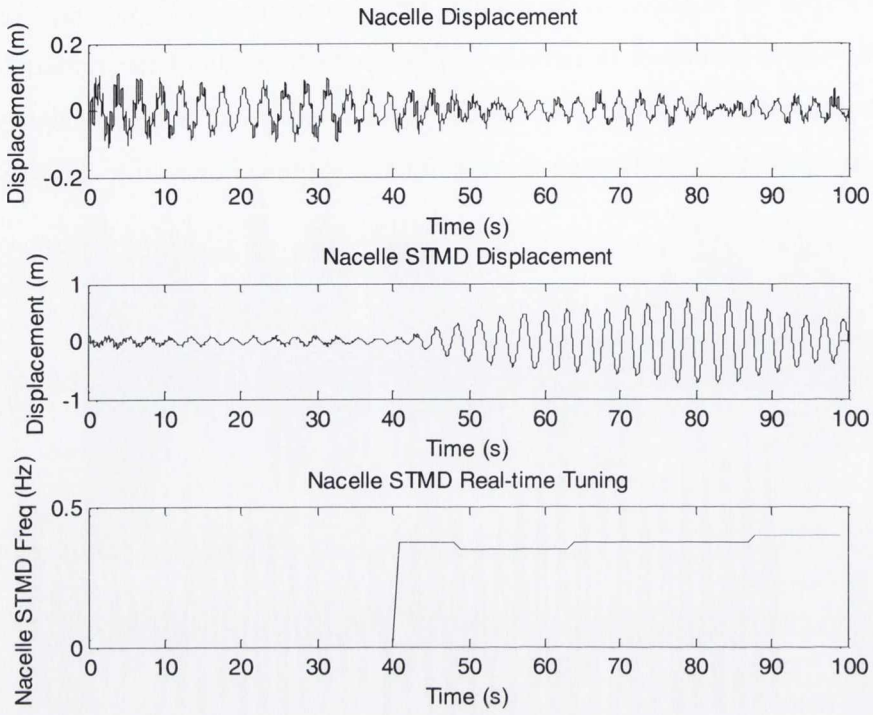

Figure 5.5: Nacelle flapwise STMD behaviour, turbulent load, Ω = 3.14rad/s

Variation in the three dynamic parameters of the system outlined previously in section 5.2.2 was then considered. This allowed assessment of the ability of the algorithm to adjust in real-time to changes in the dynamic parameters of the turbine.

5.3.1.1 Variation in the Rotational Speed, Ω

Many modern wind turbines operate at variable rotational speeds. With this in mind the rotational speed was assumed to slow down linearly from 3.14 to 1.57rad/s over 180s. Figure 5.6 shows the displacement response of blade one. A window size of 40s has again been applied with the algorithm initiating at t = 41s. Figure 5.7 shows the corresponding behaviour of the blade STMD, with figures 5.8 and 5.9 illustrating the displacement response and STMD behaviour of the nacelle. Significant reductions of up to 50% are achieved in the displacement response of the blade and nacelle when the STMD takes effect. Similar reductions were achieved for the other two blades.

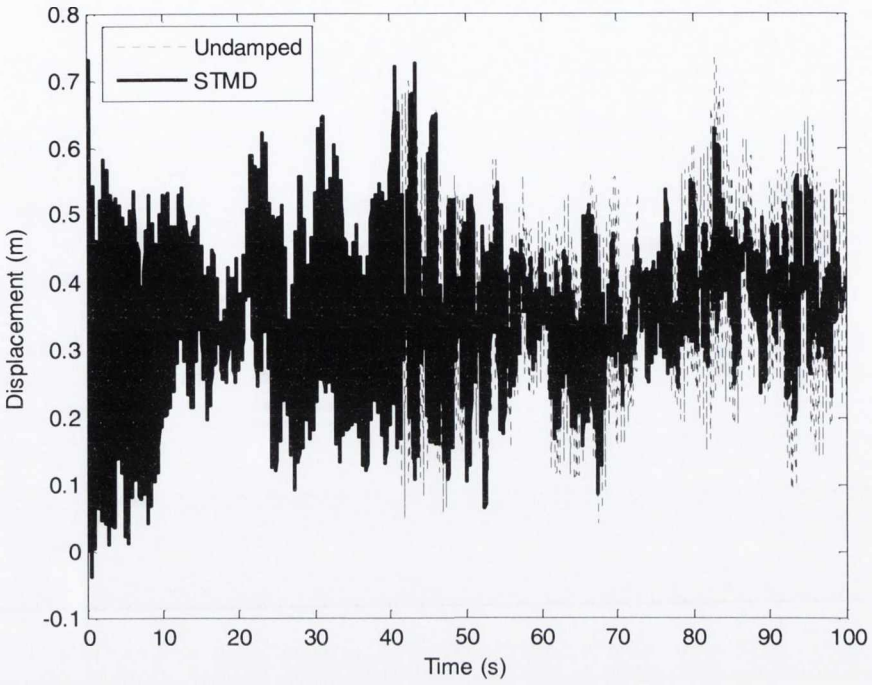

Figure 5.6: Flapwise response of blade 1, turbulent load, variable Ω

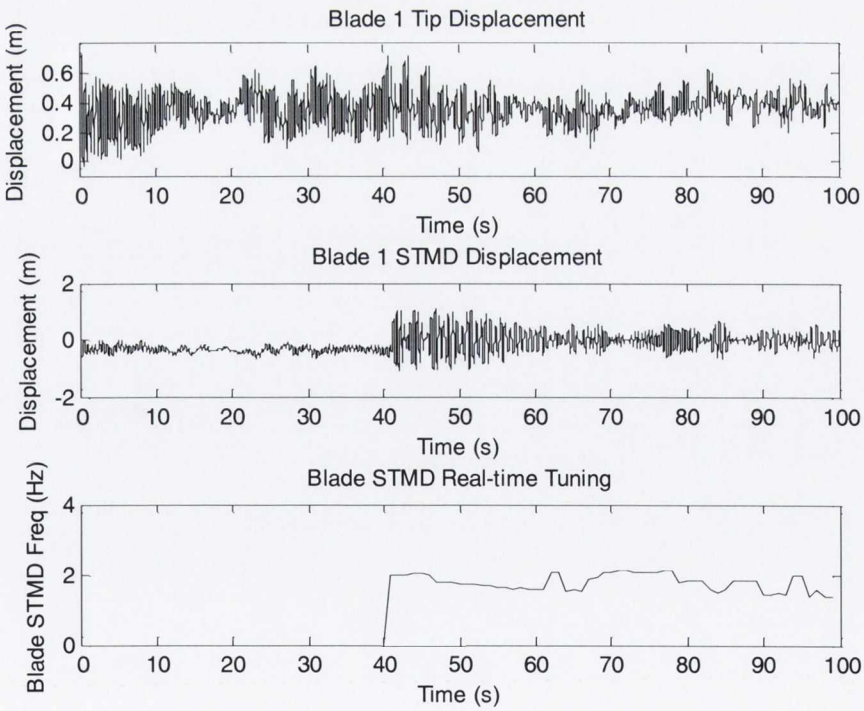

Figure 5.7: Blade flapwise STMD behaviour, turbulent load, variable Ω

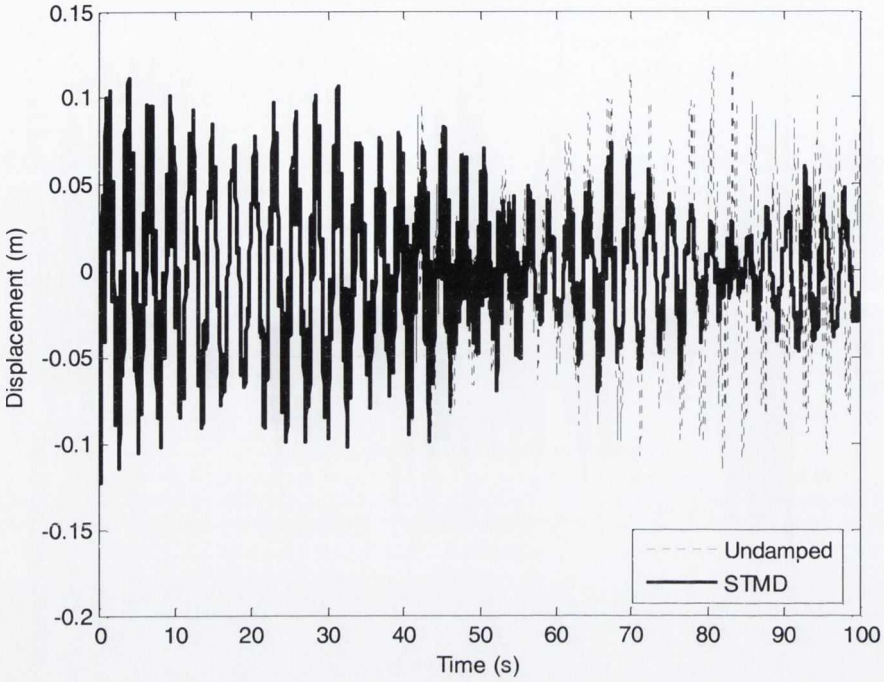

Figure 5.8: Flapwise response of the nacelle, turbulent load, variable Ω

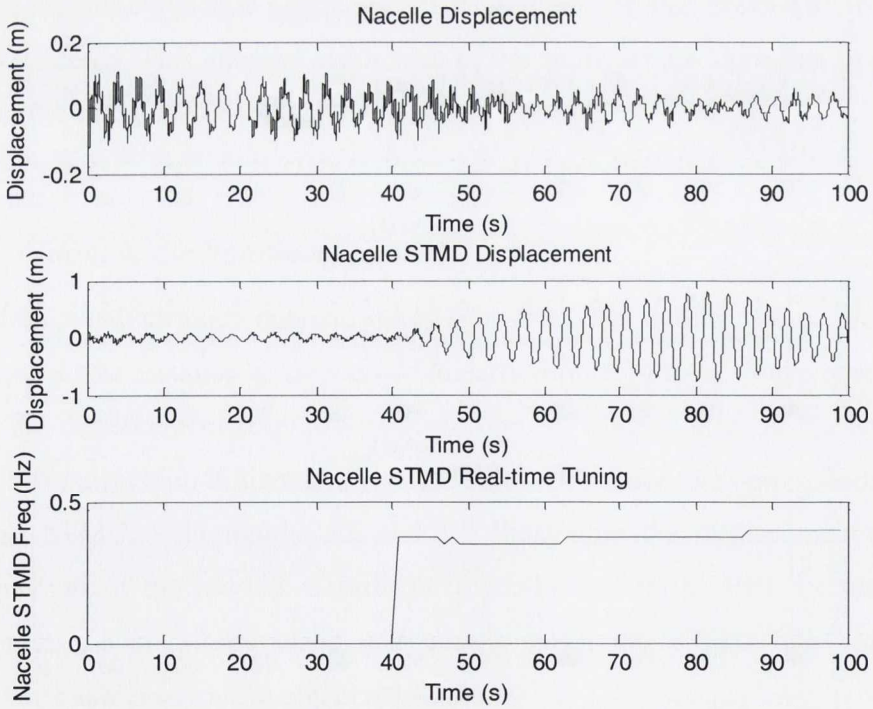

Figure 5.9: Nacelle flapwise STMD behaviour, turbulent load, variable Ω

5.3.1.2 Variation in Blade Natural Frequency, ω_b

The second parameter varied was the natural frequency of the blades. A loss in the stiffness of blade one, ω_{b1}, was considered. This represented damage occurring to the blade. The natural frequency of the blade was changed from 1.59Hz to 1.11Hz at t = 70s. Blades two and three remained unchanged. Figures 5.10 and 5.11 show the blade response and STMD behaviour, with figures 5.12 and 5.13 showing the corresponding nacelle response and STMD behaviour. As can be seen in the graphs a good reduction is achieved in the displacement of the blade and nacelle both before and after the loss in stiffness of the blade. The semi-active algorithm identifies the loss in blade stiffness and adjusts the tuning of the blade STMD just after t = 70s. The damage to the blade has no noticeable effect on the dynamic behaviour of the nacelle as can be seen in figure 5.12. The nacelle STMD again successfully identifies the dominant frequency throughout the time history achieving an excellent reduction in response.

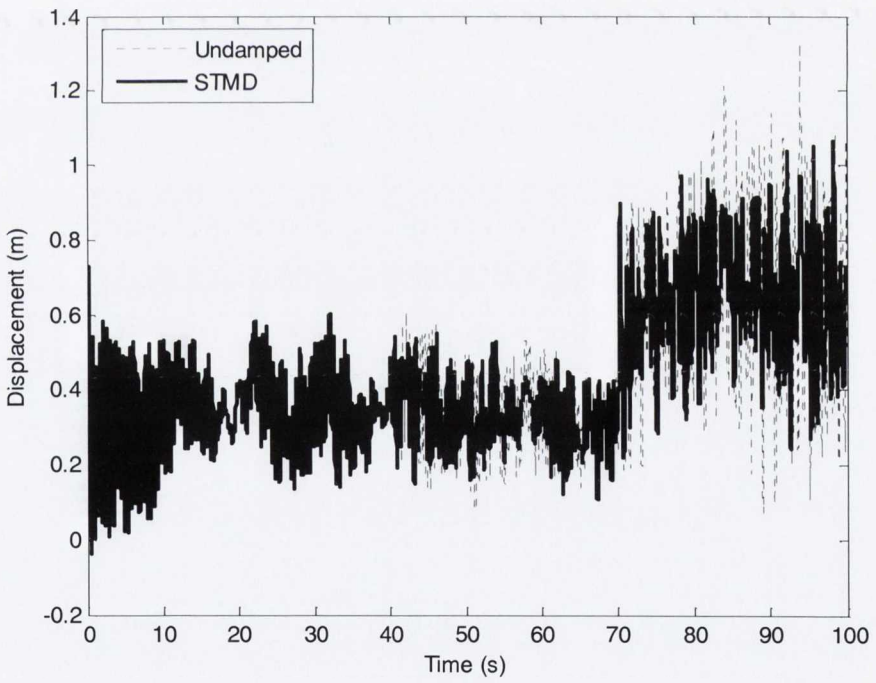

Figure 5.10: Flapwise response of blade 1, turbulent load, variable ω_{b1}

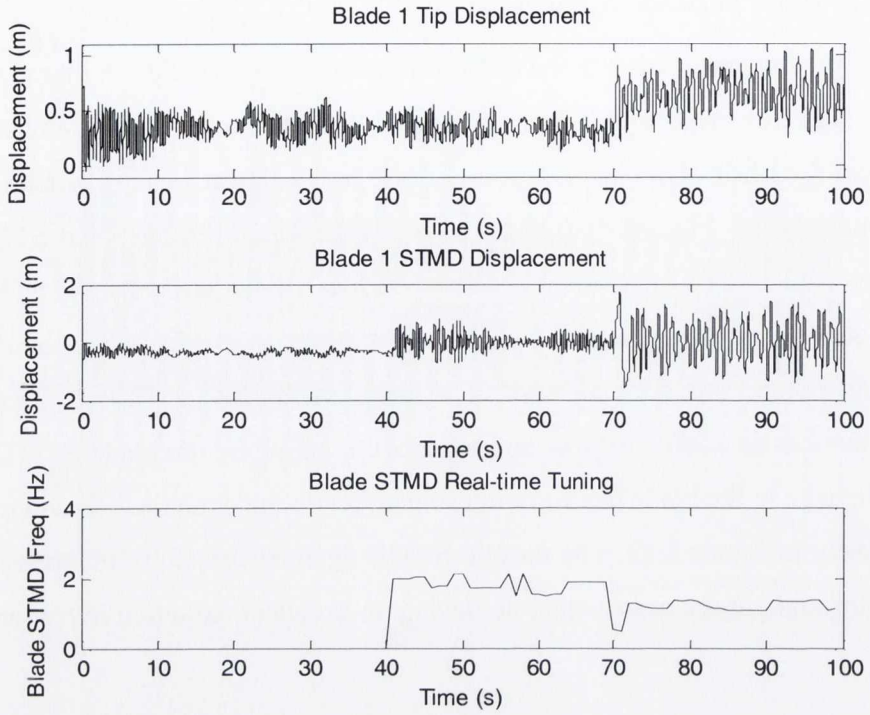

Figure 5.11: Blade flapwise STMD behaviour, turbulent load, variable ω_{bl}

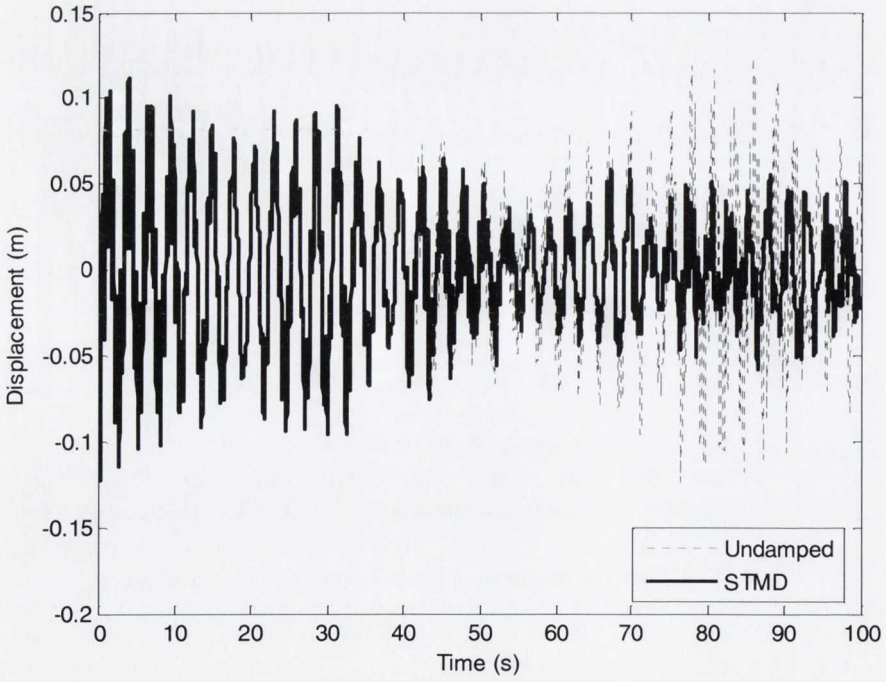

Figure 5.12: Flapwise response of the nacelle, turbulent load, variable ω_{bl}

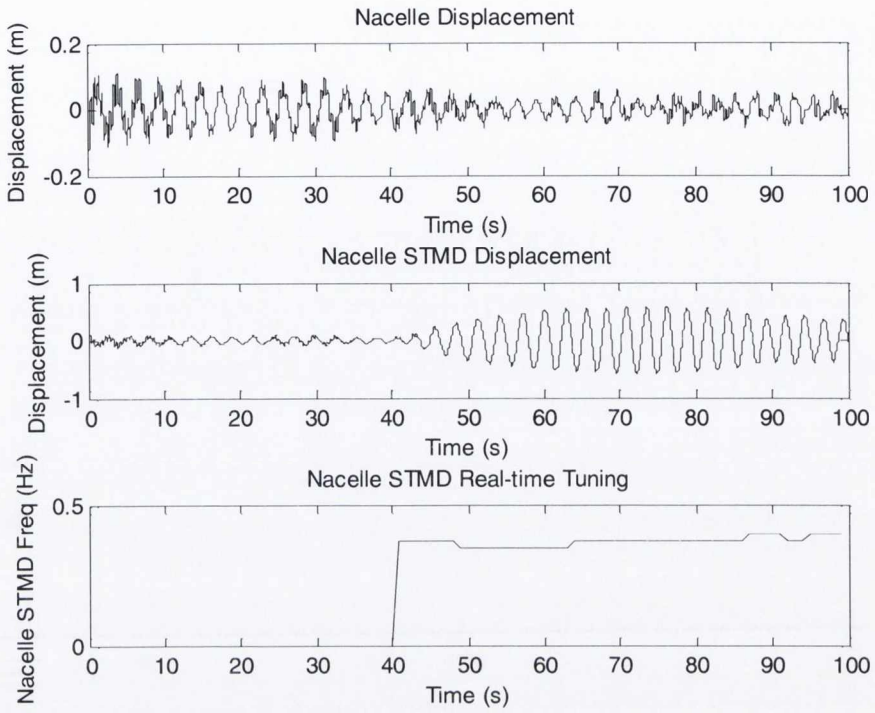

Figure 5.13: Nacelle flapwise STMD behaviour, turbulent load, variable ω_{b1}

5.3.1.3 Variation in Nacelle Natural Frequency, ω_{nac}

Finally, damage in the nacelle/tower of the turbine structure was also simulated. A loss in stiffness was assumed, represented by a change in the nacelle natural frequency from 0.57Hz to 0.48Hz at t = 70s. Figures 5.14 and 5.15 show the nacelle displacement response and STMD behaviour, while figures 5.16 and 5.17 show the corresponding plots for blade one. Again good reduction is achieved in the response of the nacelle and blade before and after the loss in stiffness. In figure 5.15 the nacelle SMTD is seen to adjust its tuning in real time just after t = 70s to cater for the loss in stiffness. As for the steady wind load, the loss in nacelle stiffness has little effect on the blade response with no significant change in the blade STMD tuning required to maintain a good reduction after the damage to the nacelle/tower.

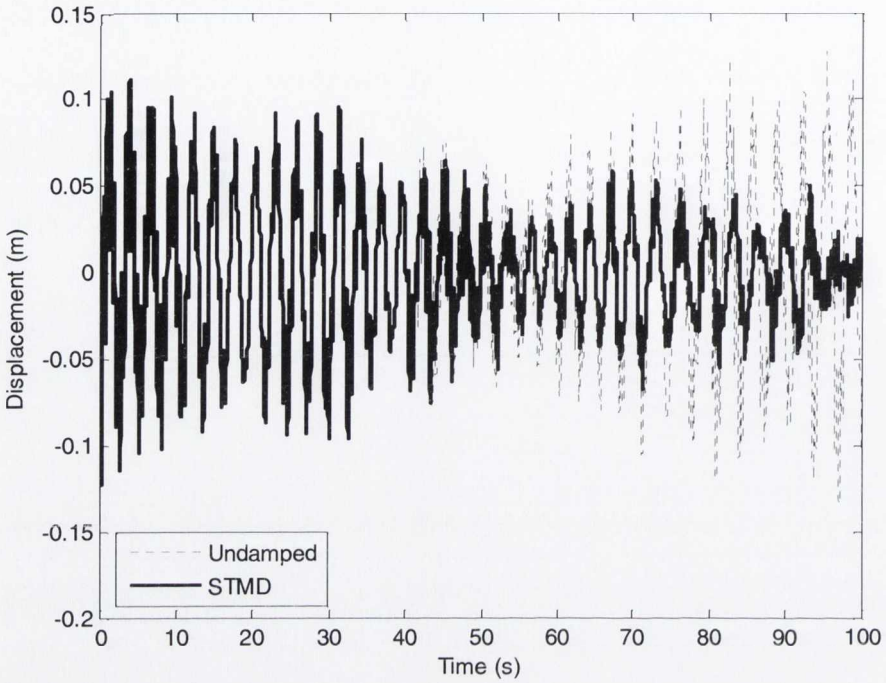

Figure 5.14: Flapwise response of the nacelle, turbulent load, variable ω_{nac}

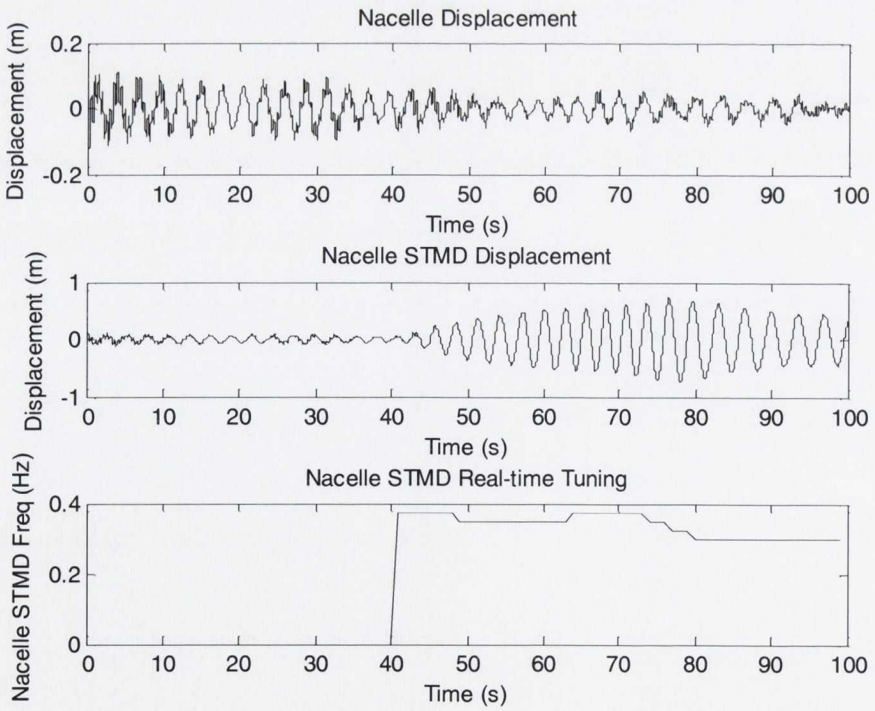

Figure 5.15: Nacelle flapwise STMD behaviour, turbulent load, variable ω_{nac}

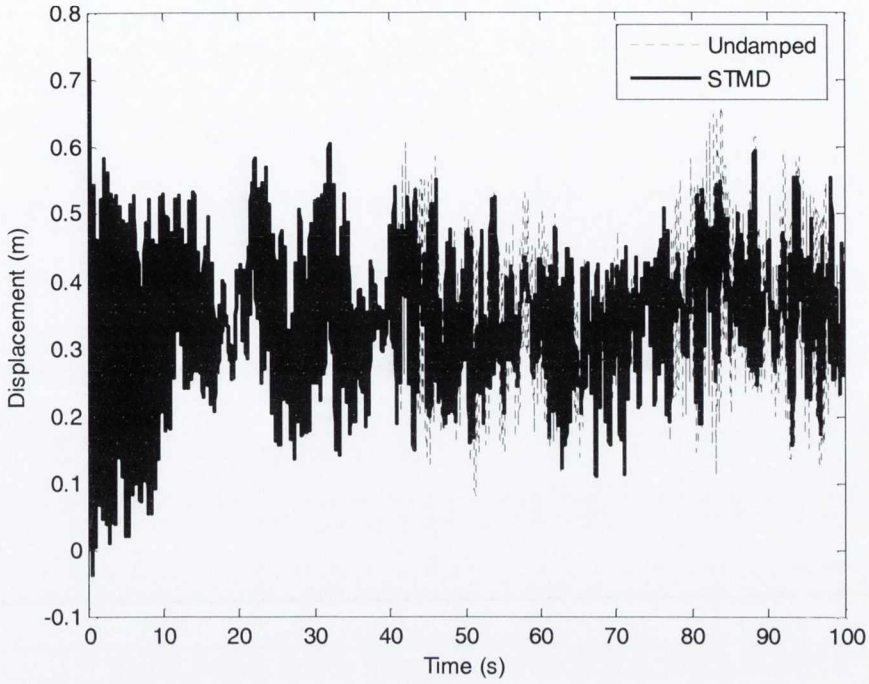

Figure 5.16: Flapwise response of blade 1, turbulent load, variable ω_{nac}

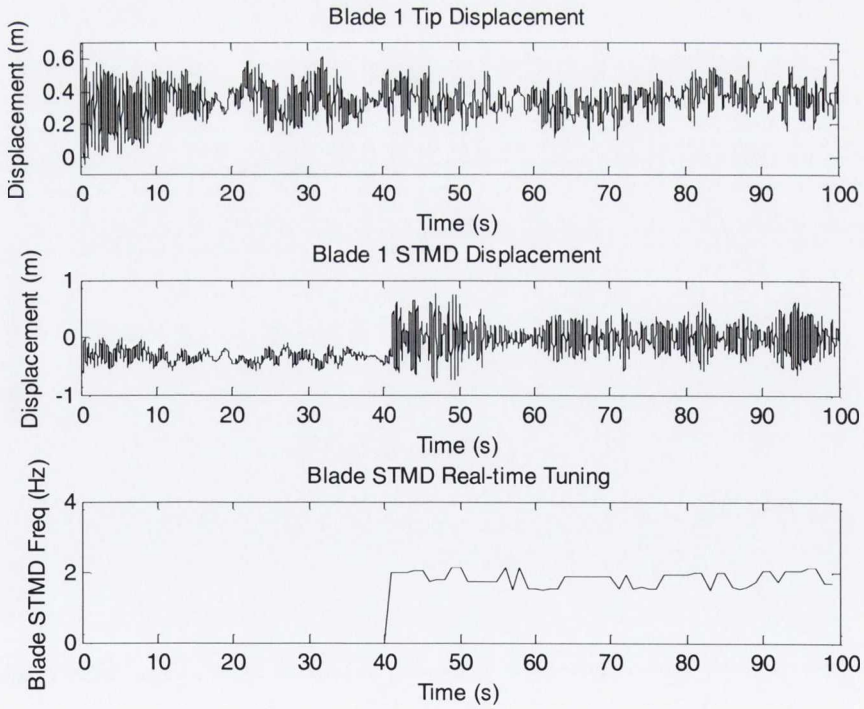

Figure 5.17: Blade flapwise STMD behaviour, turbulent load, variable ω_{nac}

5.4 Edgewise Model Results

The same semi-active STFT algorithm used for the flapwise model as outlined in section 5.2.2 was applied to the edgewise model. This allowed real time tuning of the dampers in the blades and nacelle.

5.4.1 Turbulent Wind Load

The turbulent wind load in the edgewise direction as outlined in chapter 3 was applied to the model. Figure 5.18 below shows the displacement response of the blade, again for a rotational speed of 3.14rad/s (0.5Hz).

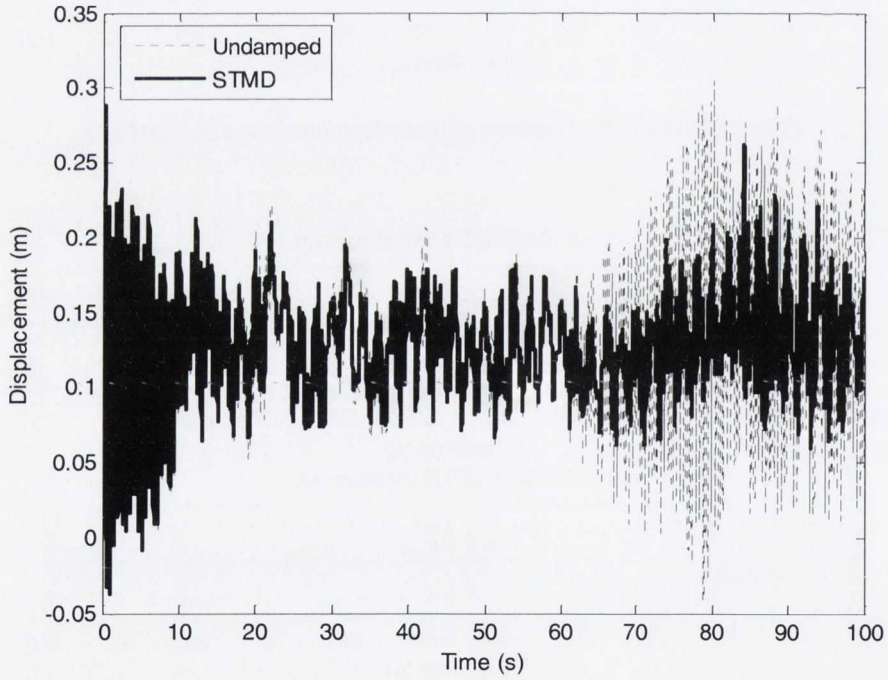

Figure 5.18: Edgewise response of blade 1, turbulent load, Ω = 3.14rad/s

As can be observed, an excellent reduction is achieved by the STMD over the undamped blade with an improvement of over 50% seen throughout most of the response. The behaviour of the STMD is illustrated in figure 5.19. The STMD again initiates at t = 41s and tunes in real-time to the dominant frequency in the blade.

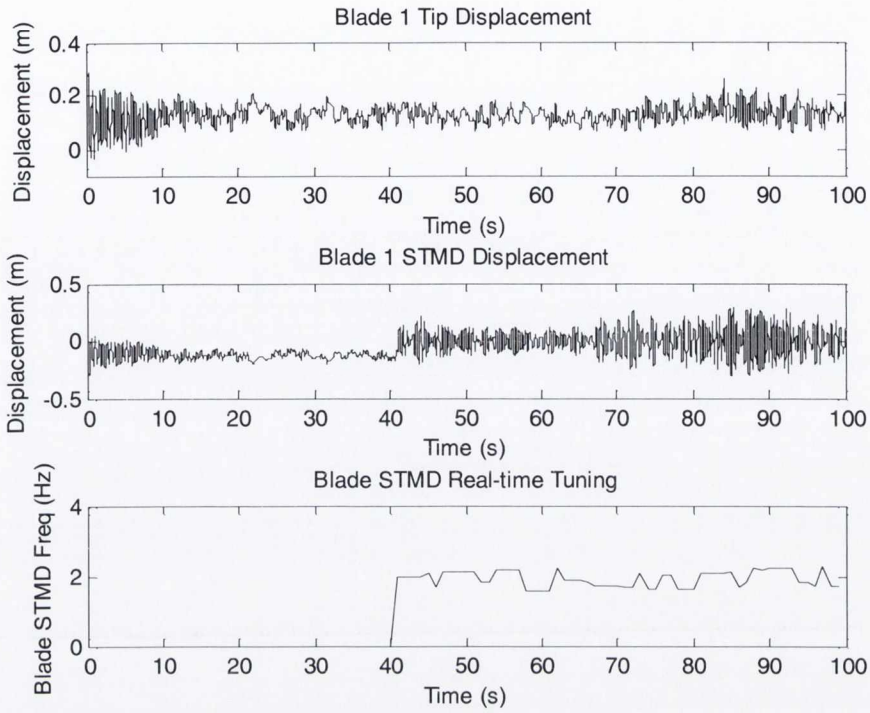

Figure 5.19: Blade edgewise STMD behaviour, turbulent load, Ω = 3.14rad/s

Figures 5.20 and 5.21 show the response of the nacelle and nacelle STMD behaviour. It is interesting to note that the response of the nacelle increases in magnitude highlighting that the STMD is ineffective in controlling the vibrations. This was investigated further by omitting the nacelle STMD from the model. However, the response of the nacelle was still seen to increase. It can be concluded that the increase in nacelle displacement is therefore purely due to the interaction with the blades. Even though the magnitude of the blade displacement has been successfully reduced by the control system, the same is not true of the nacelle. This highlights the complicated interaction that occurs between the turbine blades and nacelle/tower in the edgewise direction. It is worth noting that the magnitude of the nacelle displacement is very small compared to that of the blade. Therefore controlling the response of the blades is still desirable as an overall strategy.

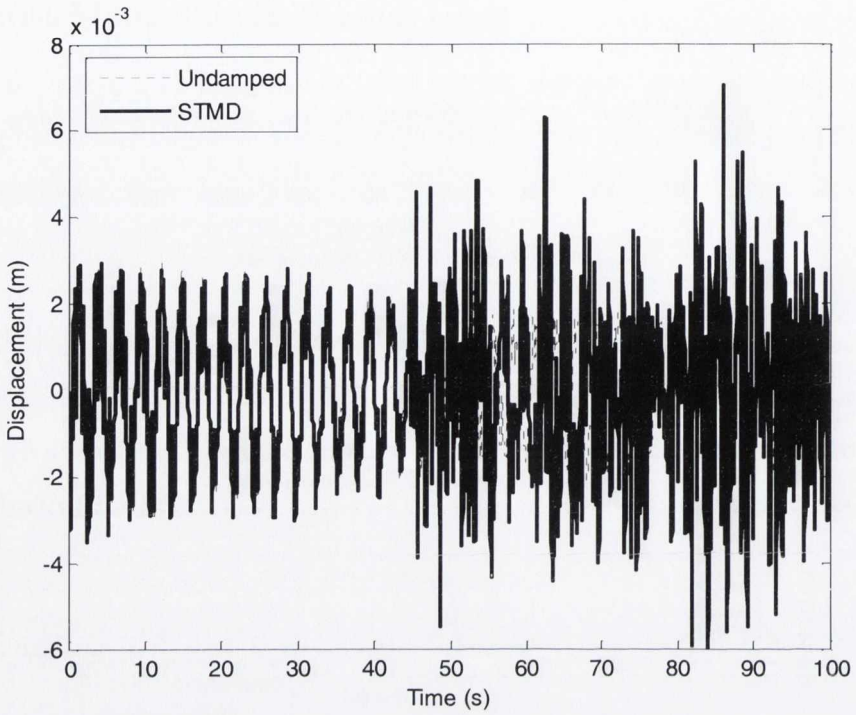

Figure 5.20: Edgewise response of the nacelle, turbulent load, Ω = 3.14rad/s

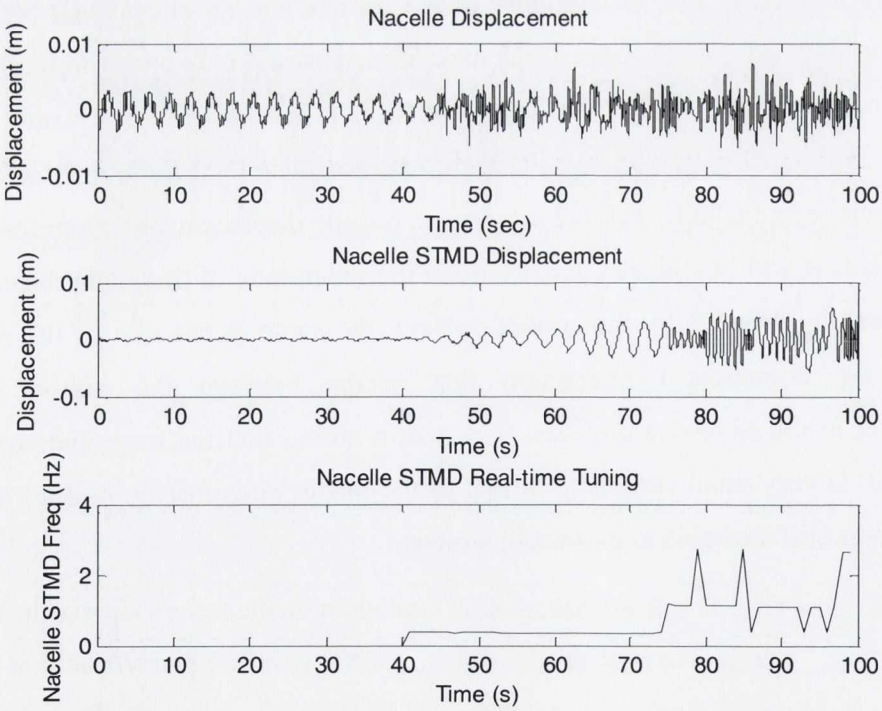

Figure 5.21: Nacelle edgewise STMD behaviour, turbulent load, Ω = 3.14rad/s

Variation in the three main dynamic parameters of the system was again considered as for the flapwise results to study the effectiveness of the algorithm for edgewise vibration.

5.4.1.1 Variation in Rotational Speed, Ω

The same variation in rotational speed was considered as for the flapwise model. Figures 5.22 and 5.23 show the blade response and STMD behaviour respectively, with figures 5.24 and 5.25 illustrating the corresponding plots for the nacelle. The semi-active algorithm again performs well for the blade, achieving a good reduction from t = 41s when the real-time tuning kicks in. Once more, an increase is seen in the nacelle response in figure 5.24 illustrating the ineffective nature of the STMD in the nacelle. Omitting the nacelle STMD from the simulations still sees a large increase in the response, again highlighting that the coupling from the blades is responsible.

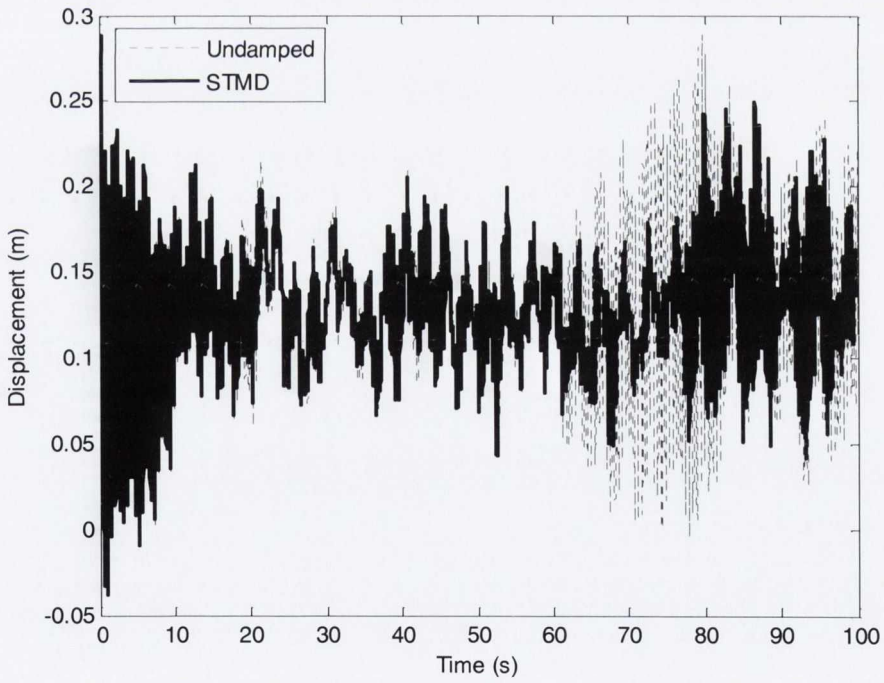

Figure 5.22: Edgewise response of blade 1, turbulent load, variable Ω

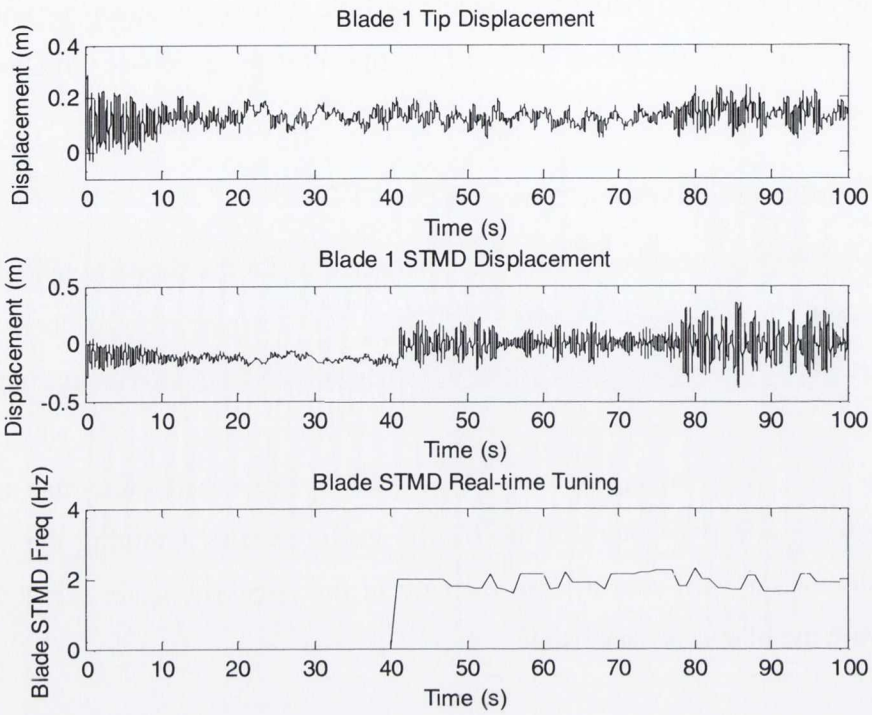

Figure 5.23: Blade edgewise STMD behaviour, turbulent load, variable Ω

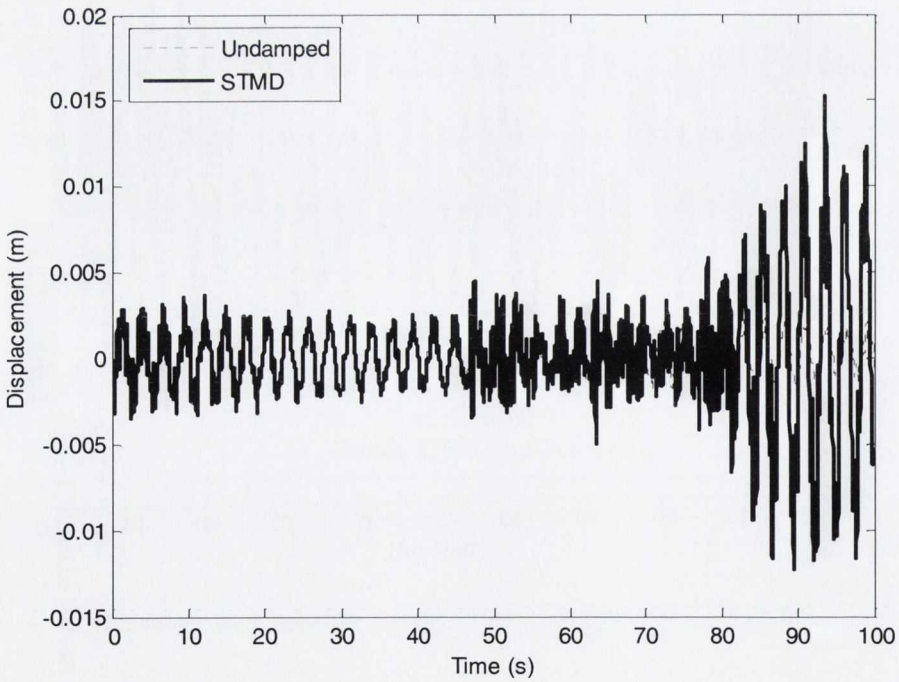

Figure 5.24: Edgewise response of the nacelle, turbulent load, variable Ω

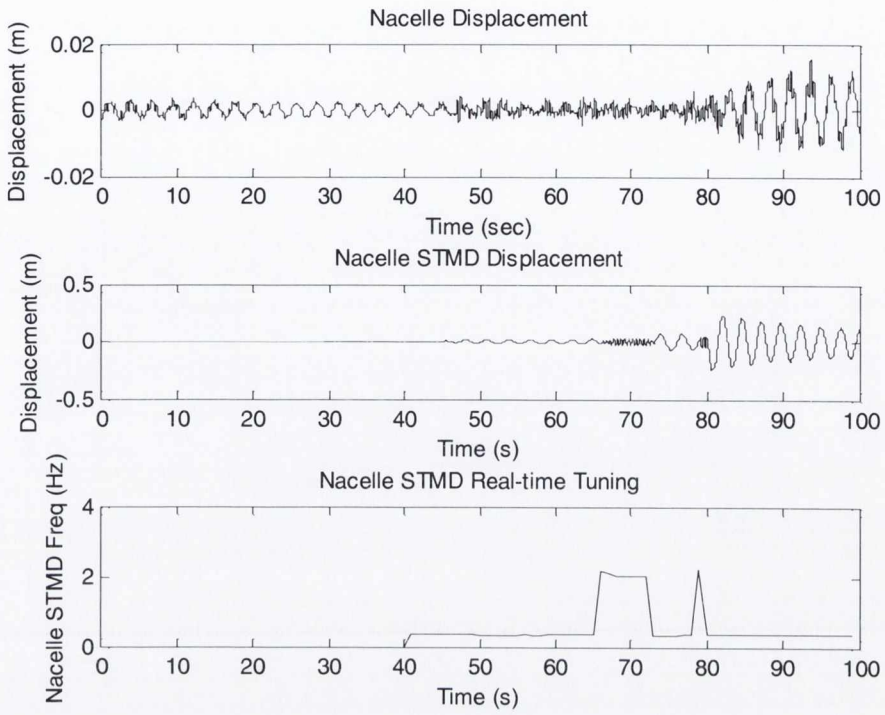

Figure 5.25: Nacelle edgewise STMD behaviour, turbulent load, variable Ω

5.4.1.2 Variable Blade Natural Frequency, ω_b

A loss in the stiffness of blade one, ω_{b1}, was again considered representing damage occurring to the blade. The natural frequency of the blade in the edgewise direction was changed from 1.91Hz to 1.43Hz at t = 70s. Blades two and three remained unchanged. An increase in the response of blade one can be seen in figure 5.26 after t = 70s due to the loss in stiffness. The STMD again achieves a notable reduction in response before and after the simulated damage to the blade. After the loss in blade stiffness a reduction in the maximum peak to peak blade tip displacement of nearly 50% is seen emphasizing the effectiveness of the STMD in the blade.

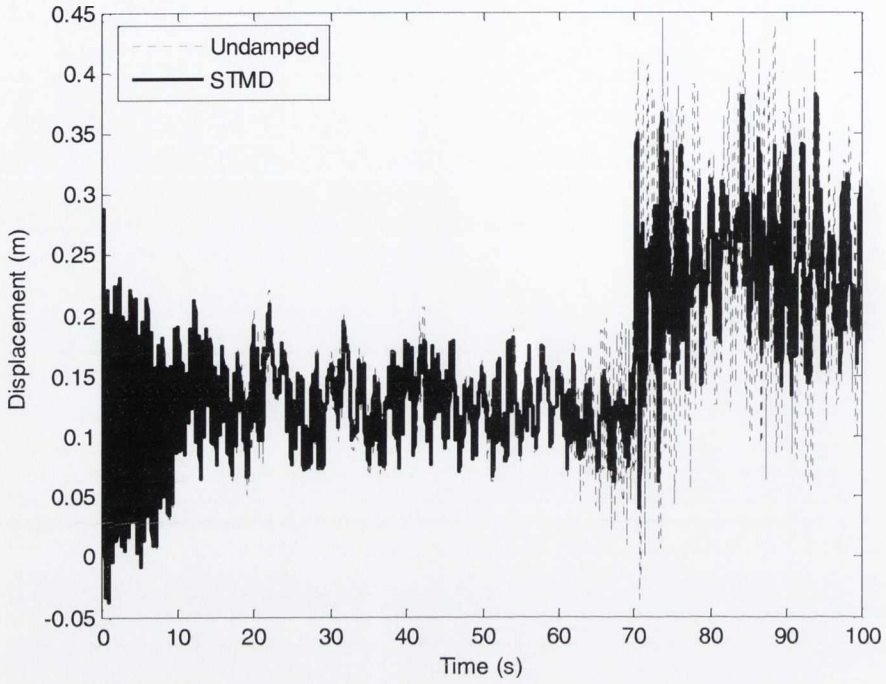

Figure 5.26: Edgewise response of blade 1, turbulent load, variable ω_{b1}

The STMD behaviour is shown in figure 5.27. As can be seen the tuning of the STMD changes after the loss in blade stiffness once more highlighting the advantages of real time tuning of the dampers. The nacelle response and STMD behaviour are shown in figures 5.28 and 5.29. A large increase in nacelle response is also seen when the loss in blade stiffness is introduced to the system. This again highlights the influence of the dynamic coupling in the turbine between the blades and nacelle. A reduction of approximately 30% is seen in the nacelle displacement after the loss in blade stiffness. However, once more omitting the nacelle STMD from the model, a reduction is still seen in the nacelle displacement highlighting that the coupling is once more responsible for the its behaviour.

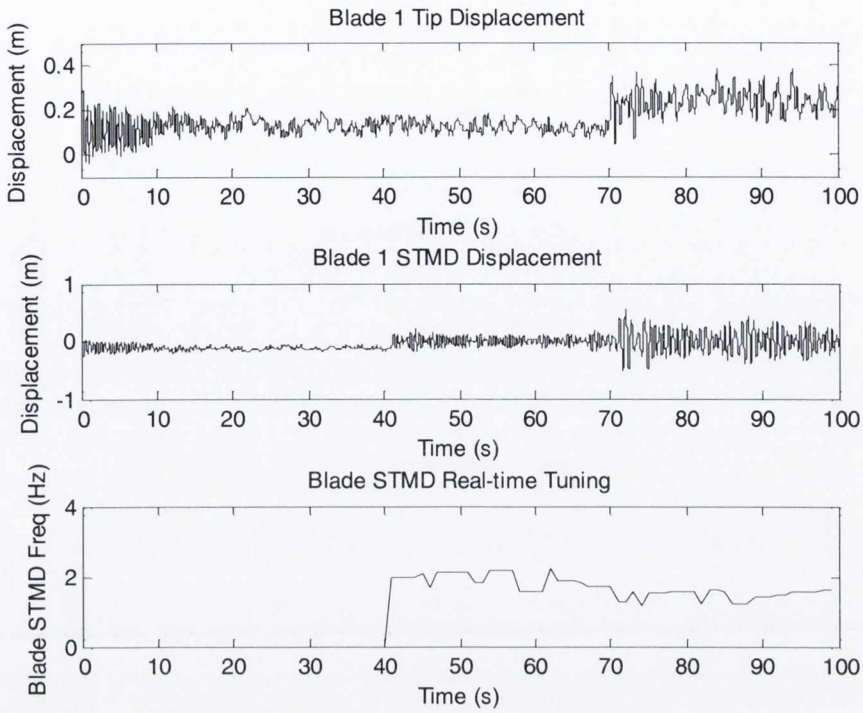

Figure 5.27: Blade edgewise STMD behaviour, turbulent load, variable ω_{b1}

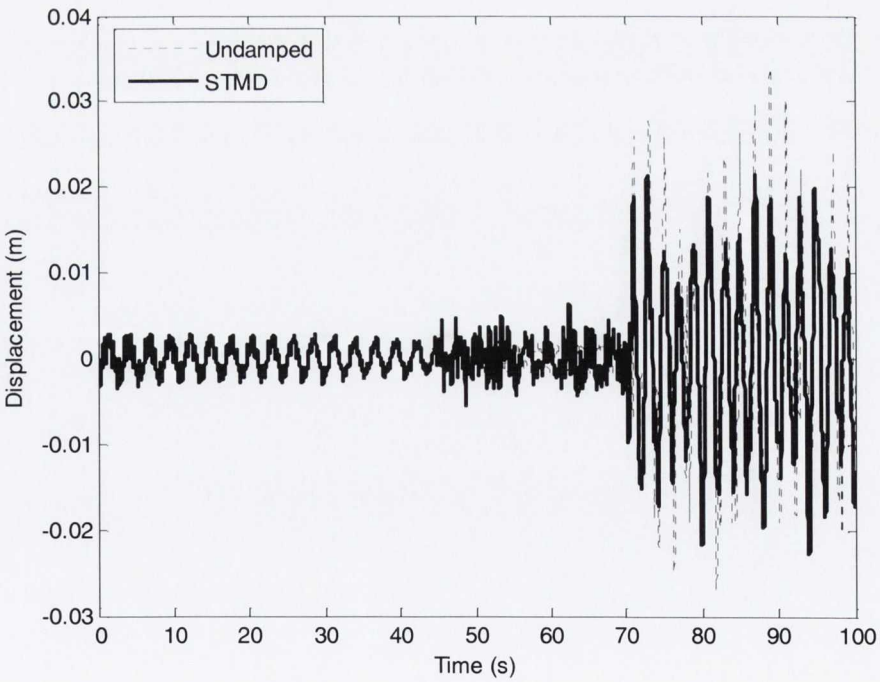

Figure 5.28: Edgewise response of the nacelle, turbulent load, variable ω_{b1}

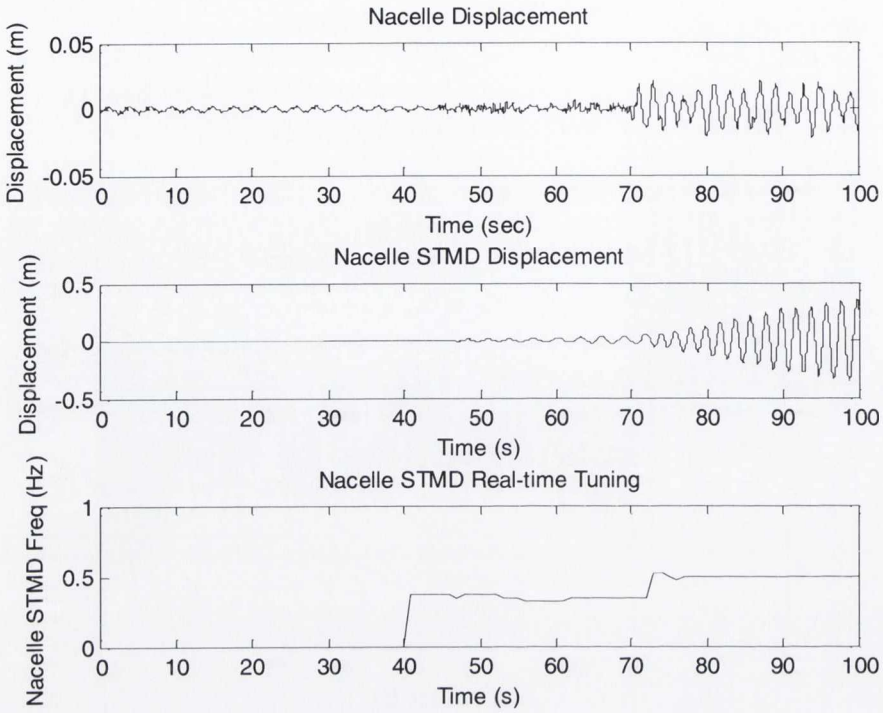

Figure 5.29: Nacelle edgewise STMD behaviour, turbulent load, variable ω_{b1}

5.4.1.3 Variable Nacelle Natural Frequency, ω_{nac}

Finally, a loss in nacelle stiffness from 0.57Hz to 0.48Hz was considered at t = 70s. This was the same as for the flapwise model due to the identical dynamic properties of the turbine tower in the flapwise and edgewise directions. The nacelle response and STMD behaviour are shown in figures 5.30 and 5.31.

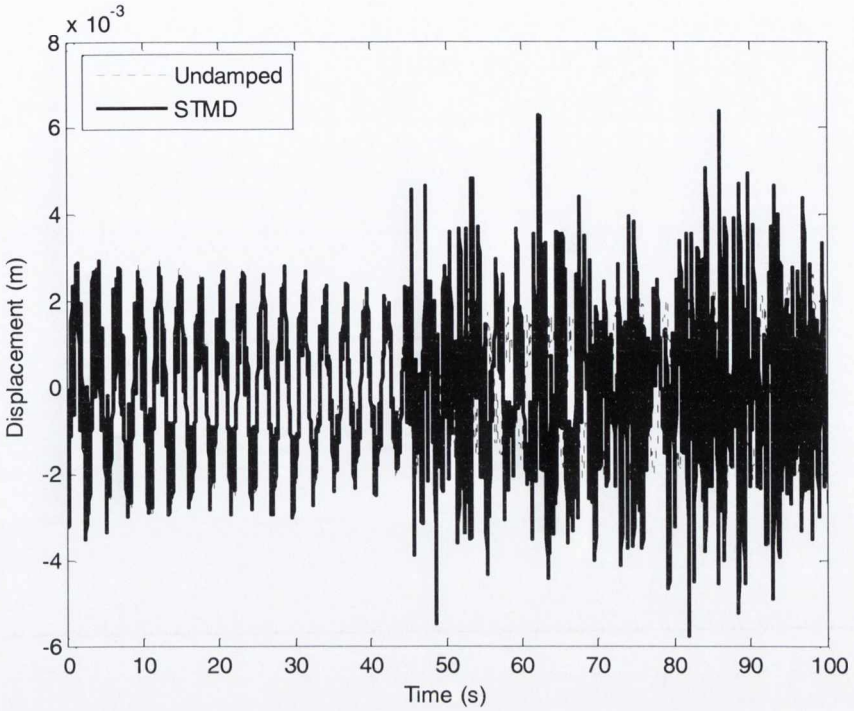

Figure 5.30: Edgewise response of the nacelle, turbulent load, variable ω_{nac}

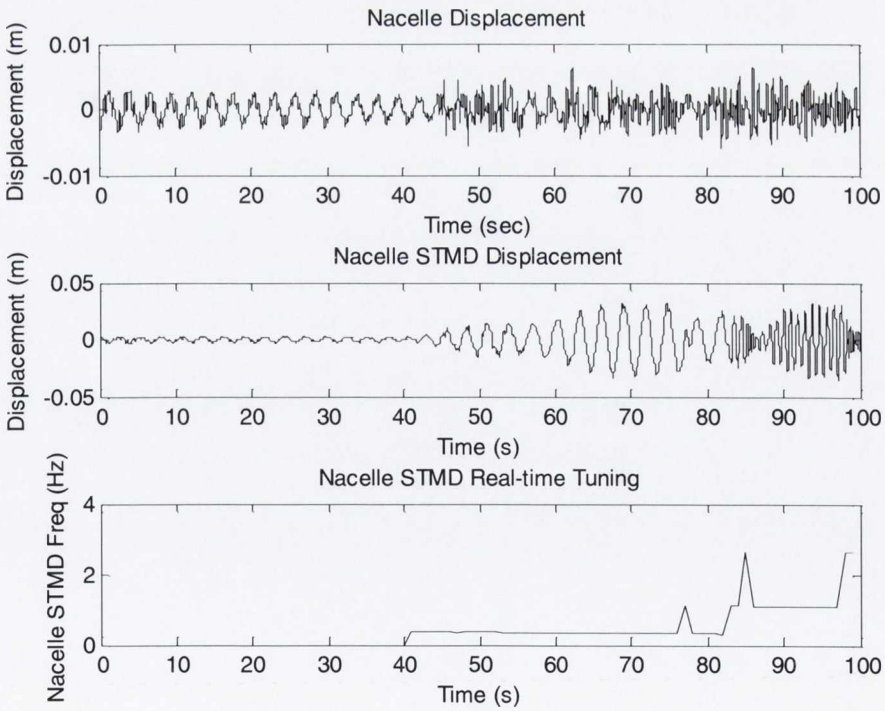

Figure 5.31: Nacelle edgewise STMD behaviour, turbulent load, variable ω_{nac}

As can be seen in figure 5.30 an increase is seen in the nacelle response once the semi-active algorithm initiates, illustrating the ineffectiveness of the STMD at the nacelle. An excellent reduction is seen in the response of blade one, plotted in figure 5.32, with the corresponding behaviour of the STMD shown in figure 5.33. Omission of the nacelle STMD again still sees an increase in the nacelle displacement emphasising that the coupling from the blades has a greater effect on the nacelle behaviour than the STMD itself.

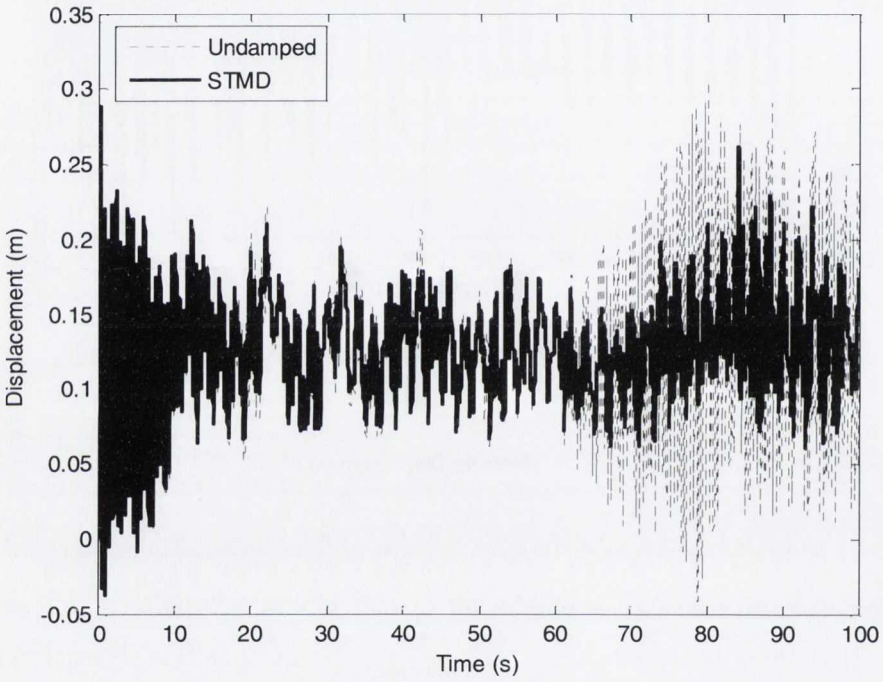

Figure 5.32: Edgewise response of blade 1, turbulent load, variable ω_{nac}

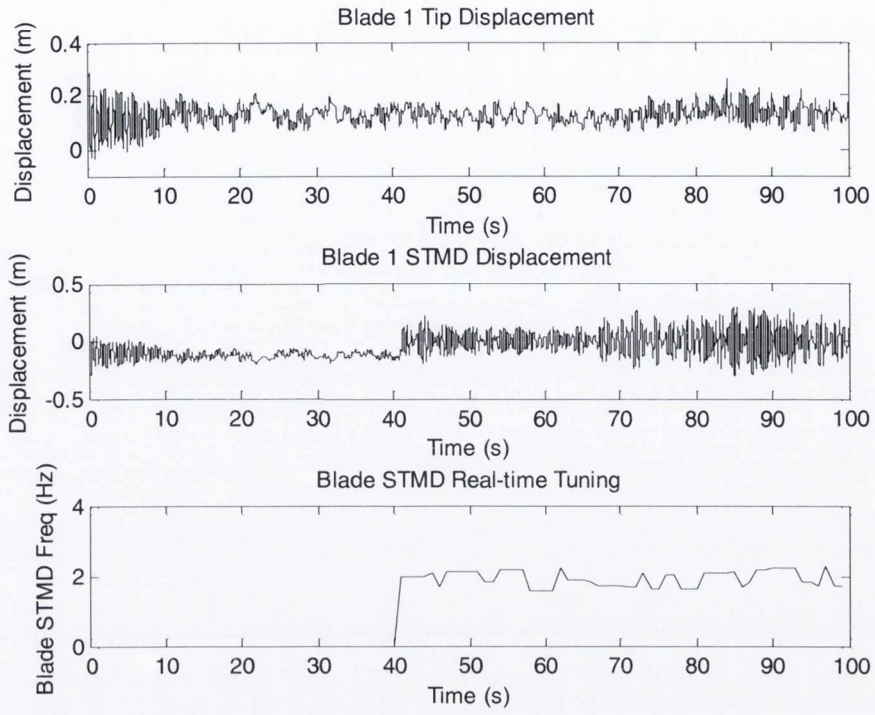

Figure 5.33: Blade edgewise STMD behaviour, turbulent load, variable ω_{nac}

5.4.2 Effect of Gravity on STMD

As mentioned previously in this thesis, the effect of gravitational forces on the turbine model was not included as these are considered small compared to the centrifugal forces experienced by the blades. However, due to the in-plane motion of the damper for edgewise control and its relatively small mass, the effect of gravity on the STMD was studied. Figure 5.34 plots the acceleration of the damper over 10s for a blade p-p displacement of approximately 0.2m. As can be observed, the STMD experiences accelerations as large as $80m/s^2$, significantly greater than the acceleration due to gravity ($9.81m/s^2$). Therefore, omission of the gravitational effect on the behaviour of the damper is considered a reasonable assumption.

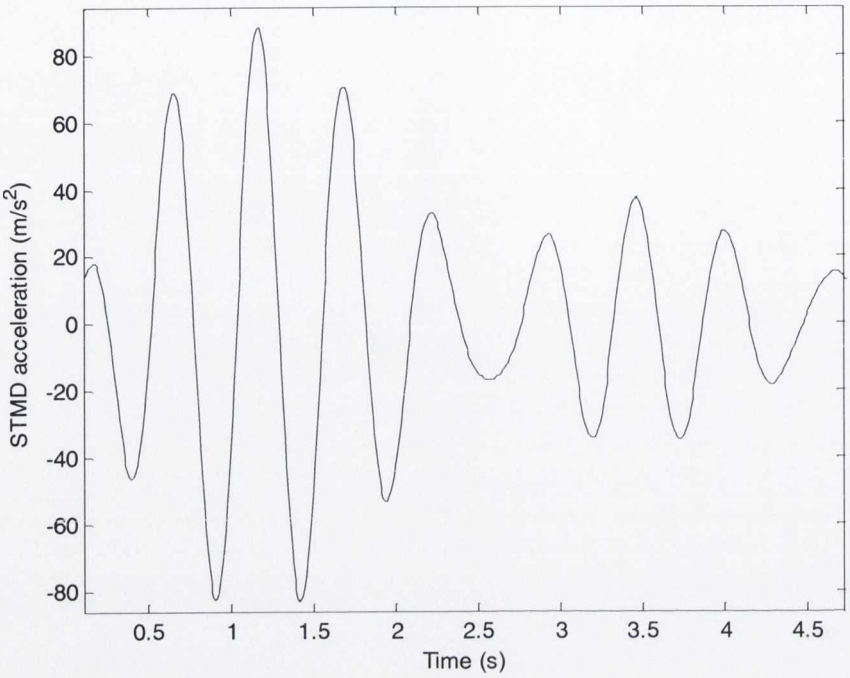

Figure 5.34: Acceleration response of blade STMD

5.5 Conclusions

In this chapter, use of an STFT algorithm for the semi-active control of both flapwise and edgewise vibrations has been presented. The time history response of the model was split up into short time segments, each of which was transformed into the time-frequency domain by means of an STFT. This allowed the frequency content of the blades and nacelle to be determined in real-time. The algorithm, outlined in the flowchart in figure 5.1, was repeated every second allowing real time tuning of the STMDs to the dominant frequencies in the response of the both the blades and nacelle of the turbine.

A detailed numerical study into the effectiveness of the semi-active algorithm was carried out with the results presented throughout the course of this chapter. Variation in the three main dynamic parameters of the system, namely the rotational speed, Ω, the natural frequency of the blades, ω_b, and the natural frequency of the nacelle/tower, ω_{nac}, were considered. This allowed the ability of the semi-active algorithm to adjust to changes in the dynamic behaviour of the system to be determined. A window size of t = 40s was used to achieve a sampling

frequency of 0.025Hz. This ensured no mistuning of the STMDs to the frequency peaks. A broad banded turbulent wind load was applied to the flapwise and edgewise models as detailed in chapter 3 of this thesis. The semi-active algorithm was shown to successfully control the response of the system for all variations to the dynamic properties of the turbine model considered. Reductions of up to 50% were frequently achieved in the blades and nacelle. However, throughout the edgewise results, increases in the response of the nacelle were observed. This was discovered to be a result of the dynamic coupling between the blades and nacelle and not a result of mistuning of the nacelle STMD. Due to the lower magnitude of the nacelle displacements in comparison to the blades, controlling the response of the blades is still deemed an effective overall control strategy. However, under larger amplitude excitation this coupling could lead to vibration problems in the nacelle/tower of the turbine.

CHAPTER 6 – Experimental Development of a Semi-Active TLD

6.1 Introduction

Chapters 4 and 5 proposed passive methods and a semi-active algorithm to control vibrations in wind turbines, in particular the blades. A theoretical model of a wind turbine including blade-tower interaction was developed and the dynamic behaviour studied by numerical simulation to ascertain the effectiveness of the proposed control method which was outlined in the previous two chapters of this thesis.

This chapter describes in detail the experimental work carried out in developing a practical and effective semi-active damping device for vibration control of these large flexible structures using the ideas previously presented in this dissertation. The hollow nature of the blades makes them inherently compatible for the installation of damping devices. Step by step development of a semi-active TLD is described in detail based on the STFT control method of Chapter 5. This TLD can adapt in real-time to changing frequency content in the vibration response due to variation in environmental or operating conditions. Real-time adjustment of the liquid level in the damper is performed to achieve the desired TLD tuning. As mentioned in chapter 4 the mass-spring-dashpot systems used to model a TMD can also equivalently represent a TLD. A TLD was chosen over a TMD due its simplicity in construction, and hence low cost of installation and maintenance, and the zero trigger level needed for the damper to operate. The damping provided by a TLD from its tuning is supplemented by additional damping due to the liquid sloshing inside the tank. Furthermore, the self contained nature of a TLD means motion of the damper is not an issue as the liquid is contained inside a sealed tank. In contrast, a TMD's motion may need to be limited due to space constraints inside the turbine blades. Finally, a passive TLD is effective over a greater frequency range than that of an equivalent TMD.

6.2 Passive TLD

6.2.1 Test Structure

A single degree of freedom structure with a fundamental frequency similar in nature to a wind turbine blade was used to test the proposed semi-active TLD. It consisted of a single mass in the form of a steel plate (=1.93kg) connected to 4 flexible columns. Figure 6.1 shows a photo of the structure with TLD attached.

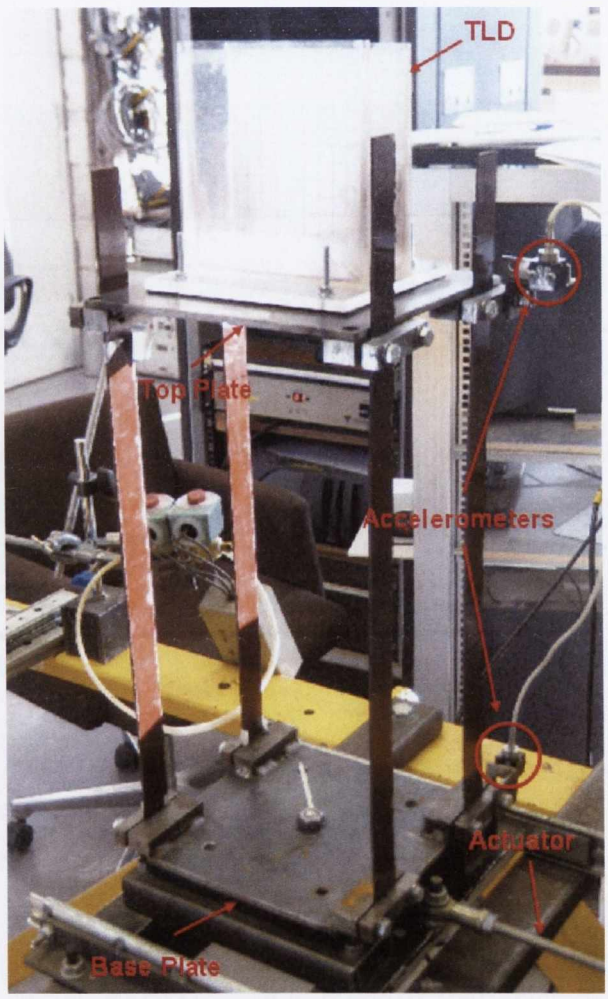

Figure 6.1: SDOF test structure

The fundamental frequency was designed to be in the low frequency range, around 1.5Hz. Cross bracing in the form of string was later added to stiffen the structure to 2.2Hz, approximately equal to the natural frequency of the wind turbine blades used in the numerical

studies performed in chapters 4 and 5 of this thesis. This allowed the TLD to be tested in the range of interest. The structure is connected to an actuator at its base as shown in figure 6.1. This actuator was used to excite the structure to study its dynamic behaviour. Two accelerometers (one connected to the top plate and one connected to the base plate), were used to record the response of the structure. A passive TLD was first designed and tested on the SDOF structure as shown in figure 6.1 before extending the device to include semi-active behaviour.

6.2.2 Initial Characterisation of Passive TLD

Two passive rectangular TLDs of different sizes were tested to study their range of effectiveness. The dimensions of the tanks considered were 73x45mm and 111x45mm (length x breadth). Figure 6.2 shows a photograph of the 111x45mm tank. Both tanks were constructed from clear perspex allowing the sloshing of the water to be clearly seen. The water was also dyed and graph paper attached to the back of the TLD to allow the amplitude of liquid motion to be easily identified.

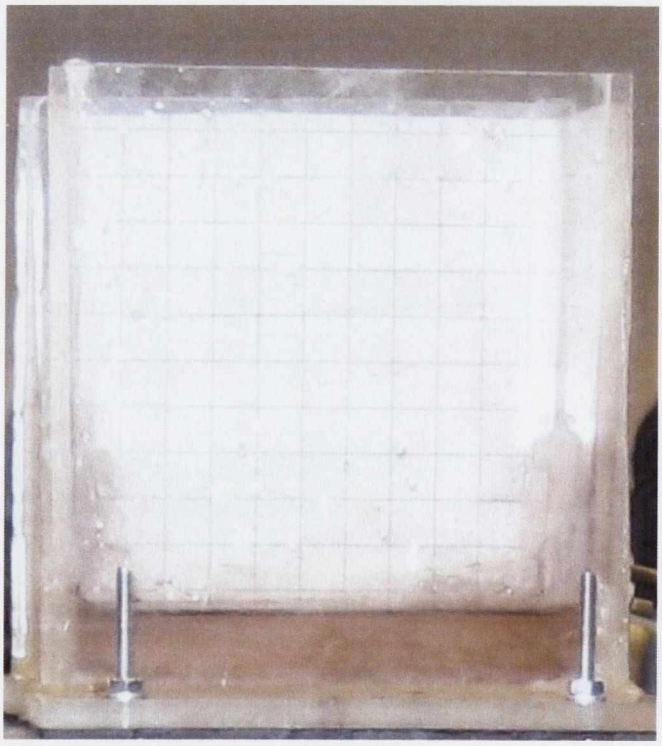

Figure 6.2: Rectangular TLD 111x45mm

6.2.2.1 Experimental Characterisation

The two TLDs were first characterised experimentally. The TLD was mounted directly on a base plate which was connected to the actuator. The experimental steps carried out are outlined as follows:

- An initial volume of water was added to the tank. In the case of the 73x45mm tank, this was 30ml.
- The tank was then excited by the actuator using a sine function of different frequencies and the liquid motion recorded on video. Increments of 0.05Hz were used between each excitation.
- The video was then reviewed to identify at what frequency maximum liquid motion occurred. This gave the experimental natural frequency for that volume/depth of water.
- The amplitude of excitation at the base of the TLD was also noted for theoretical calculations which are explained in section 6.2.2.2.
- The procedure was then repeated for different water volumes allowing the relationship between water volume/depth and natural frequency to be determined for each tank.

6.2.2.2 Theoretical Analysis

The fundamental frequency of water sloshing in a rectangular tank was originally derived by Lamb (1932) using linear water theory (i.e. this assumes small amplitude oscillations), and is expressed as

$$f_w = \frac{1}{2\pi}\sqrt{\frac{\pi g}{L}\tanh\left(\frac{\pi h_0}{L}\right)} \tag{6.1}$$

where g = acceleration due to gravity, h_0 = still water depth and L is the length of the tank in the direction of liquid motion. This was previously stated in equation 2.5 of this thesis. Reed et al. (1998) went on to study TLDs under large amplitude excitation. They noted the occurrence of non-linear behaviour in the TLD due to the large amplitude motion of the

water. The TLD was seen to exhibit a so-called 'hardening spring' behaviour if the amplitude of motion exceeded a certain critical value. This resulted in a natural frequency higher than that predicted by the linear wave water theory from equation 6.1 above. The liquid motion essentially becomes 'stiffer'; hence the hardening spring comparison. Above this frequency the amplitude of liquid motion suddenly dies off. This is known as the jump phenomenon and highlights the non-linear behaviour of the TLD under large amplitude excitation. Depending on the amplitude of excitation, Yu et al. (1999) noted that the TLD could behave as a 'soft' or 'hard' spring. They carried out experimental studies to determine the threshold between these regions. They defined these two regions as 'weak wave breaking' and 'strong wave breaking'. They expressed the non-dimensional amplitude of excitation as

$$\Lambda = \frac{A}{L} \tag{6.2}$$

where A is the amplitude of base motion and L is the length of the tank. The threshold between weak wave breaking and strong wave breaking was found to be at a non-dimensional amplitude of 0.03. In their study they developed a formula similar to that originally derived by Lamb but which accounted for the non-linear behaviour of the TLD when subjected to large amplitude excitations. This is expressed in equation 6.3 below.

$$f_{nl} = \frac{\psi}{2\pi}\sqrt{\frac{\pi g}{L}\tanh\left(\frac{\pi h_0}{L}\right)} \tag{6.3}$$

or

$$f_{nl} = \psi f_w \tag{6.4}$$

where f_{nl} is the non-linear natural frequency and ψ is the frequency shift ratio. Experimental investigation allowed ψ to be expressed in terms of the non dimensional amplitude as follows

$$\psi = 1.038\Lambda^{0.0034} \text{ for } \Lambda < 0.03 \text{ or weak wave breaking}$$

(this gives an $\psi \approx 1$, i.e. linear theory is accurate)

and

$$\psi = 1.59\Lambda^{0.125} \text{ for } \Lambda > 0.03 \text{ or strong wave breaking}$$

This allows the hardening spring or strong wave breaking behaviour to be taken into account. Explanations for the occurrence of this hardening behaviour with excitation amplitude generally point towards the fact that for large amplitude excitation more of the liquid mass is involved in the liquid motion. If some of the liquid mass in the TLD is not moving erroneous results can occur when comparing the theoretical natural frequencies to those obtained from experimentation.

6.2.2.3 TLD Characterisation Results

The theoretical natural frequencies for the two TLDs were calculated using both linear wave water theory (equation 6.1) and the non-linear equation developed by Reed et al. (equation 6.3). These calculations were compared to the results obtained from the experimental investigation described in section 6.2.2.1.

The linear, non-linear and experimental results for the 73x45mm tank are shown in table 6.1 below. In the experimental tests, significant liquid motion was seen over a range of frequencies due to the large amplitude excitation. Above this the jump phenomenon mentioned above was observed. The natural frequency of the TLD for each water depth was therefore taken as the highest frequency that exhibited this large amplitude motion just above which the jump phenomenon occurred.

Volume (ml)	Linear Natural Frequency (Hz)	Non-dimensional Amplitude, A	Non-Linear Natural Frequency (Hz)	Experimental Natural Frequency (Hz)
30	2.00	0.043	2.15	2.25
40	2.27	0.050	2.47	2.40
50	2.48	0.054	2.74	2.50
60	2.65	0.056	2.94	2.60

Table 6.1: Theoretical and experimental natural frequencies, 73x45mm tank

Figure 6.3 shows a plot of natural frequency with respect to water volume. As can be seen in the graph for the lower liquid volumes, the experimentally observed natural frequencies agree closely with the non-linear wave water theory. However, for the higher liquid volumes the natural frequencies approach closer to the frequencies predicted by linear wave water theory. This is in spite of the fact that in table 6.1 above we can see that we should be in the strong wave breaking zone based on the non-dimensional amplitudes (A>0.03). In the experimental characterisation of the TLD it was noted that for these greater liquid volumes (and hence greater liquid depths) not all the mass of the water seemed to be active which is an assumption in the theory outlined above. This would result in a smaller 'active' mass and hence the lower observed natural frequency compared to that predicted by non-linear theory which assumes all the liquid mass to be active.

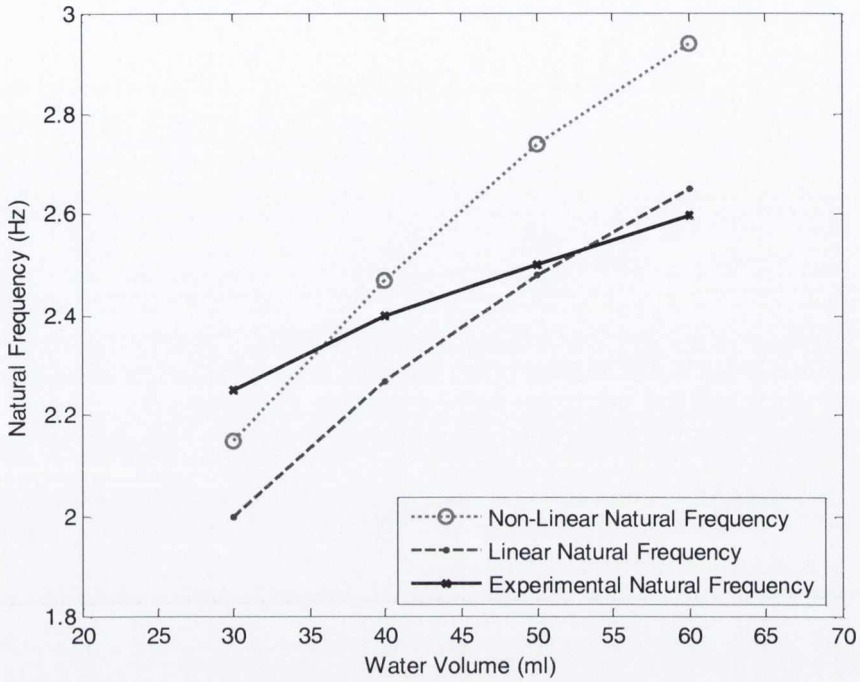

Figure 6.3: Characterisation of 73x45mm TLD

Table 6.2 shows the results for the larger 111x45mm tank. Greater water volumes were studied as volumes of 30/40ml resulted in insignificant fluid motion due to the low depths of liquid in the tank. This made the natural frequency too difficult to identify.

Volume (ml)	Linear Natural Frequency (Hz)	Non-dimensional Amplitude, A	Non-Linear Natural Frequency (Hz)	Experimental Natural Frequency (Hz)
50	1.39	0.054	1.54	1.7
60	1.52	0.060	1.70	1.8
70	1.63	0.063	1.83	1.85
80	1.73	0.063	1.95	1.9

Table 6.2: Theoretical and experimental natural frequencies, 111x45mm tank

These linear, non-linear and experimental natural frequencies are again plotted below in figure 6.4.

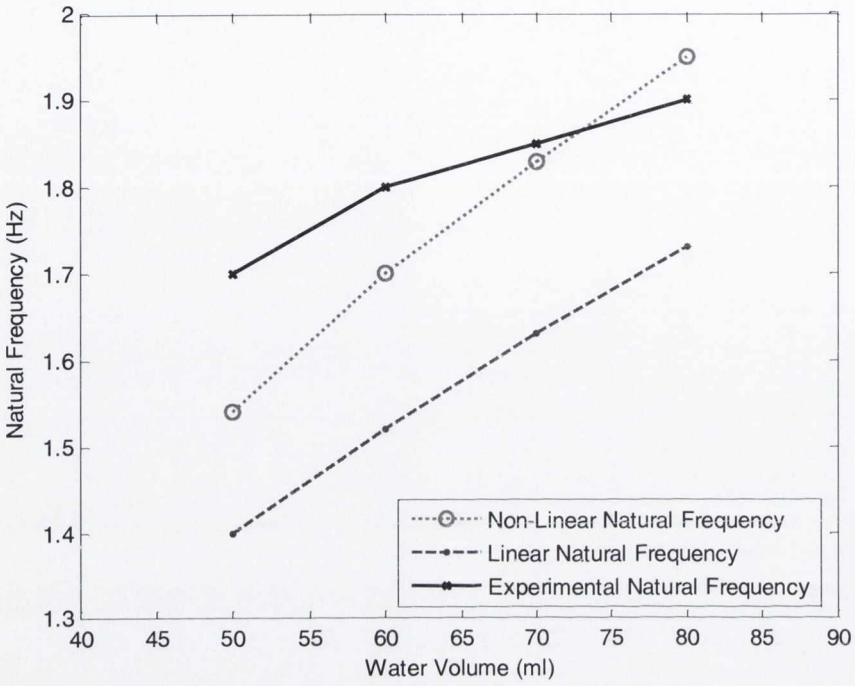

Figure 6.4: Characterisation of 111x45mm TLD

As can be seen above the experimental results for the 111x45mm tank agree more closely with non-linear wave theory than those seen for the 73x45mm tank. This is due to the fact that the longer tank means shallower water for greater liquid volumes compared to the previous tank. Hence there was no 'dead mass' as was observed for the previous tank. This explains why the 73x45mm tank results do not agree as closely with the theory as those shown here for the 111x45mm tank. It is also important to note that TLDs are effective over a range of frequencies due to the damping provided by liquid sloshing as well as the TLD tuning itself. For example, for a liquid volume of 50ml in the 111x45ml tank, the non-linear theory (equation 6.3) predicted a natural frequency of 1.54Hz while the experimental results showed 1.7Hz. Significant liquid motion was seen from a frequency of 1.5Hz in the experiment; however the liquid motion did not reduce in magnitude until just over 1.7Hz. Hence the experimental natural frequency was deemed to be 1.7Hz. This wide range of effectiveness of the TLD is a well known advantage over other vibration mitigating devices such as TMDs and this range increases with the amplitude of liquid motion (Reed et al., 1998).

As the 111x45mm TLD has tuning capabilities in the desired range of the test structure this TLD was selected for development into a semi-active device. As shown in the results above

the non-linear theory developed by Reed et al. (1998) was seen to accurately predict the natural frequency of the TLD for different water volumes, and was used as a basis for calculating the tuning of the TLD.

6.2.3 Passive Testing of TLD

The TLD was first tested as a passive device on the test structure (without cross-bracing) described in section 6.2.1.

6.2.3.1 Harmonic Testing

The TLD was initially tested for a simple harmonic load case. The structure was excited by a sinusoidal load and the response compared for the undamped and damped scenarios. Figure 6.5 shows the response of the undamped and damped structure to a sinusoidal load with a frequency of 1.5Hz. This corresponds to the natural frequency of the SDOF system. The TLD was tuned to 1.5Hz with a water volume of 50ml. This gave a mass ratio of just over 2%.

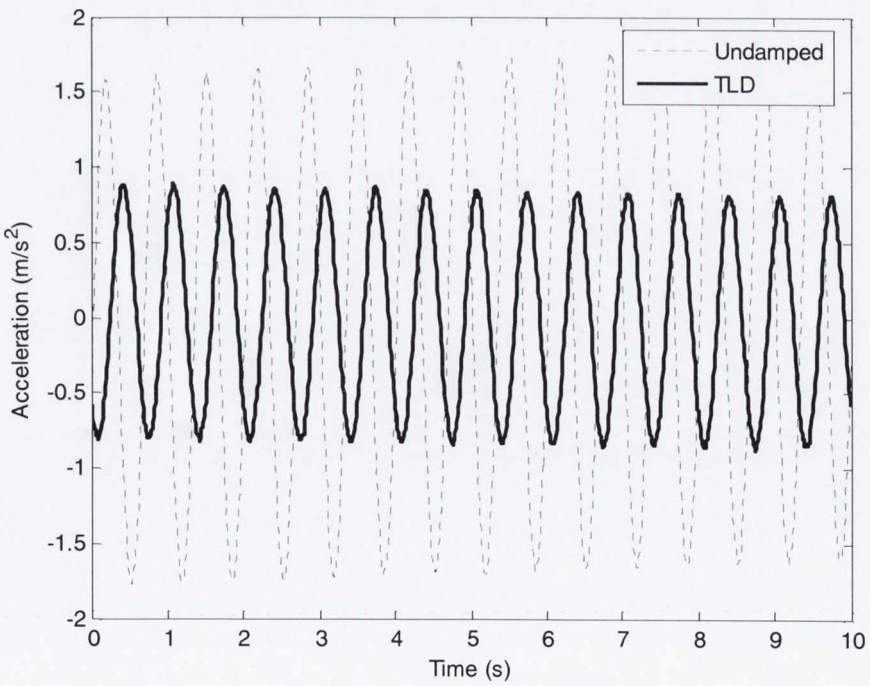

Figure 6.5: Acceleration response of SDOF structure, Harmonic load – 1.5Hz

As can be seen in the plot, an excellent reduction is achieved in the response of the structure when water is added to the TLD. This highlights that accurate tuning of the TLD leads to a large reduction in the response of the primary structure.

Figure 6.6 shows the response of the structure for a sinusoidal load of 1.6Hz. As can be seen a small reduction is again achieved by the TLD despite the structure being excited off resonance. This highlights the range of effectiveness of a TLD which was mentioned in the experimental characterisation in section 6.2.2.3.

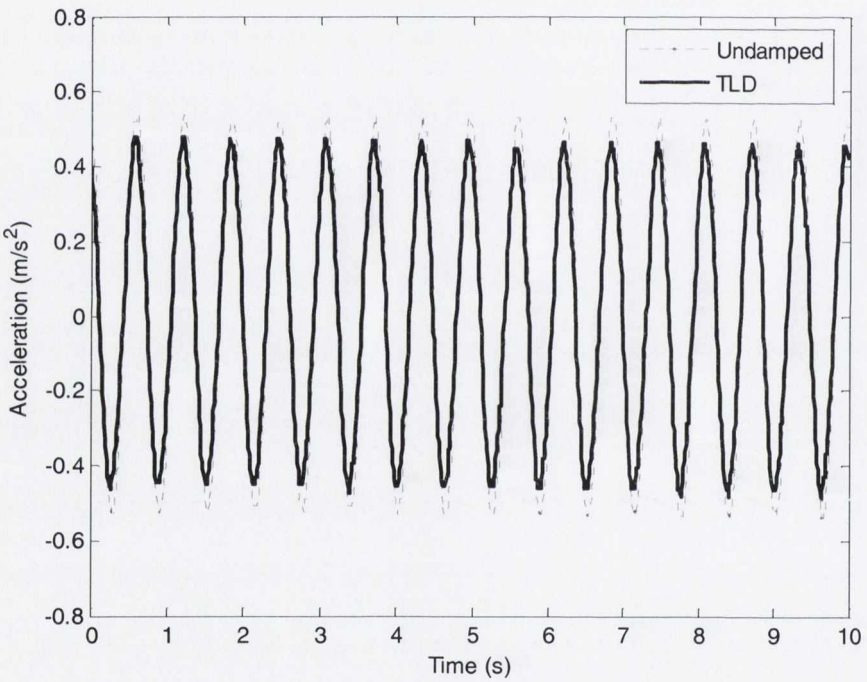

Figure 6.6: Acceleration response of SDOF structure, Harmonic load – 1.6Hz

6.2.3.2 Kaimal Loading

The behaviour of the passively tuned TLD was also studied for a turbulent wind load, represented by a Kaimal spectrum as described in section 3.2.3.2 of this thesis. As before, the TLD was passively tuned to the natural frequency of the structure at 1.5Hz by a water volume of 50ml. This achieved a mass ratio of approximately 2% as for the harmonic results presented in the previous section. Figure 6.7 below shows the time history response of the

structure to the Kaimal loading. A good reduction is seen with the addition of the TLD. This highlights the ability of the TLD to mitigate vibrations due to broad banded excitations such as those experienced by a wind turbine.

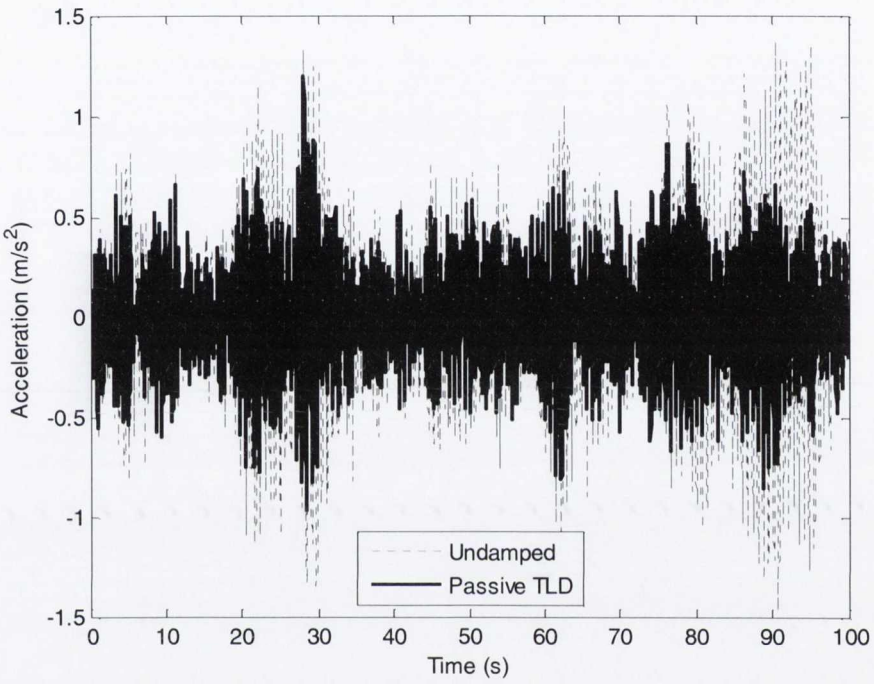

Figure 6.7: Acceleration response of SDOF test structure with passive TLD, Kaimal load

As can be seen in the plot above, the TLD is most effective during periods of high structural motion. This induces greater liquid motion in the TLD, and hence higher damping forces. Figure 6.8 shows the corresponding frequency spectrum. The single peak at 1.5Hz is significantly reduced by addition of the TLD.

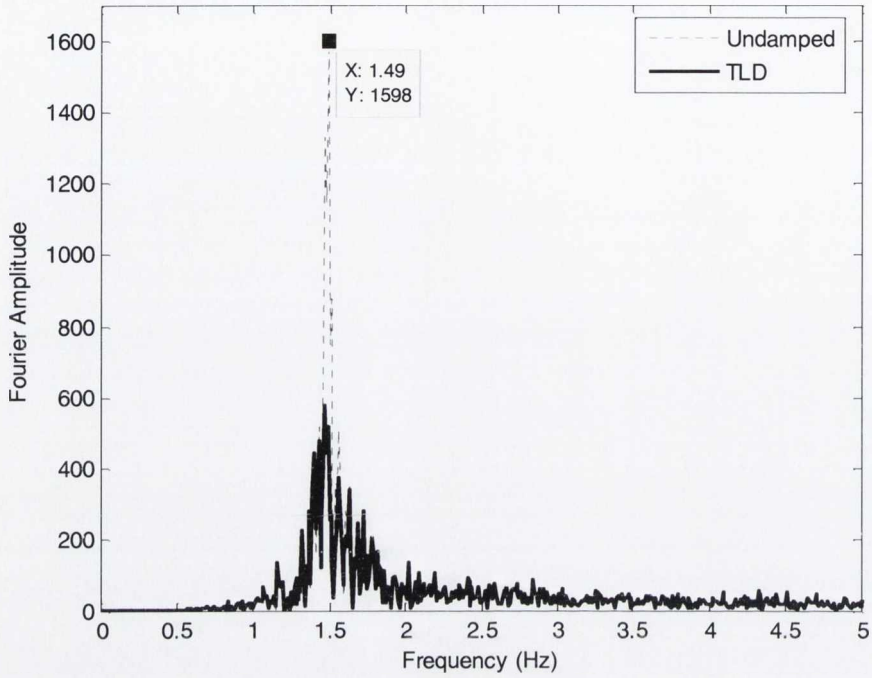

Figure 6.8: Frequency response of SDOF test structure with passive TLD, Kaimal load

6.3 Development of Semi-active TLD

After initial characterisation of the behaviour of the TLD as described above, the device was then developed into a semi-active damper to cater for stiffness loss or damage occurring in the primary system. This was achieved through real-time adjustment of the depth of liquid in the container.

6.3.1 Design of Semi-active TLD

A small hole was drilled in the base of the TLD and a drainage pipe installed. This pipe was attached to a valve which controlled the flow of liquid out of the TLD. This allowed the tuning of the TLD to be reduced to cater for any loss in the stiffness of the structure. A photograph of the semi-active TLD is shown below in figure 6.9.

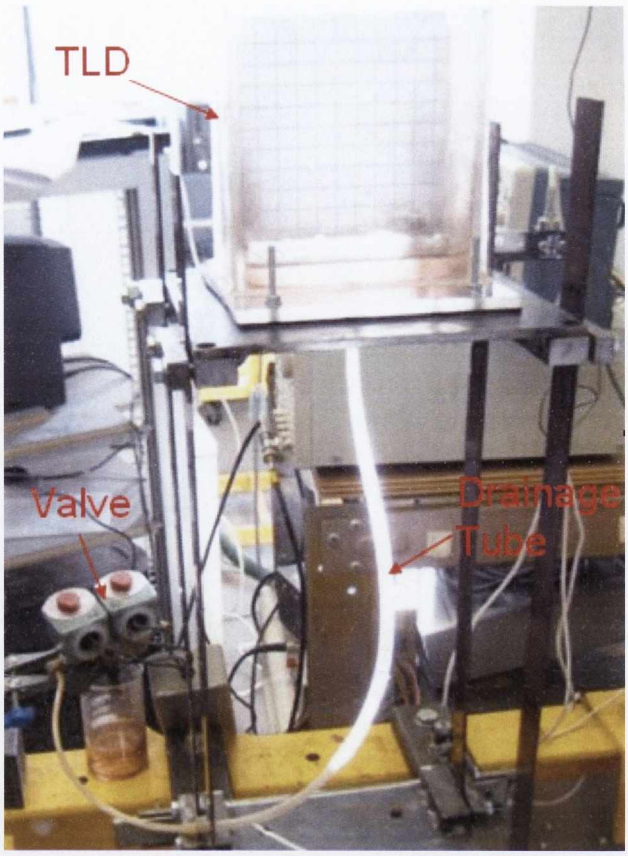

Figure 6.9: Semi-active TLD

The valve was connected to an automated computer system which, upon identification of a loss in the stiffness of the primary system, drained water from the damper to retune the TLD in real-time. The system developed was one way, catering for any loss in structural stiffness. For a more complex multi-modal structure whose dominant frequency may increase, a two way valve system would be required to allow the TLD to increase its tuning. The algorithm used for real-time frequency tracking was similar in nature to that described in Chapter 5 of this thesis and is outlined in the next section.

6.3.2 Semi-active Algorithm

As for the numerical results in Chapter 5, the control algorithm used for the experimental testing of the semi-active TLD was based on an STFT approach. The simple nature of the stiffness adjustable SDOF structure used to test this adaptive control system allowed the algorithm to be simplified. The resulting algorithm is shown below in figure 6.10.

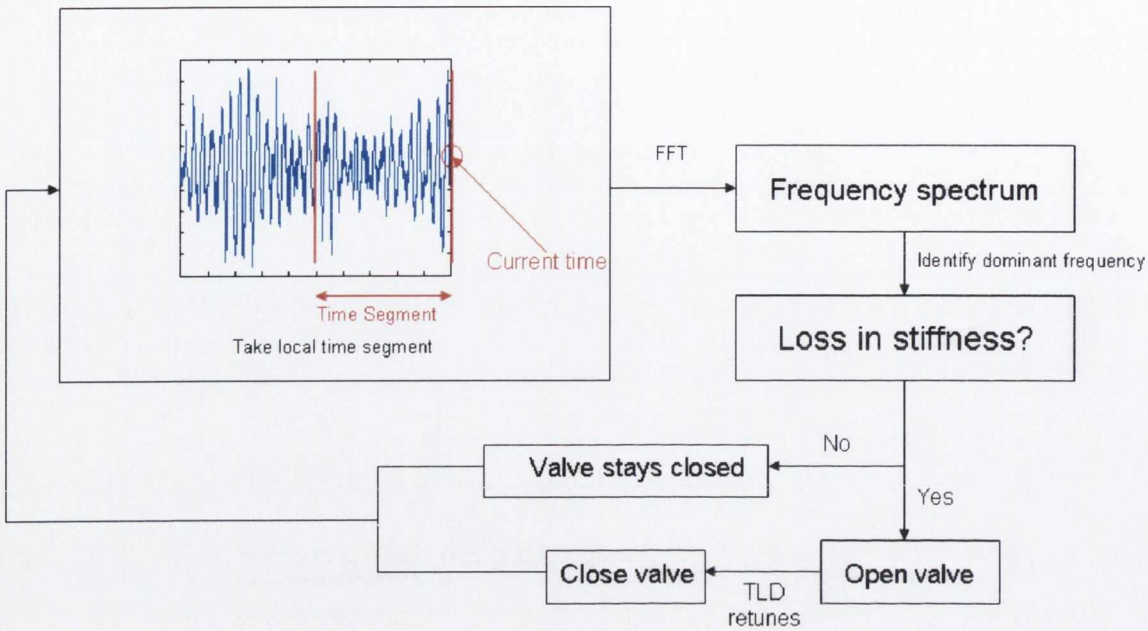

Figure 6.10: Semi-active TLD control algorithm

The response of the structure is split into short time segments or windows, as shown in figure 6.10. A window size of 10 seconds was used achieving a sampling frequency of 0.1Hz. A labview program was devised to record the accelerometer data in real-time and pass it into Matlab for STFT analysis. The dominant frequency of the response was calculated by transforming the response to the frequency domain. This was then compared to the dominant frequency for the previous window. If a loss in stiffness occurred the valve was opened to allow retuning of the TLD to the new dominant frequency. The time for which to open the valve was calculated based on the flow rate through the drainage tube and the magnitude of the loss in stiffness. The water volume in the TLD was tuned in real time according to the non-linear natural frequency plot in figure 6.4. Every 10 seconds a new window was passed into the algorithm for analysis allowing real-time frequency tracking and tuning of the semi-active TLD to the structure's dominant frequency.

6.3.3 Experimental Testing of Semi-active TLD

The semi-active adaptive control system was then tested to determine its effectiveness in mitigating vibrations and adjusting its tuning for changes in the dynamic properties of the primary system. The algorithm was first tested on the flexible structure to determine if it could accurately tune the TLD to the natural frequency of the primary system when the TLD was initially detuned. Tests on the stiffened structure with cross bracing described above were then also carried out.

6.3.3.1 Flexible Structure Results

Exact prior knowledge of the natural frequency of a structure is hard to estimate before the installation of a vibration mitigating device. This can lead to the mistuning of dampers and hence a less effective performance in terms of vibration mitigation. This is one of the main disadvantages of passive devices as, once installed in the structure, their tuning cannot be adjusted. The semi-active TLD was therefore initially detuned to the SDOF test structure. 100ml of water was initially placed in the TLD, tuning it to approximately 2.2Hz. This allowed determination of the algorithm's ability to identify the natural frequency of the structure and hence retune the TLD.

A Kaimal load was used to excite the structure, similar to that used for the passive tests in figure 6.7. Figure 6.11 below first compares the response of the undamped structure to the structure with the detuned TLD.

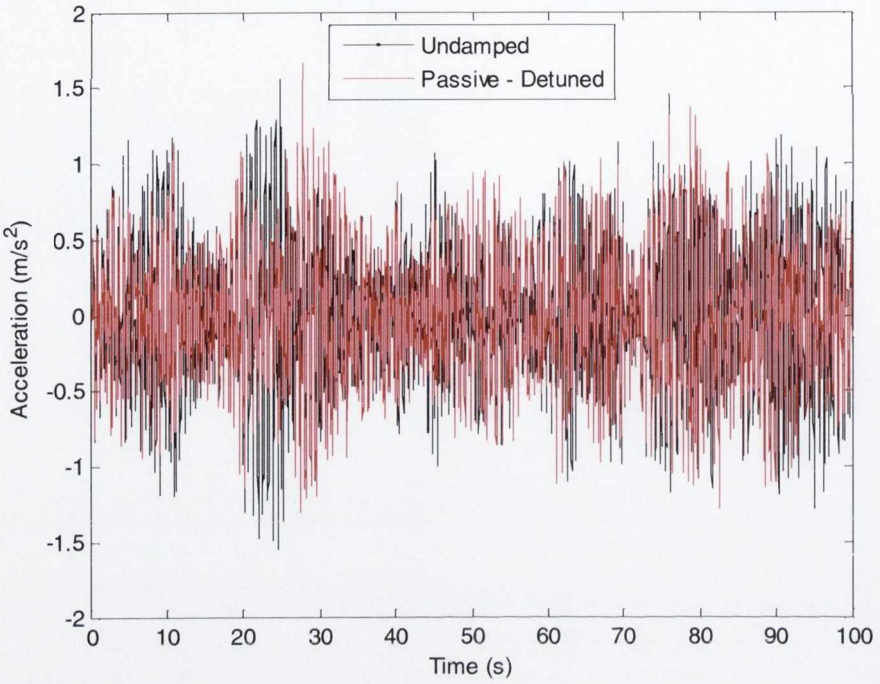

Figure 6.11: Acceleration response of flexible structure, Kaimal load

As can be observed some reduction is seen in the response of the structure despite the TLD being detuned, in particular when the magnitude of the structural motion is high. This is a result of more of the liquid mass being active from the large amplitude excitation, hence a reduction is achieved. This again highlights the advantage of a passive TLD over a TMD as it is effective over a wider frequency range. However, the response of the structure with the TLD is also seen to increase at other points in the time history emphasising that the TLD is not accurately tuned.

Figure 6.12 below compares the passive detuned response to the response for the semi-active TLD. On analysis of response of the system the algorithm identifies the TLD is not accurately tuned to the structure and hence gives the command to open the valve, reducing the volume of water to 50ml, thus retuning the TLD. As expected an improvement is seen in the response of the system when the TLD retunes.

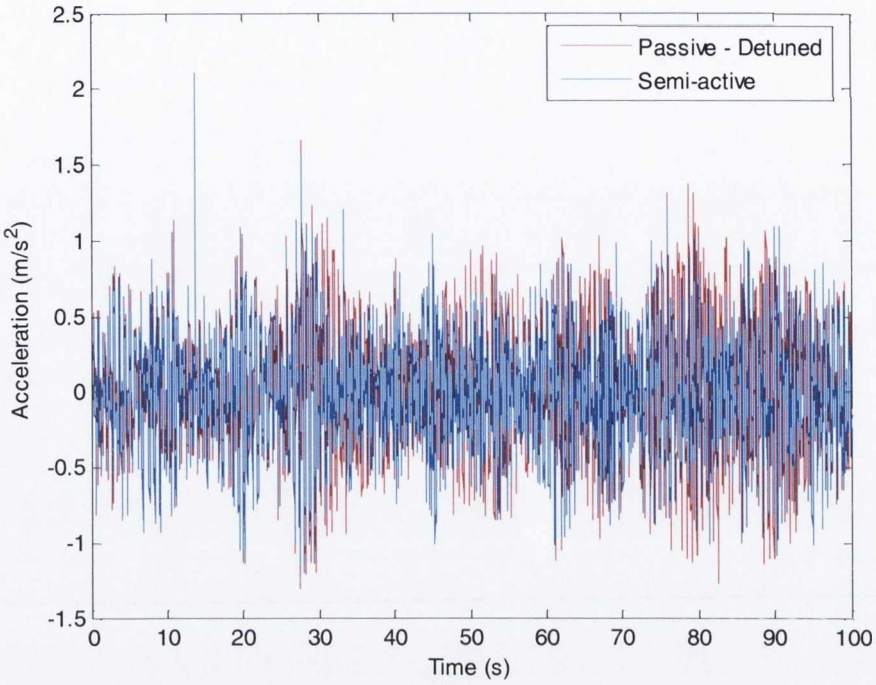

Figure 6.12: Acceleration response of flexible structure, Kaimal load

It is worth noting that, despite the loss in mass ratio, a greater reduction is seen in the response due to the more accurate tuning achieved by the semi-active algorithm. The temporal Root Mean Square (RMS) values for each of the vectors in figure 6.11 and 6.12 were calculated to determine the reduction in response achieved by the semi-active TLD over the course of the response. The results are shown in table 6.3 below.

Response	Temporal RMS Acceleration (m/s^2)
Undamped	0.440
Passive - Detuned	0.399
Semi-Active	0.360

Table 6.3: Temporal RMS acceleration

As can be observed the semi-active reduction is twice that of the passive detuned response highlighting the ability of the algorithm to identify and tune to the natural frequency of the structure in real-time. Figure 6.13 below plots all three responses highlighting a section of the

time history from 60 to 70s allowing clear identification of the performance of the semi-active TLD compared to the passive and undamped plots.

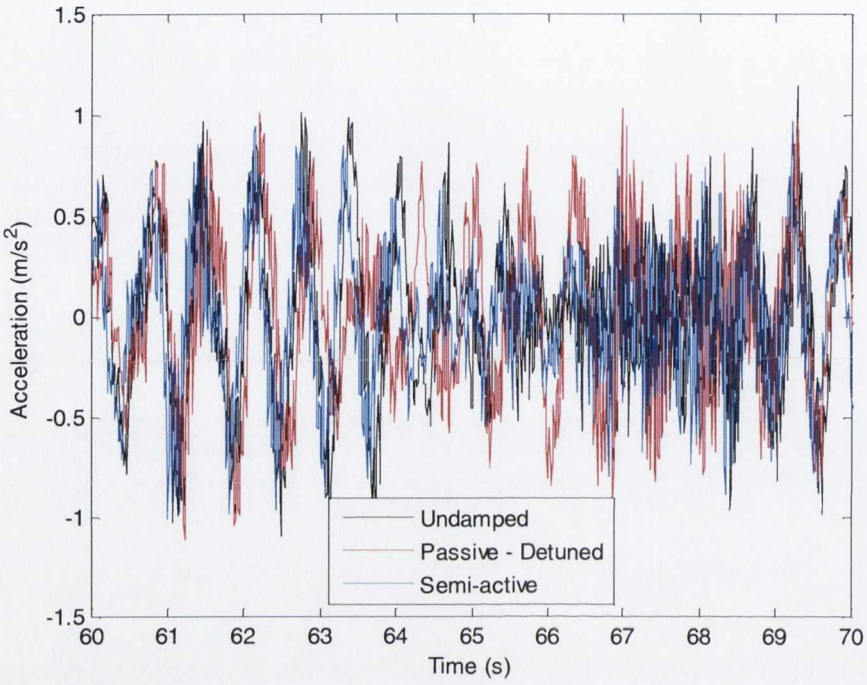

Figure 6.13: Acceleration response of flexible structure, 60-70s, Kaimal load

6.3.3.2 Stiffness Adjustable Structure Results

The semi-active control scheme was then tested on the stiffened SDOF structure with cross bracing in the form of string as described in section 6.2.1. A photograph of the structure with the semi-active TLD attached is shown in figure 6.14. The cross bracing allowed the structure to be stiffened to approximately 2.2Hz. The string was then cut during the excitation to change the natural frequency of the structure and study the ability of the control system to adjust for the change in the dynamic behaviour of the primary structure.

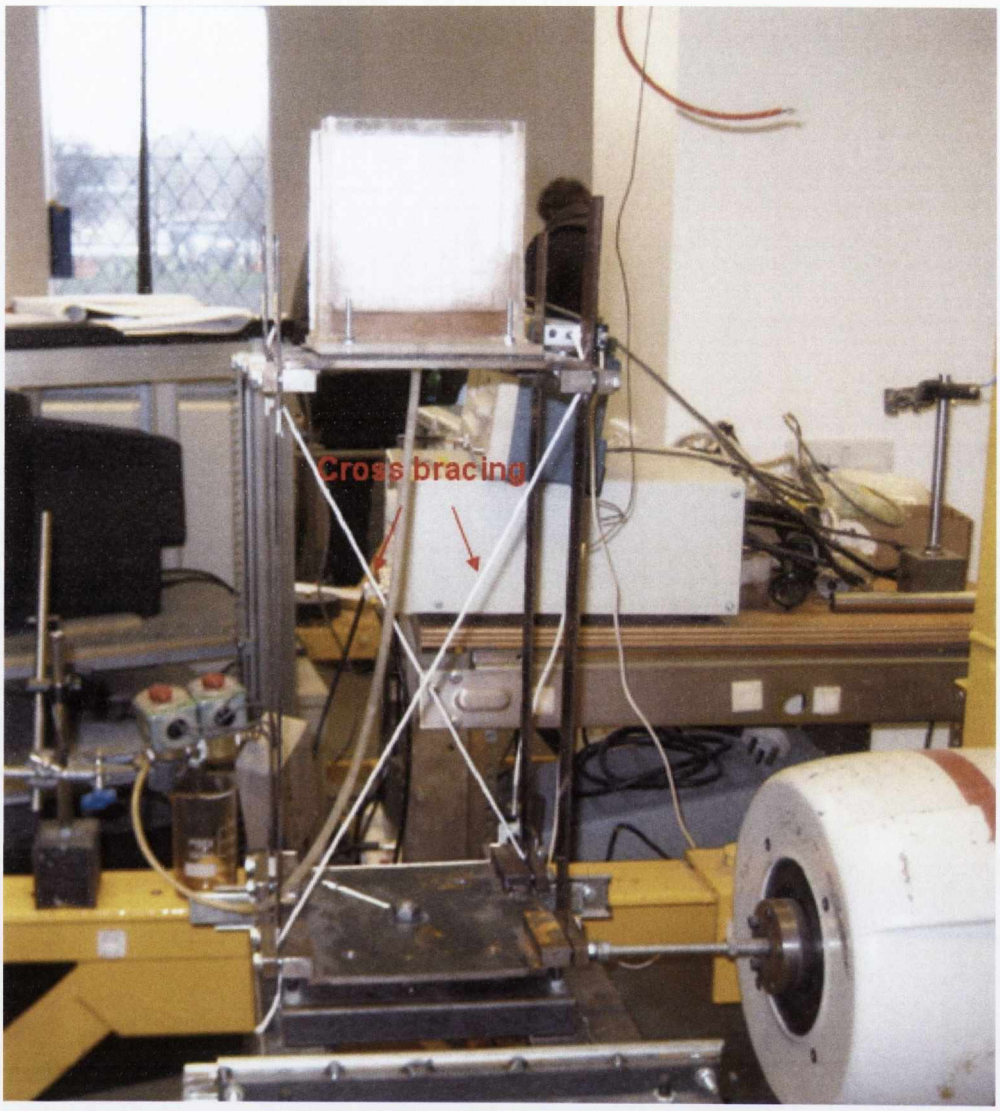

Figure 6.14: SDOF test structure with cross bracing

Figures 6.15 and 6.16 show the frequency plot before and after the string was cut (at t = 40s) highlighting the change in stiffness.

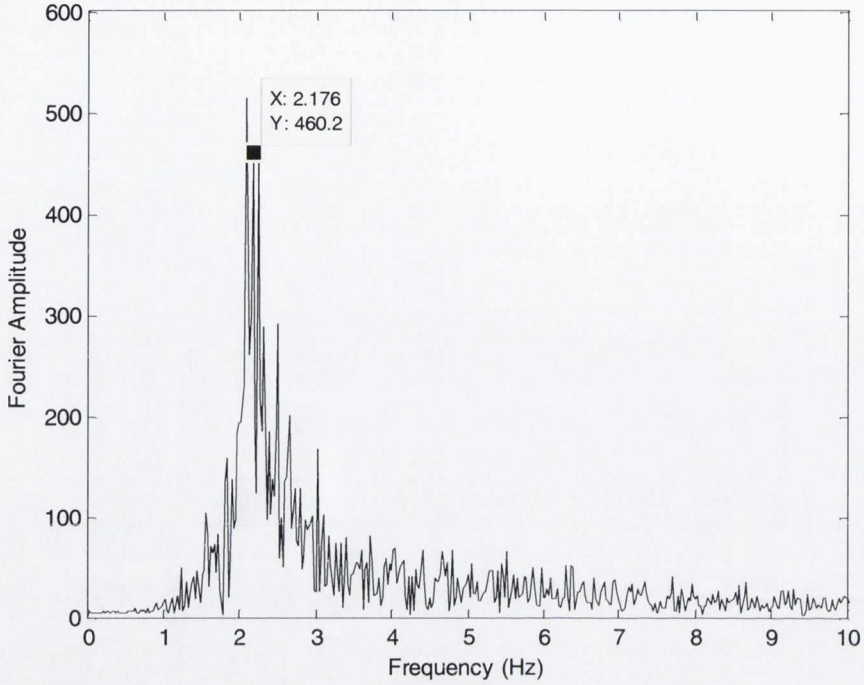

Figure 6.15: Frequency plot of structure before loss in stiffness

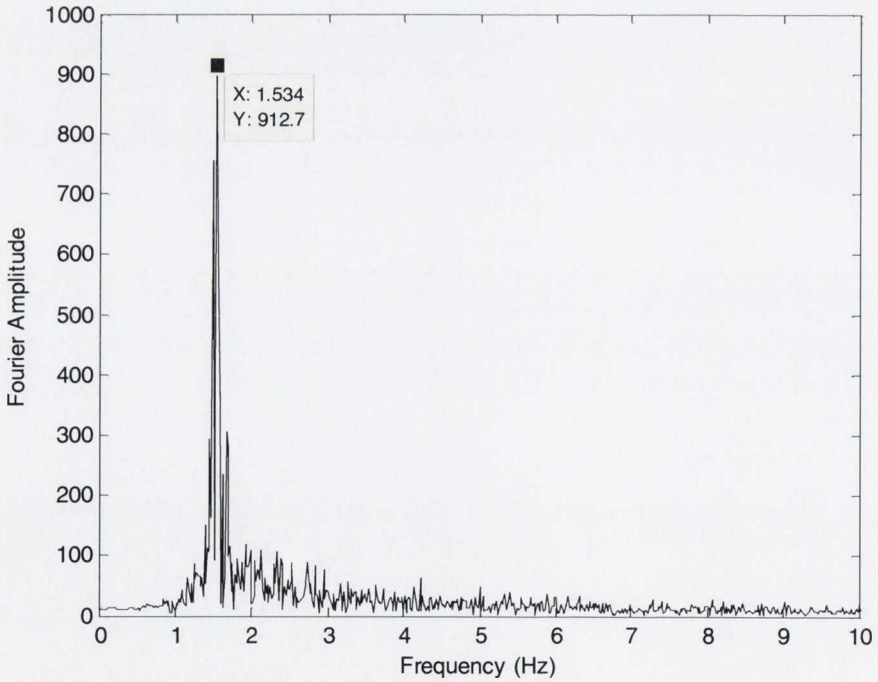

Figure 6.16: Frequency plot of structure after loss in stiffness

Figure 6.17 shows the acceleration response of the structure, comparing the undamped response to the passive and semi-active plots. The passive response was for a TLD tuned to 2.2Hz, i.e. the natural frequency of the structure before the change in stiffness. Once the stiffness change occurred in the structure the passive TLD would therefore be detuned for the rest of the time history.

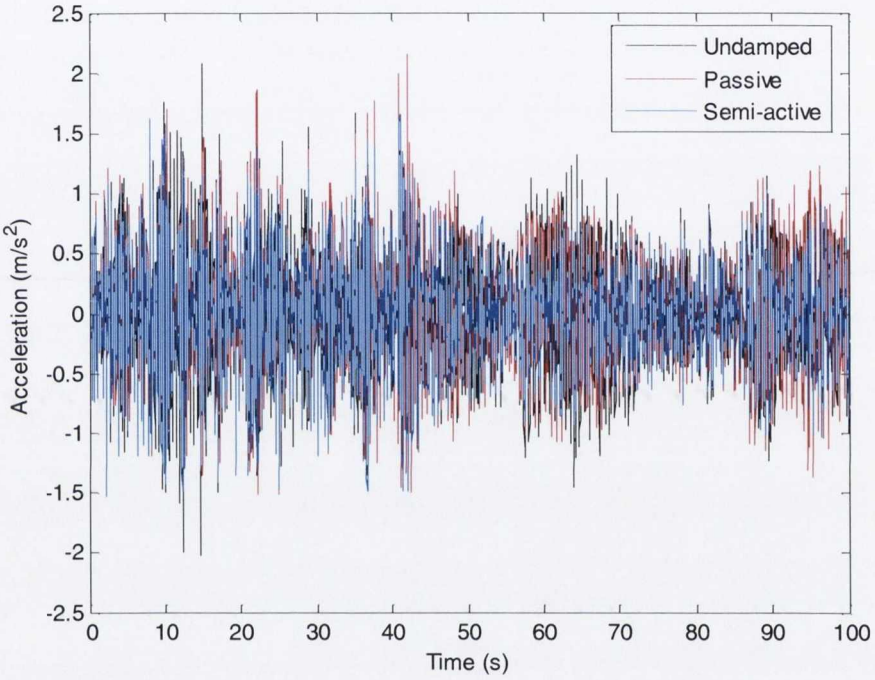

Figure 6.17: Acceleration response, change in structure stiffness, Kaimal load

As can be observed, the passive and semi-active plots show approximately the same response reduction for the first forty seconds as they have the same initial tuning. However, once the loss in the stiffness of the structure occurs at t = 40s the semi-active algorithm achieves a better reduction for the remainder of the time history as it adjusts the tuning of the TLD in real-time to cater for the change in the dynamic properties of the structure. The temporal RMS acceleration values for the response were again calculated to determine the reduction achieved by the semi-active algorithm. The results shown in table 6.4 below compare the RMS values after the loss in structural stiffness.

Response	Temporal RMS Acceleration (m/s^2)
Undamped	0.432
Passive	0.417
Semi-Active	0.324

Table 6.4: Temporal RMS acceleration after loss in stiffness

Again despite the loss in mass ratio which reduces from 4% to 2%, the improved tuning results in an increase in the effectiveness of the TLD after the loss in structural stiffness. As can be seen in table 6.4 the passive RMS value is only slightly smaller than the undamped RMS value indicating that little reduction is achieved by the passive TLD after the loss in structural stiffness as it is no longer accurately tuned to the structure. The semi-active RMS acceleration is significantly lower achieving a reduction of 25% over the undamped response. This again highlights the effectiveness of the adaptive control system developed in adjusting to changes in the dynamic parameters of the primary structure and hence achieving a reduction in the response.

Figure 6.18 shows an enhanced plot of figure 6.17 from 90 to 100s. This allows the improvement achieved by the semi-active algorithm to be clearly seen.

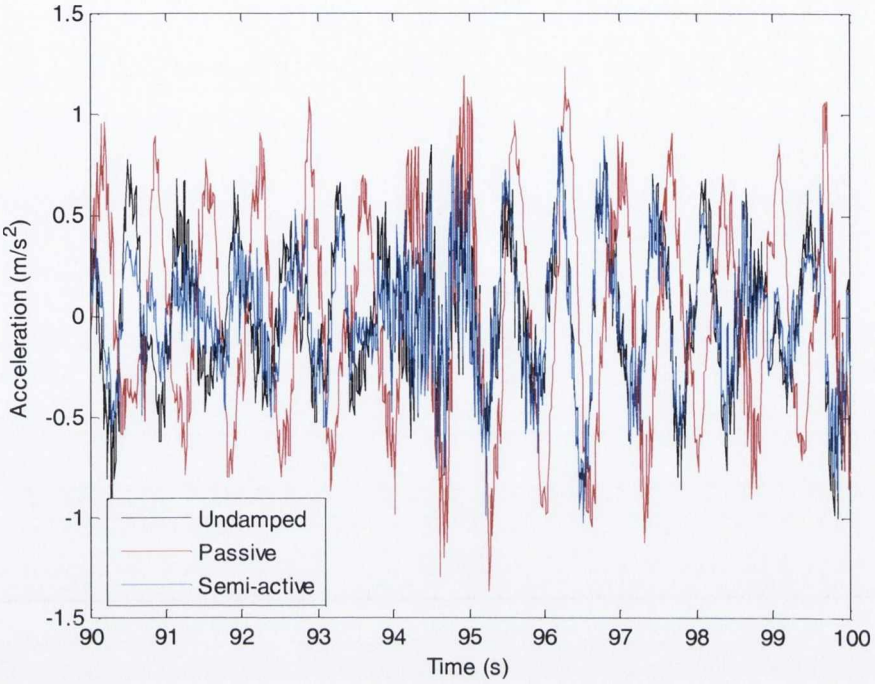

Figure 6.18: Acceleration response, change in structure stiffness, 90-100s, Kaimal load

Figure 6.19 below plots the dominant frequency of the structure with respect to time corresponding to the time history response plotted in figure 6.17. As can be seen the algorithm successfully identifies the change in stiffness at t = 40s which triggers opening of the valve to adjust the tuning of the TLD. This results in the improved performance achieved by the semi-active control system over the passive device as can be seen in the acceleration response above.

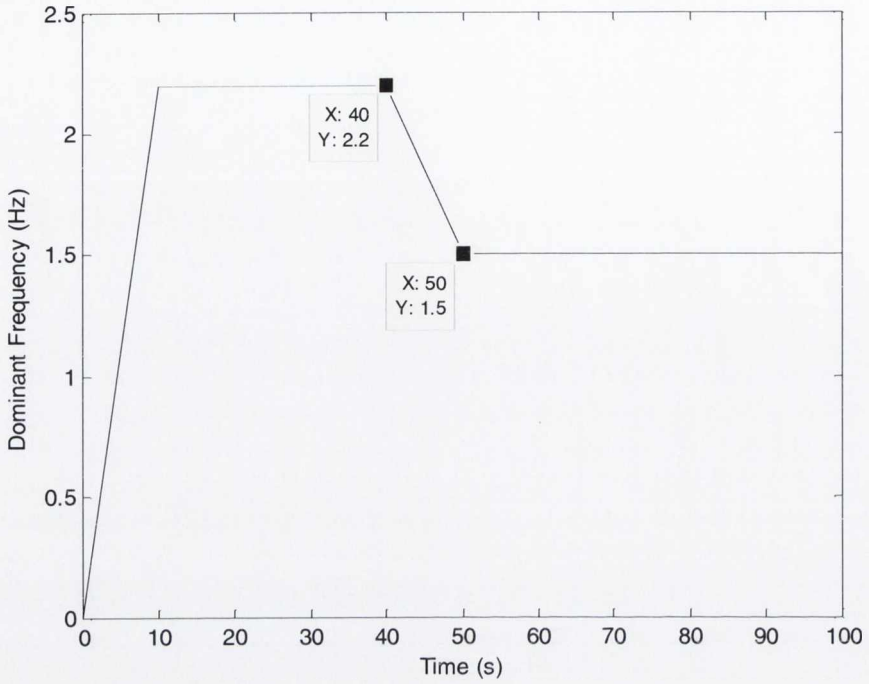

Figure 6.19: Frequency tracking, stiffness change at t = 40s

These tests were repeated a total of five times with the undamped, passive and semi-active acceleration responses measured for five different Kaimal loads, all generated by the method outlined in section 3.2.3.2 of this thesis. Figure 6.20 shows the RMS acceleration response for the five time histories.

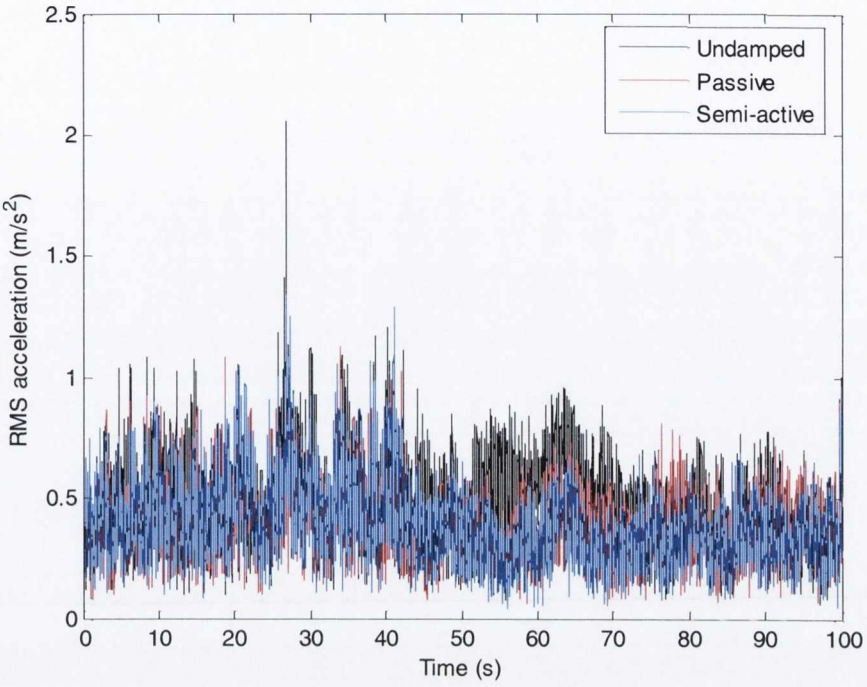

Figure 6.20: RMS acceleration response, Kaimal loading, stiffness change at t = 40s

As can be observed in the plot above the semi-active TLD achieves a greater reduction in the response of the structure as compared to the passive results after the change in stiffness at t = 40s. The improvement in reduction starts at approximately t = 55s as it takes time for the water to drain retuning the TLD to the new dominant frequency. This improved reduction once more emphasises the ability of the adaptive control system developed to cater for a loss in the stiffness of the primary structure by automatically adjusting the tuning of the TLD in real-time to the new dominant frequency.

6.4 Numerical Modelling of a TLD as an Equivalent TMD

As mentioned in Chapter 4 the mass-spring-dashpot systems used to represent the dampers in the numerical simulations can represent a TMD or equivalent TLD. Figure 6.21 shows a diagram of a TLD modelled as an equivalent mass-spring-dashpot system.

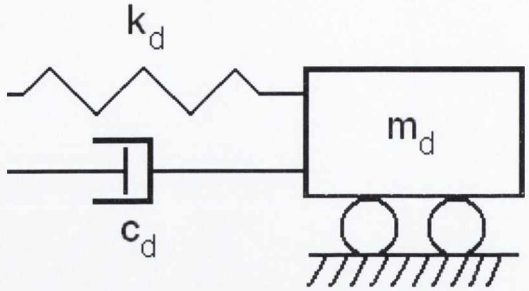

Figure 6.21: TLD equivalent TMD

Modelling a TLD as an equivalent TMD was investigated by Yu et al. (1999). They identified the equivalent damping ratio of a TLD, ξ_d as

$$\xi_d = 0.5\Lambda^{0.35} \tag{6.5}$$

where as before Λ is the non-dimensional amplitude of excitation, defined previously in equation 6.2. Assuming a very conservative non dimensional amplitude, $\Lambda = 0.01$ results in a damping ratio, $\xi_d = 0.1$ or 10%. This value increases with amplitude of excitation before leveling off at some maximum value. The damping, c_d can then be identified from

$$c_d = 2\xi_d \omega_d m_d \tag{6.6}$$

where ω_d is the natural frequency of the TLD and m_d is the mass of the damper. Assuming all the liquid to be active, the mass of the damper is simply taken as the mass of the water in the TLD. Finally the stiffness is calculated from

$$k_d = \omega_d^{\,2} m_d \tag{6.7}$$

The numerical studies in chapters 4 and 5 of this thesis assumed a small damping ratio, $\xi_d = 0.005$ or 0.5%. Even with this small amount of damping a good reduction was achieved in the response of the turbine model. The amplitude of motion of the blades and nacelle will easily achieve a non-dimensional amplitude, $\Lambda = 0.01$ which gives an equivalent damping, $\xi_d = 0.1$ or 10%. Therefore the dampers used in the numerical studies can be representative of TLDs

which easily achieve the assumed damping ratio of 0.005. The advantages of using TLDs as the vibration mitigating devices of choice in wind turbines are outlined in the following section.

6.5 Suitability of TLDs for use in Wind Turbines

TLDs exhibit several properties which make them particularly suitable for use in the vibration control of wind turbines. Due to the flexible nature of the blades and tower (especially in the large multi-Megawatt turbines), and hence their low fundamental frequencies, TLDs have an ideal range of effectiveness to accurately tune to the fundamental frequencies of these components. As stated above TLDs are also effective over a wide frequency range and increase in effectiveness with amplitude of vibration. Their zero trigger level is a further advantage over other damping devices as they provide damping even for very small amplitude oscillations.

Due to the rotation of the blades when a turbine is operational, the behaviour of a rectangular TLD will vary periodically over time. To counteract this for flapwise vibrations a simple hinge system could be installed to ensure the base of the TLD is horizontal at all times during rotation of the blades. This would ensure uniform behaviour of the TLDs during operation of the turbine. Furthermore, blades tend to suffer most damage during high loading events such as a storm. During these adverse conditions the turbines are shut down with their blades in the 'Y' position. Therefore correct orientation of the dampers to mitigate vibrations when the turbine is offline is another approach worth considering. This will result in mitigation of the most severe vibrations experienced by the blades, reducing fatigue and thus improving their design life.

For edgewise vibrations the motion of the liquid cannot always be kept perpendicular to direction of vibration due to the rotation of the blades. However, the TLD should still provide some damping to the blades through the sloshing of the liquid. Danish company LM used passive TLDs for mitigation of edgewise vibrations (Grabau, 1999). However, no analysis was done on their tuning or the mitigation effect they had on the edgewise vibrations

experienced by the blades. The TLD developed in this chapter aims to address this lack of knowledge.

6.5.1 Example TLD Design for Wind Turbine Blades

This section outlines the design of a simple passive TLD using linear theory suitable for the control of vibrations in wind turbine blades.

A tank size of 0.18x0.18m (length x breadth) was chosen. Equation 6.2 was used to determine the height of water needed to achieve the desired TLD frequency. Since the TLD is likely to experience high amplitude motion (i.e. A>0.03) a conservative estimate of non-dimensional amplitude, $A = 0.05$ was used in the calculations. The TLD was tuned to the blade flapwise frequency peak in figure 3.4 of 2.03Hz. To achieve this damper tuning a still water depth, h_0 = 0.092m is needed. This gives a required water volume in the TLD of 3l. Due to the blade mass of approximately 4500kg, fifteen TLDs of size 0.18x0.18m are required to achieve the mass ratio (μ = 1%) used in the numerical simulations in chapters 4 and 5. These passive TLDs could then be extended to semi-active behaviour as described above. With this damper simulations for semi-active vibration control of wind turbine blades can be carried out with the TLDs modelled as equivalent mass-spring-dashpot systems. This leads to the results seen in chapter 5 such as figures 5.2 and 5.4.

Finally, the small size of these tanks allow them to be places inside the turbine blades near the blade tip to achieve maximum response reduction. This was an assumption of the numerical model in the previous chapters. The space constraints in the nacelle/tower of the turbine would be less constricting allowing a larger TLD to be designed.

6.6 Conclusions

This chapter described the development of a semi-active TLD for use in the vibration control of wind turbine blades. A passive TLD was initially characterized with its tuning in the range of interest. The experimental characterisation was shown to be in good agreement with the theoretical natural frequencies. The TLD was tested on a SDOF test structure with a natural

frequency similar to that of the wind turbines blades used in the numerical studies of this thesis. Good reduction was achieved in the response of the structure for both harmonic and turbulent wind loading by accurate tuning of the TLD to the natural frequency of the primary system.

The device was extended to semi-active behaviour by use of an STFT based control algorithm similar to that used in Chapter 5. This allowed the tuning of the TLD to be adjusted in real-time by controlling the depth of water in the damper using a computer automated valve. The semi-active TLD was tested on a structure which experienced a loss in stiffness during its excitation. The control algorithm successfully identified the loss in the stiffness of the structure and retuned the TLD to cater for the new dynamic behaviour of the primary system. The structure was excited at its base by a Kaimal load representative of a real life wind load experienced by an operational turbine.

Modelling of a TLD as an equivalent TMD was also discussed and a simple method presented for the design of a passive TLD suitable for use in wind turbine blades. The suitability of TLDs for use as vibration control devices in wind turbines was also highlighted. Their advantages include their simplicity and self contained nature, zero trigger level and wide range of effectiveness compared to other damping devices.

CHAPTER 7 – Summary and Conclusions

7.1 Summary of Work

The aim of this thesis is to propose structural vibration control methods for wind turbines. This will address the lack of studies on the effectiveness of vibration mitigating devices in controlling the dynamic behaviour of wind turbines, in particular the blades. Over the last decade interest in renewable energy technologies has gained huge momentum, becoming an area of significant research. Wind energy is now paving the way forward as an alternative, environmentally friendly and affordable method of electricity generation. Multi-Megawatt turbines with tower heights and rotor diameters of 80m and 120m respectively are being installed in huge numbers, particularly across Europe and the USA. Ireland itself has huge potential to become a world leader in wind energy technology given the enormous resources present, particularly offshore. The huge size of these modern turbines has resulted in increased vibration problems with the dynamic behaviour of these structures critical to their overall feasibility.

A theoretical model of a three blade wind turbine was first developed to study the structural dynamic behaviour of the system. The blades were modelled as rotating cantilever beams attached at their root to the nacelle to allow inclusion of the dynamic coupling that occurs between the blades and tower. Models for both flapwise and edgewise vibrations were derived, including the effects from centrifugal stiffening of the blades. Dynamic coupling in the edgewise model between the tower and blades resulted in the occurrence of time varying system matrices. It is important to note that time varying damping arose in the edgewise model before the addition of structural damping. These terms were purely a result of the dynamic interaction present in the edgewise model. Structural damping was added to the models in the form of stiffness proportional damping.

Numerical simulations were carried out in Matlab allowing the response of the system to be analysed in the time domain. The results were transformed to the frequency domain by means of an FFT to determine the resonant frequencies present. Two loading scenarios were

considered. The first considered a uniform wind load that varied with height. Due to the rotation each blade experienced a periodic time varying load as it rotated through the wind field. The second load case considered the same uniform wind load with an added turbulent component. This turbulence was generated from a Kaimal spectrum to accurately represent a real-life wind flow experienced by an operational wind turbine. No load was considered on the nacelle. This allowed the coupling in the model to be clearly seen. Any motion of the nacelle was therefore a result of the dynamic interaction between it and the turbine blades.

Dynamic control of the turbine model was then considered. Dampers were added to both the flapwise and edgewise models to study their effect in mitigating vibrations in the structural system. These were modelled as mass-spring dashpot systems, represented of a TMD or equivalent TLD. One damper was added to the nacelle of the turbine with three more added to the blades, one at each blade tip. The hollow nature of wind turbine blades makes them automatically suitable for the installation of damping devices to mitigate their dynamic response without compromising their aerodynamic behaviour. However, little or no published literature exists investigating their potential in controlling vibrations in these structures. The equations of motion for the flapwise and edgewise models were then reformulated to include the effects of the TMDs. This gave each model a total of eight dof.

The passive behaviour of these dampers was first analysed. The behaviour of the nacelle and blade TMDs were studied separately to allow the dynamic interaction between the components to be understood. This allowed the coupled frequencies in the nacelle and blades to be easily identified. The dampers were tuned in turn to each frequency peak in the response of the system to study their vibration mitigation effects.

A semi-active algorithm was then developed based on an STFT approach to allow real-time tuning of the dampers to the dominant frequencies in the system. The response of the system was split into short time segments which were transformed into the time-frequency domain by an STFT. This allowed the time varying frequency content of the turbine model to be determined. The algorithm was repeated every second to allow real-time tracking of the dominant frequencies in both the nacelle and blades. The TMDs were then tuned in real-time to these dominant frequency peaks. The effectiveness of this algorithm in mitigating

vibrations in the structure was then studied for variations in the three main dynamic parameters of the turbine. Variation in the rotational speed, Ω, was first considered. A sudden loss in the stiffness of the nacelle and blades was also studied simulating the occurrence of damage in these components.

Finally, experimental development of a semi-active TLD was investigated for its potential use as a vibration mitigation device in a wind turbine. A passive TLD was first designed and experimentally characterised to verify the relationship between the natural frequency of the TLD and the still water depth. The TLD was tested on a simple SDOF structure consisting of four flexible columns with a mass on top. The natural frequency of the structure was similar to that of the wind turbine blades used in the numerical model. This allowed the behaviour of the TLD to be studied in the range of interest. The damper was first tested as a passive device to study its vibration mitigation effects. The passive TLD was then extended to a semi-active device by means of an STFT control algorithm, similar to that used for the numerical studies carried out in chapter 5. Real-time tuning of the TLD was achieved by controlling the depth of water in the container using an automated computer controlled valve. The semi-active TLD was tested on the SDOF test structure which experienced a loss in stiffness during its excitation. This allowed the ability of the adaptive control system in catering for a change in system dynamics to be determined. A Kaimal load similar to that applied in the numerical studies was used to excite the test structure through an actuator connected at its base. This allowed the effectiveness of the adaptive control system in mitigating vibrations due a real life wind load experienced by a wind turbine to be analysed. Modelling of a TLD as a mass-spring-dashpot system was also carried out to highlight how the damping in a TLD can be represented by an equivalent TMD.

7.2 Conclusions

This section outlines the conclusions that may be drawn from the numerical and experimental studies presented in this thesis.

The studies performed on the flapwise and edgewise Lagrangian models showed significant dynamic coupling to occur between the blades and tower of the turbine. In the flapwise

model, the nacelle motion induced through coupling with the turbine blades was of a similar order of magnitude. The coupling in the edgewise model was observed to be approximately 10%. As previously mentioned the dynamic interaction between the blades and tower resulted in the occurrence of time varying system matrices in the edgewise model. No time varying behaviour was seen in the flapwise model.

The addition of dampers to the dynamic model (one at each blade tip and one at the nacelle) was then studied. These were first passively tuned to the resonant peaks of the system, determined by transferring the response of the system to the frequency domain. It was seen that for a low rotational speed, typical of a modern wind turbine, the blades were not excited at resonance. The presence of coupled peaks in the system meant that tuning the nacelle TMD to a coupled peak achieved a reduction in the response of the blades as well as the nacelle itself. This was also true in the reverse case. For both the flapwise and edgewise models a frequency peak occurred at the rotational speed of the blades and forcing function frequency. Tuning the blade TMDs to this frequency peak was found to have no effect on the response of the system as it was far from the resonant peaks of the turbine itself. If a higher rotational speed was considered corresponding to the main frequency peak in the blade, a large reduction in the nacelle and blade displacements for both the flapwise and edgewise models was achieved.

While passive dampers were shown to be effective in controlling the response of the turbine system they have some limitations. Their main disadvantage is the inability to cater for changes in the dynamic parameters of the system being damped due to changes in operating and/or environmental conditions. Furthermore accurate tuning of passive devices can also be an issue as once installed their properties cannot be altered. This can lead to mistuning and hence poor performance of the dampers. Therefore it is advantageous to use so-called 'smart control devices' which can successfully identify and tune in real time to the dominant frequencies of the primary structure. As shown in the edgewise model wind turbines exhibit time varying behaviour, and variations in dynamic parameters such as the rotational speed of the blades can alter the dynamic characteristics. Therefore development of a semi-active control strategy was undertaken to provide a more robust method for vibration control of these structures.

As described in section 7.1, the semi-active algorithm developed was based on an STFT approach. A window size of 40s was used, achieving a sampling frequency of 0.025Hz. This ensured accurate tuning of the semi-active dampers to the dominant frequencies in the response of the turbine model. The dampers retuned every second to the current dominant frequency of the blades and nacelle. The adaptive control system was found to successfully track the dominant frequencies in the turbine model achieving a significant reduction in the response of both the blades and nacelle. Since many modern multi-Megawatt wind turbines operate at variable rotational speeds the performance of the control system for a varying rotational speed was studied. A loss in nacelle and blade stiffness was also considered simulating damage in the tower and blades of the structure. The control algorithm was shown to achieve a good reduction in the response of the system for all the variations considered in the dynamic parameters of the turbine when excited by a turbulent wind load. This highlights the suitability of the control scheme proposed for use in the dynamic control of wind turbines.

The experimental tests carried out looked at the development of a semi-active TLD. TLDs are deemed to be particularly suitable for use in wind turbine blades due to their simplicity and self contained nature. Furthermore, space constraints in the blades may require the restriction of damper motion if TMDs were used. This would reduce the amount of damping they could provide to the blades. However, no such issue exists with the use of TLDs as the damping is provided by the liquid motion inside the sealed container. TLDs are also effective over a wide frequency range due to the damping provided from not only the tuning but also the liquid sloshing. Their natural frequencies also lie in the low frequency range making them suitable for the vibration control of large wind turbines due to the flexible nature of the blades and tower.

The designed passive TLD was experimentally characterised and shown to be in close agreement with the non-linear theoretically predicted natural frequencies. This device was then extended to semi-active behaviour by installation of a small drainage tube and computer controlled valve which allowed the depth of water in the TLD to be reduced, catering for any loss in structural stiffness. The semi-active TLD was first initially detuned and seen to successfully identify the natural frequency of the SDOF system and tune in real-time to achieve an effective reduction in response. Further tests on a structure which experienced a

loss in stiffness while excited by a turbulent wind load were carried out. These demonstrated that the control system was able to successfully identify the loss in structural stiffness, and hence tune to the new dominant frequency, achieving an improved reduction in response over a passive TLD.

Modelling of a TLD as an equivalent TMD was also discussed. It has been highlighted that the damping ratio of a TLD is dependent on the non-dimensional amplitude and even for very small excitations a TLD can achieve significant damping. The TMDs used in the numerical studies required a very small damping ratio of just 1% to achieve a good reduction in response and it is deemed a reasonable assumption that TLDs will be able to provide this damping. A simple design method for TLDs suitable for use in turbine blades was finally presented. Their small size allows them to be placed inside the blades near the blade tip, thus maximising their vibration mitigation effects.

7.3 Recommendations for Future Work

With wind energy technology focusing towards offshore development due to the higher wind speeds and hence greater energy capabilities, it would be of significant relevance to extend the numerical model derived in this thesis to model an offshore wind turbine. This would involve modelling the offshore platform used to support a wind turbine in a marine environment. The loading experienced by an offshore turbine is more intricate in nature due the added wave loading at its base which would need to be taken into account. Furthermore the motion of the base would also be coupled to the tower and blades affecting the dynamics of the entire structure. Research into the dynamic control of an offshore wind turbine has been performed by Colwell and Basu (2009) who studied the use of TLCDs in the turbine tower. However, the application of the semi-active control scheme developed in this thesis to an offshore turbine would be of particular interest to determine its ability to cater for the more complicated system dynamics.

The semi-active TLD developed in the laboratory could also be developed further. The extension of the system to allow the level of water in the TLD to be increased should be performed. Due to the complicated dynamics of real life wind turbines, the ability of the

damper to tune to higher frequencies is also desirable. The semi-active TLD developed was shown to cater adequately for losses in structural stiffness. However, the dominant frequency in the primary system (whether a wind turbine or other structure) could also increase due to non-linearity in the system dynamics or excitation of a higher vibration mode. Therefore development of a semi-active TLD which could cater for this possibility would result in a more robust damping device.

Experimental tests looking at TLDs installed on real life turbine blades should also be explored. The possibility of experimentally investigating the behaviour of a TLD on a rotating blade, while ambitious, would be of great interest in determining how the TLD performs during rotation. As proposed in this thesis, a simple rotating hinge system could be developed for flapwise vibration control to ensure uniform behaviour of the TLD during the rotation of the blade.

Above are just a few of the possibilities when it comes to further research in the area of wind turbine dynamics and control. Due to the complicated nature of the system and the huge drive towards renewable energy technologies, it is expected that this will be an area of significant research for many years to come.

REFERENCES

Ackermann, T. & Söder, L. (2000) Wind energy technology and current status: a review. *Renewable and Sustainable Energy Reviews,* 4, 315-374.

Ahlstrom, A. (2005) Influence of Wind Turbine Flexibility on Loads and Power Production. *Wind Energy,* 9, 237-249.

Archer, C. L. & Jacobson, M. Z. (2005) Evaluation of global wind power. *J. Geophys. Res.,* 110.

Balendra, T., Wang, C. M. & Cheong, H. F. (1995) Effectiveness of tuned liquid column dampers for vibration control of towers. *Engineering Structures,* 17, 668-675.

Banerji, P., Murudi, M., Shah, A. H. & Popplewell, N. (2000) Tuned liquid dampers for controlling earthquake response of structures. *Earthquake Engineering and Structural Dynamics,* 29, 587-602.

Baumgart, A. (2002) A Mathematical Model for Wind Turbine Blades. *Journal of Sound and Vibration,* 251, 1-12.

Bazeos, N., Hatzigeorgiou, G. D., Hondros, I. D., Karamaneas, H., Karabalis, D. L. & Beskos, D. E. (2002) Static, seismic and stability analyses of a prototype wind turbine steel tower. *Engineering Structures,* 24, 1015-1025.

Bechly, M. E. & Clausen, P. D. (1997) Structural Design of a composite wind turbine blade using Finite Element Analysis. *Computers and Structures,* 63, 639-646.

Chang, C. C. (1999) Mass dampers and their optimal designs for building vibration control. *Engineering Structures,* 21, 454-463.

Chaviaropoutos, P. K. (2001) Flap/Lead-Lag Aeroelastic Stability of Wind Turbine Blades. *Wind Energy,* 4, 183-200.

Chaviaropoutos, P. K., Nikolaou, I. G., Aggelis, K. A., Sorensen, N. N., Johansen, J., Hansen, M. O. L., Gaunaa, M., Hambraus, T., von Geyr, H. F., Hirsch, C., Shun, K., Voutsinas, S. G., Tzabiras, G., Perivolaris, J. & Dyrmose, S. Z. (2003) Viscous and Aeroelastic Effects on Wind Turbine Blades. The VISCEL Project. Part 1: 3D Navier-Stokes Rotor Simulations. *Wind Energy,* 6, 365-385.

Chaviaropoutos, P. K., Politis, E. S., Lekou, D. J., Sorensen, N. N., Hansen, M. H., Bulder, B. H., Winkelaar, D., Lindenburg, C., Saravanos, D. A., Philippidis, T. P., Galiotis, C., Hansen, M. O. L. & Kossivas, T. (2006) Enhancing the Damping of Wind Turbine Rotor Blades, the DAMPBLADE Project. *Wind Energy,* 9, 163-177.

Clough, R. W. & Penzien, J. (1993) *Dynamics of Structures,* New York, McGraw Hill.

Colwell, S. & Basu, B. (2009) Tuned liquid column dampers in offshore wind turbines for structural control. *Engineering Structures,* 31, 358-368.

Den Hartog, J. P. (1985) *Mechanical Vibrations,* New York, Dover.

EWEA (2009a) Wind Energy - The Facts Executive Summary. European Wind Energy Association.

EWEA (2009b) Wind Energy Map 2008. European Wind Energy Association.

Fujino, Y., Sun, L., Pacheco, B. M. & Chaiseri, P. (1992) Tuned Liquid Damper (TLD) for Suppressing Horizontal Motion of Structures. *Journal of Engineering Mechanics,* 118, 2017-2030.

Gardarsson, S., Yeh, H. & Reed, D. (2001) Behaviour of Sloped Bottom Tuned Liquid Dampers. *Journal of Engineering Mechanics,* 127, 266-271.

Grabau, P. (1999) Windmill Blade with Vibration Damper. IN W.I.P.O (Ed.) F03D 1/06, 7/02, 11/00, F01D 5/16 ed. Denmark.

GWEC (2008) The Global Wind 2008 Report. Global Wind Energy Council.

Hansen, M. H. (2003) Improved Modal Dynamics of Wind Turbines to Avoid Stall-Induced Vibrations. *Wind Energy,* 6, 179-195.

Henderson, A. R. & Patel, M. H. (2003) On the Modelling of a Floating Offshore Wind Turbine. *Wind Energy,* 6, 53-86.

Henderson, A. R., Zaaijer, M. B. & Camp, T. R. (2003) Hydrodynamic Loading on Offshore Wind Turbines.

Hijmissen, J. W. & Van Horssen, W. T. (2007) On aspects of damping for a vertical beam with a tuned mass damper at the top. *Nonlinear Dynamics,* 50, 169-190.

J. C. Kaimal, J. C. Wyngaard, Y. Izumi & Coté, O. R. (1972) Spectral characteristics of surface-layer turbulence. *Quarterly Journal of the Royal Meteorological Society,* 98, 563-589.

Jensen, F. M., Falzon, B. G., Ankersen, J. & Stang, H. (2006) Structural testing and numerical simulation of 34m composite wind turbine blade. *Composite Structures,* 76, 52-61.

Joshi, A. S. & Jangid, R. S. (1997) Optimum Parmaters of Multiple Tuned Mass Dampers for Base-excited Damped Systems. *Journal of Sound and Vibration,* 202, 657-667.

Kallesøe, B. S. (2007) Equations of motion for a rotor blade, including gravity, pitch action and rotor speed variations. *Wind Energy,* 10, 209-230.

Kareem, A. (1983) Mitigation of wind induced motion of tall buildings. *Journal of Wind Engineering and Industrial Aerodynamics,* 11, 273-284.

Kareem, A. & Kline, S. (1995) Performance of multiple mass dampers under random loading. *Journal of Structural Engineering,* 121, 348-361.

Kong, C., Bang, J. & Sugiyama, Y. (2005) Structural investigation of composite wind turbine blade considering various load cases and fatigue life. *Energy,* 30, 2101-2114.

Kwok, K. C. S. & Samali, B. (1995) Performance of tuned mass dampers under wind loads. *Engineering Structures,* 17, 655-667.

Lamb, H. (1932) *Hydrodynamics*, Cambridge University Press.

Larsen, J. W., Nielsen, S. R. K. & Krenk, S. (2007) Dynamic stall model for wind turbine airfoils. *Journal of Fluids and Structures,* 23, 959-982.

Lavassas, I., Nikolaidis, G., Zervas, P., Efthimiou, E., Doudoumis, I. N. & Baniotopoulos, C. C. (2003) Analysis and design of the prototype of a steel 1-MW wind turbine tower. *Engineering Structures,* 25, 1097-1106.

Lee, D., Hodges, D. H. & Patil, M. J. (2002) Multi-Flexible-Body Dynamic Analysis of Horizontal Axis Wind Turbines. *Wind Energy,* 5, 281-300.

Li, H.-N., Jia, Y. & Wang, S.-Y. (2004) Theoretical and Experimental Studies on Reduction for Multi-Modal Seismic Responses of High-Rise Structures by Tuned Liquid Dampers. *Journal of Vibration and Control,* 10, 1041-1056.

Li, H.-N. & Ni, X.-L. (2007) Optimization of non-uniformly distributed multiple tuned mass damper. *Journal of Sound and Vibration,* 308, 80-97.

Li, S. J., Li, G. Q., Tang, J. & Li, Q. S. (2002) Shallow rectangular TLD for structural control implementation. *Applied Acoustics,* 63, 1125-1135.

Manwell, J. F., McGowan, J. G. & Rogers, A. L. (2002) *Wind Energy Explained: Theory, Design and Applications,* Chichester, Wiley.

Marín, J. C., Barroso, A., París, F. & Cañas, J. (2009) Study of fatigue damage in wind turbine blades. *Engineering Failure Analysis,* 16, 656-668.

Martínez, E., Sanz, F., Pellegrini, S., Jiménez, E. & Blanco, J. (2009) Life cycle assessment of a multi-megawatt wind turbine. *Renewable Energy,* 34, 667-673.

Murtagh, P. J., Basu, B. & Broderick, B. M. (2004a) Mode acceleration approach for rotating wind turbine blades. *Journal of Multi-body Dynamics,* 218, 159-166.

Murtagh, P. J., Basu, B. & Broderick, B. M. (2004b) Simple models for natural frequencies and mode shapes of towers supporting utilities. *Computers & Structures,* 82, 1745-1750.

Murtagh, P. J., Basu, B. & Broderick, B. M. (2005) Along-wind response of a wind turbine tower with blade coupling subjected to rotationally sampled wind loading. *Engineering Structures,* 27, 1209-1219.

Murtagh, P. J., Ghosh, A., Basu, B. & Broderick, B. M. (2008) Passive control of wind turbine vibrations including blade/tower interaction and rotationally sampled turbulence. *Wind Energy,* 11, 305-317.

Nagarajaiah, S. & Basu, B. (2009) Output only modal identification and structural damage detection using time frequency & wavelet techniques. *Earthquake Engineering and Engineering Vibration,* 8, 583-605.

Nagarajaiah, S. & Sonmez, E. (2007) Structures with Semiactive Variable Stiffness Single/Multiple Tuned Mass Dampers,. *Journal of Structural Engineering,* 133, 67-77.

Nagarajaiah, S. & Varadarajan, N. (2005) Short time Fourier transform algorithm for wind response control of buildings with variable stiffness TMD. *Engineering Structures,* 27, 431-441.

Naguleswaran, S. (1994) Lateral Vibration of a Centrifugally Tensioned Uniform Euler-Bernoulli Beam. *Journal of Sound and Vibration,* 176, 613-624.

Olson, D. E. & Reed, D. A. (2001) A nonlinear numerical model for sloped-bottom tuned liquid dampers. *Earthquake Engineering and Structural Dynamics,* 30, 731-743.

Özdemir, Ö. & Kaya, M. O. (2006) Flapwise bending vibration analysis of a rotating tapered cantilever Bernoulli-Euler beam by differential transform method. *Journal of Sound and Vibration,* 289, 413-420.

Pinkaew, T. & Fujino, Y. (2001) Effectiveness of semi-active tuned mass dampers under harmonic excitation. *Engineering Structures,* 23, 850-856.

Quarton, D. C. (1998) The evolution of wind turbine design analysis - a twenty year progress review. *Wind Energy,* 1, 5-24.

Rana, R. & Soong, T. T. (1998) Parametric study and simplified design of tuned mass dampers. *Engineering Structures,* 20, 193-204.

Rasmussen, F., Hansen, M. H., Thomson, K., Larsen, T. J., Bertagnolio, F., Johansen, J., Madsen, H. A., Bak, C. & Hansen, A. M. (2003) Present Status of Aeroelasticity of Wind Turbines. *Wind Energy,* 6, 213-228.

Reed, D., Yeh, H., Yu, J. & Gardarsson, S. (1998) Tuned liquid dampers under large amplitude excitation. *Journal of Wind Engineering and Industrial Aerodynamics,* 74-76, 923-930.

Ricciardelli, F., Occhiuzzi, A. & Clemente, P. (2000) Semi-active Tuned Mass Damper control strategy for wind-excited structures. *Journal of Wind Engineering and Industrial Aerodynamics,* 88, 57-74.

Ronold, K. O. & Larsen, G. C. (2000) Reliability-based design of wind-turbine rotor blades against failure in ultimate loading. *Engineering Structures,* 22, 565-574.

Ronold, K. O., Wedel-Heinen, J. & Christensen, C. J. (1999) Reliability-based fatigue design of wind turbine rotor blades. *Engineering Structures,* 21, 1101-1114.

Schreck, S. & Robinson, M. (2005) Blade Three-Dimensional Dynamic Stall Response to Wind Turbine Operating Condition. *Journal of Solar Engineering,* 127, 488-495.

Shokrieh, M. M. & Rafiee, R. (2006) Simulation of fatigue failure in a full composite wind turbine blade. *Composite Structures,* 74, 332-342.

Shum, K. M. & Xu, Y. L. (2004) Multiple tuned liquid column dampers for reducing coupled lateral and torsional vibration of structures. *Engineering Structures,* 26, 745-758.

Sicot, C., Devinant, P., Loyer, S. & Hureau, J. (2008) Rotational and turbulence effects on a wind turbine blade. Investigation of the stall mechanisms. *Journal of Wind Engineering and Industrial Aerodynamics,* 96, 1320-1331.

Simiu, E. & Scanlan, R. (1996) *Wind Effects on Structures,* New York, John Wiley & Sons.

Snel, H. (2003) Review of Aerodynamics for Wind Turbines. *Wind Energy,* 6, 203-211.

Stol, K., Balas, M. & Bir, G. (2002) Floquet Modal Analysis of a Teetered-Rotor Wind Turbine. *Journal of Solar Energy Engineering,* 124, 364-371.

Sutherland, H. J. (2000) A Summary of the Fatigue Properties of Wind Turbine Materials. *Wind Energy,* 3, 1-34.

Tait, M. J., Damatty, A. A. E. & Isyumov, N. (2005a) An investigation of tuned liquid dampers equipped with damping screens under 2D excitation. *Earthquake Engineering & Structural Dynamics,* 34, 719-735.

Tait, M. J., El Damatty, A. A., Isyumov, N. & Siddique, M. R. (2005b) Numerical flow models to simulate tuned liquid dampers (TLD) with slat screens. *Journal of Fluids and Structures,* 20, 1007-1023.

Tavner, P. J., Xiang, J. & Spinato, F. (2006) Reliability Analysis for Wind Turbines. *Wind Energy.*

Thomson, K., Petersen, J. T., Nim, E., Oye, S. & Petersen, B. (2000) A Method for Determination of Damping for Edgewise Blade Vibrations. *Wind Energy,* 3, 233-246.

UNFCCC (1992) United Nations Framework Convention on Climate Change.

Uys, P. E., Farkas, J., Jármai, K. & van Tonder, F. (2007) Optimisation of a steel tower for a wind turbine structure. *Engineering Structures,* 29, 1337-1342.

Van de Vegte, J. & de Silva, C. W. (1976) Design of passive vibration controls for internally damped beams by modal control techniques. *Journal of Sound and Vibration,* 45, 417-425.

Veldkamp, H. F. & van der Tempel, J. (2005) Influence of Wave Modelling on the Prediction of Fatigue for Offshore Wind Turbines *Wind Energy,* 8, 49-65.

Wang, J. Y., Ni, Y. Q., Ko, J. M. & Spencer Jr., B. F. (2005) Magneto-rheological tuned liquid column dampers (MR-TLCDs) for vibration mitigation of tall buildings: modelling and analysis of open loop control. *Computers and Structures,* 83, 2023-2034.

Wu, J. & Chen, G. (2000) Optimization of multiple tuned mass dampers for seismic response reduction. *American Control Conference.* Chicago, Illinois.

Yang, G., Spencer Jr., B. F., Carlson, J. D. & Sain, M. K. (2002) Large-scale MR Fluid Dampers: Modelling and Dynamic Performance Considerations. *Engineering Structures,* 24, 309-323.

Yoo, H. H. & Shin, S. H. (1998) Vibration analysis of rotating cantilever beams. *Journal of Sound and Vibration,* 212, 807-828.

Yoshioka, H., Ramallo, J. C. & Spencer Jr., B. F. (2002) "Smart" Base Isolation Strategies Employing Magnetorheological Dampers. *Journal of Engineering Mechanics,* 128, 540-551.

Yu, J.-K., Wakahara, T. & Reed, D. A. (1999) Non-linear numerical model of the tuned liquid damper. *Earthquake Engineering and Structural Dynamics,* 28, 671-686.

Zaaijer, M. B. (2006) Foundation modelling to assess dynamic behaviour of offshore wind turbines. *Applied Ocean Research,* 28, 45-57.

Zang, J. & Roschke, P. N. (1999) Active Control of a Tall Structure Excited by Wind. *Journal of Wind Engineering and Industrial Aerodynamics,* 83, 209-223.

Appendix A - Model Formulation

A.1 Flapwise Model

The undamped model was formulated first for a single rotating blade coupled to the nacelle in the flapwise direction, depicted below in figure A.1. The blade was modelled as a cantilever beam as mentioned in chapter 3. The displacement of the blade was expressed as

$$u_{1,f}(x,t) = \phi(x) q_{1,f}(t) \tag{A.1}$$

where $q_{1,f}$ is the blade tip displacement. This allowed the continuous beam to be reduced to a SDOF system. The fundamental modeshape, $\phi(x)$, was taken as a quadratic function given by

$$\phi(x) = \frac{x^2}{L^2} \tag{A.2}$$

where L is the total length of the blade and x is the distance from the blade root.

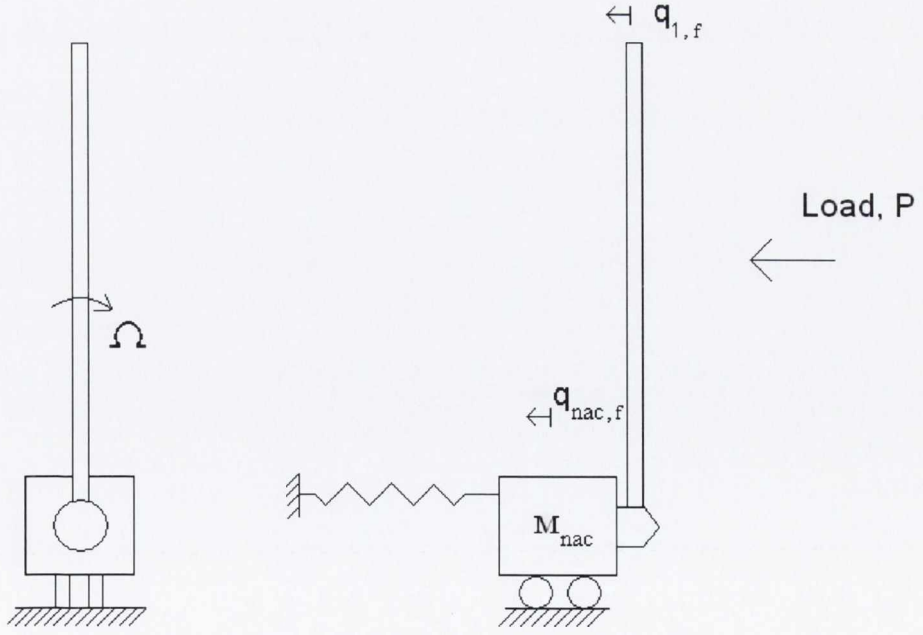

Figure A.1: Single blade flapwise model with nacelle coupling

The total kinetic energy of the single blade system, T_{fl} is given by

$$T_{f1} = \frac{1}{2}\overline{m}\int_0^L v_{b1,f}(x,t)^2\,dx + \frac{1}{2}M_{nac}\dot{q}_{nac,f}{}^2 \tag{A.3}$$

where $v_{b1,f}$ is the total velocity of blade 1 in the flapwise direction, including the nacelle motion that causes blade displacement. This ensures inclusion of the coupling between the blade and nacelle and is expressed below in equation A.4. The overdots represent the first derivative with respect to time.

$$v_{b1}(x,t) = \phi(x)\dot{q}_{1,f} + \dot{q}_{nac,f} \tag{A.4}$$

Subbing equation A.4 into equation A.3 and performing the integration gives the final expression for the kinetic energy as

$$T_{f1} = \frac{m_b}{10}\dot{q}_{1,f}{}^2 + \frac{m_b}{3}\dot{q}_{1,f}\dot{q}_{nac,f} + \frac{m_b}{2}\dot{q}_{nac,f}{}^2 + \frac{1}{2}M_{nac}\dot{q}_{nac,f}{}^2 \tag{A.5}$$

The potential energy of the cantilever blade in bending is given by

$$V = \frac{1}{2}\int_0^L EI_f(x)\left(\frac{\partial^2 u_{1,f}}{\partial x^2}\right)^2 dx \tag{A.6}$$

Where E is the Young's Modulus and I_f is the second moment of area. These are constant along the length of the blade as it has a uniform cross-section. Differentiating the flapwise blade displacement, $u_{1,f}$, twice with respect to x gives

$$\frac{\partial^2 u_{1,f}}{\partial x^2} = \frac{2}{L^2}q_{1,f} \tag{A.7}$$

The potential energy of the blade can then be expressed by

$$V_{b,f} = \frac{1}{2}\int_0^L EI_f \left(\frac{2}{L^2} q_{1,f}\right)^2 dx \tag{A.8}$$

The potential energy of the blade from centrifugal stiffening was outlined in chapter 3 of the thesis in equation 3.8 and is expressed here in equation A.9

$$V_{ci} = \frac{1}{2}\Omega^2 \int_0^L \left(q_i \frac{d\phi(x)}{dx}\right)^2 \int_x^L m(\zeta)\zeta d\zeta dx \tag{A.9}$$

where Ω is the rotational speed of the blade. This results in another term in the potential energy of the blade

$$V_{ci} = \frac{2\Omega^2 m_b}{15} {q_{1,f}}^2 \tag{A.10}$$

Adding this to equation A.8 above and performing the integration gives the total potential energy of the rotating blade as

$$V_{b1} = \left(\frac{2EI_f}{L^3} + \frac{2\Omega^2 m_b}{15}\right) {q_{1,f}}^2 \tag{A.11}$$

Finally, addition of the potential energy of the nacelle results in the final expression for the flapwise potential energy of the whole system

$$V_{f1} = \left(\frac{2EI_f}{L^3} + \frac{2\Omega^2 m_b}{15}\right) {q_{1,f}}^2 + \frac{1}{2} K_{nac} {q_{nac,f}}^2 \tag{A.12}$$

where K_{nac} is the stiffness of the nacelle/tower. The Lagrangian formulation in equation A.13 was then applied to the single blade model to derive the equations of motion for the system.

$$\frac{d}{dt}\left(\frac{\delta T_{f1}}{\delta \dot{q}_i}\right)-\frac{\delta T_{f1}}{\delta q_i}+\frac{\delta V_{f1}}{\delta q_i}=Q_i \tag{A.13}$$

where Q_i is the generalized loading on degree of freedom i. Applying the formulation to each degree of freedom results in the equations of motion below.

$$\begin{bmatrix} \frac{m_b}{5} & \frac{m_b}{3} \\ \frac{m_b}{3} & M_{nac}+m_b \end{bmatrix}\begin{Bmatrix} \ddot{q}_{1,f} \\ \ddot{q}_{nac,f} \end{Bmatrix}+\begin{bmatrix} \frac{4EI_f}{L^3} & 0 \\ 0 & K_{nac} \end{bmatrix}\begin{Bmatrix} q_{1,f} \\ q_{nac,f} \end{Bmatrix}=\begin{Bmatrix} Q_{1,f} \\ Q_{nac,f} \end{Bmatrix} \tag{A.14}$$

The loading on the nacelle was assumed to be zero so that any motion of the nacelle was purely a result of dynamic interaction with the blade. The loading on the blade $Q_{1,f}$ was detailed in chapter 3. Structural damping was added to the system in the form of stiffness proportional damping.

Equation A.14 can then be simply extended to a three blade turbine, giving the final equations for the flapwise model which are expressed in equation 3.10.

$$\begin{bmatrix} \frac{m_b}{5} & 0 & 0 & \frac{m_b}{3} \\ 0 & \frac{m_b}{5} & 0 & \frac{m_b}{3} \\ 0 & 0 & \frac{m_b}{5} & \frac{m_b}{3} \\ \frac{m_b}{3} & \frac{m_b}{3} & \frac{m_b}{3} & M_{nac}+3m_b \end{bmatrix}\begin{Bmatrix} \ddot{q}_{1,f} \\ \ddot{q}_{2,f} \\ \ddot{q}_{3,f} \\ \ddot{q}_{nac,f} \end{Bmatrix}+\begin{bmatrix} c_{st,b} & 0 & 0 & 0 \\ 0 & c_{st,b} & 0 & 0 \\ 0 & 0 & c_{st,b} & 0 \\ 0 & 0 & 0 & c_{st,nac} \end{bmatrix}\begin{Bmatrix} \dot{q}_{1,f} \\ \dot{q}_{2,f} \\ \dot{q}_{3,f} \\ \dot{q}_{nac,f} \end{Bmatrix}+$$
$$\begin{bmatrix} \frac{4EI_f}{L^3}+\frac{4\Omega^2 m_b}{15} & 0 & 0 & 0 \\ 0 & \frac{4EI_f}{L^3}+\frac{4\Omega^2 m_b}{15} & 0 & 0 \\ 0 & 0 & \frac{4EI_f}{L^3}+\frac{4\Omega^2 m_b}{15} & 0 \\ 0 & 0 & 0 & K_{nac} \end{bmatrix}\begin{Bmatrix} q_{1,f} \\ q_{2,f} \\ q_{3,f} \\ q_{nac,f} \end{Bmatrix}=\{Q_f\} \tag{A.15}$$

where $q_{1,f}$ and $q_{2,f}$ represent the motion of blades 2 and 3. The damping matrix contains the terms due to the assumed structural damping in the system. These are labelled $c_{st,b}$ and $c_{st,nac}$ representing the structural damping in the blades and nacelle respectively.

A.2 Edgewise Model

As for the flapwise model the edgewise model was first formulated for a single blade attached to the nacelle as shown in figure A.2 below.

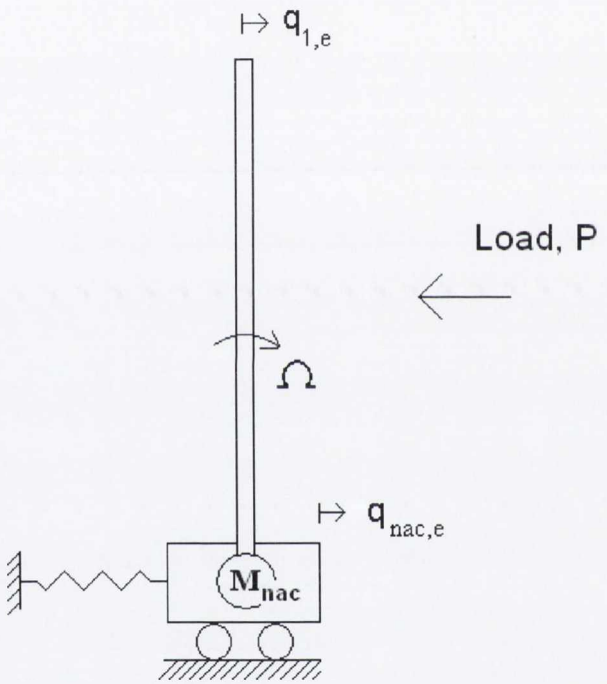

Figure A.2: Single blade edgewise model with nacelle coupling

As for the flapwise model the blade was represented by a cantilever beam vibrating in its fundamental mode.

$$u_{1,e}(x,t) = \phi(x) q_{1,e}(t) \tag{A.16}$$

where $q_{1,e}$ is the edgewise blade tip displacement. The fundamental modeshape, $\phi(x)$, was as before assumed to be a quadratic function as per equation A.2.

Due to the rotation of the blades the model was formulated from a fixed point of reference, O, as shown in figure A.3 below.

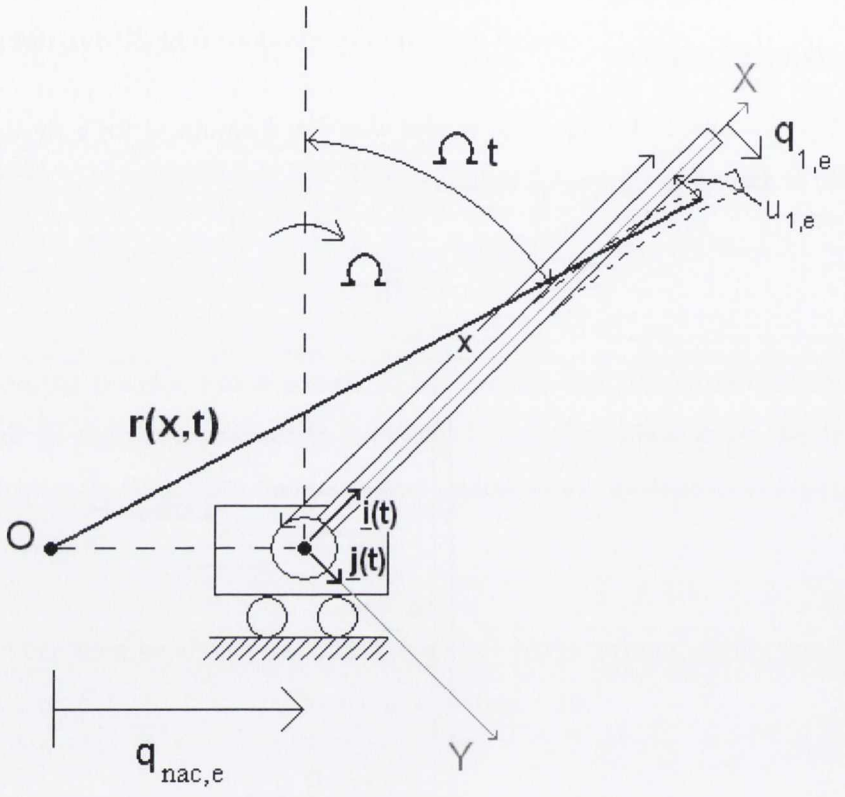

Figure A.3: Edgewise model formulation

The vector r(x,t) represents the position of any point, x, along the blade from the reference point, O. This includes the motion of the nacelle and the rotation and bending of the blade in the edgewise direction. The coordinate frame X, Y rotates with the blade at a rotational speed of Ω. The vectors i(t) and j(t) hence change with time due to the rotating frame of reference X, Y. By using basic trigonometry r(x,t) can be expressed in terms of i(t) and j(t) as

$$r(x,t) = \left(q_{nac,e}\sin(\Omega t) + x\right)\underline{i}(t) + \left(q_{nac,e}\cos(\Omega t) + u_{1,e}(x,t)\right)\underline{j}(t) \qquad \text{(A.17)}$$

The velocity of the blade is hence given as the first derivative of equation A.17 with respect to time, which by applying the product and chain rules results in

$$v_{b1,e}(x,t) = \dot{r}(x,t) = \left(\dot{q}_{nac,e}\sin(\Omega t) - \Omega u_{1,e}(x,t)\right)\underline{i}(t) + \left(\dot{q}_{nac,e}\cos(\Omega t) + \Omega x + \dot{u}_{1,e}(x,t)\right)\underline{j}(t) \quad \text{(A.18)}$$

The square of the velocity is thus

$$v_{b1,e}(x,t)^2 = \left(\dot{q}_{nac,e}\sin(\Omega t) - \Omega u_{1,e}(x,t)\right)^2 + \left(\dot{q}_{nac,e}\cos(\Omega t) + \Omega x + \dot{u}_{1,e}(x,t)\right)^2 \quad \text{(A.19)}$$

The total kinetic energy of the system is thus represented by

$$T_{e1} = \frac{1}{2}\overline{m}\int_0^L v_{b1,e}(x,t)^2 dx + \frac{1}{2}M_{nac}\dot{q}_{nac,e}^{\ 2} \quad \text{(A.20)}$$

The potential energy of the blade is formulated in the same way as for the flapwise model. This results in the total potential energy of the model being expressed as

$$V_{e1} = \frac{1}{2}\int_0^L EI_e\left(\frac{2}{L^2}q_{1,e}\right)^2 dx + V_{ci} + \frac{1}{2}K_{nac}q_{nac,e}^{\ 2} \quad \text{(A.21)}$$

where as before V_{ci} is the potential energy of the blade due to centrifugal stiffening. The Lagrangian formulation is then again applied giving the equations of motion of the single blade edgewise model as

$$\begin{bmatrix} \frac{m_b}{5} & \frac{m_b}{3}\cos(\Omega,t) \\ \frac{m_b}{3}\cos(\Omega,t) & M_{nac}+m_b \end{bmatrix}\begin{Bmatrix} \ddot{q}_{1,e} \\ \ddot{q}_{nac,e} \end{Bmatrix} + \begin{bmatrix} 0 & 0 \\ -\frac{2}{3}m_b\Omega\sin(\Omega t) & 0 \end{bmatrix}\begin{Bmatrix} \dot{q}_{1,e} \\ \dot{q}_{nac,e} \end{Bmatrix} + \begin{bmatrix} \frac{4EI_e}{L^3}+\frac{\Omega^2 m_b}{15} & 0 \\ -\frac{m_b\Omega^2}{3}\cos(\Omega,t) & K_{nac} \end{bmatrix}\begin{Bmatrix} q_{1,e} \\ q_{nac,e} \end{Bmatrix} = \begin{Bmatrix} Q_1 \\ Q_2 \end{Bmatrix} \quad \text{(A.22)}$$

As can be seen, the edgewise system is time varying in nature. Damping also arises in the system through the dynamic interaction between the blade and nacelle before any inclusion of

structural damping. Extending to the three blade model results in the final equations of motion for the undamped edgewise model expressed previously in chapter 3. The equations of motion for blade 2 and 3 are identical to blade one but shifted by $\frac{2}{3}\pi$ and $\frac{4}{3}\pi$ respectively.

$$
\begin{bmatrix}
\frac{m_b}{5} & 0 & 0 & \frac{m_b}{3}\cos(\Omega t) \\
0 & \frac{m_b}{5} & 0 & \frac{m_b}{3}\cos\left(\Omega t+\frac{2}{3}\pi\right) \\
0 & 0 & \frac{m_b}{5} & \frac{m_b}{3}\cos\left(\Omega t+\frac{4}{3}\pi\right) \\
\frac{m_b}{3}\cos(\Omega t) & \frac{m_b}{3}\cos\left(\Omega t+\frac{2}{3}\pi\right) & \frac{m_b}{3}\cos\left(\Omega t+\frac{4}{3}\pi\right) & M_{nac}+3m_b
\end{bmatrix}
\begin{Bmatrix} \ddot{q}_{1,e} \\ \ddot{q}_{2,e} \\ \ddot{q}_{3,e} \\ \ddot{q}_{nac,e} \end{Bmatrix} +
$$

$$
\begin{bmatrix}
c_{st,b} & 0 & 0 & 0 \\
0 & c_{st,b} & 0 & 0 \\
0 & 0 & c_{st,b} & 0 \\
-\frac{2}{3}m_b\Omega\sin(\Omega t) & -\frac{2}{3}m_b\Omega\sin\left(\Omega t+\frac{2}{3}\pi\right) & -\frac{2}{3}m_b\Omega\sin\left(\Omega t+\frac{4}{3}\pi\right) & c_{st,nac}
\end{bmatrix}
\begin{Bmatrix} \dot{q}_{1,e} \\ \dot{q}_{2,e} \\ \dot{q}_{3,e} \\ \dot{q}_{nac,e} \end{Bmatrix} +
$$

$$
\begin{bmatrix}
\frac{4EI_e}{L^3}+\frac{\Omega^2 m_b}{15} & 0 & 0 & 0 \\
0 & \frac{4EI_e}{L^3}+\frac{\Omega^2 m_b}{15} & 0 & 0 \\
0 & 0 & \frac{4EI_e}{L^3}+\frac{\Omega^2 m_b}{15} & 0 \\
-\frac{m_b}{3}\Omega^2\cos(\Omega t) & -\frac{m_b}{3}\Omega^2\cos\left(\Omega t+\frac{2}{3}\pi\right) & -\frac{m_b}{3}\Omega^2\cos\left(\Omega t+\frac{4}{3}\pi\right) & K_{nac}
\end{bmatrix}
\begin{Bmatrix} q_{1,e} \\ q_{2,e} \\ q_{3,e} \\ q_{nac,e} \end{Bmatrix} =
\begin{Bmatrix} Q_{1,e} \\ Q_{2,e} \\ Q_{3,e} \\ Q_{nac,e} \end{Bmatrix}
\qquad \text{(A.23)}
$$

The dampers were modelled as mass spring dashpot systems and the equations of motion formulated using the same technique as that outlined above. The resulting equations of motion for the damped flapwise and edgewise models were outlined in chapter 3.